DOKUZ EYLÜL UNIVERSITY

GRADUATE SCHOOL OF NATURAL AND APPLIED SCIENCES

MONITORING AND NUMERICAL ANALYSIS OF OPEN PIT MINE SLOPES IN GNEISSES

by

Enes KALHAN

August, 2021

İZMİR

MONITORING AND NUMERICAL ANALYSIS OF OPEN PIT MINE SLOPES IN GNEISSES

A Thesis Submitted to the
Graduate School of Natural and Applied Sciences of Dokuz Eylül University
In Partial Fulfillment of the Requirements for the Degree of Master of Science in Geological Engineering, Applied Geology Program

by

Enes KALHAN

August, 2021

İZMİR

M.Sc THESIS EXAMINATION RESULT FORM

We have read the thesis entitled **"MONITORING AND NUMERICAL ANALYSIS OF OPEN PIT MINE SLOPES IN GNEISSES"** completed by **ENES KALHAN** under supervision of **ASSOC. PROF. DR. CEM KINCAL** and we certify that in our opinion it is fully adequate, in scope and in quality, as a thesis for the degree of Master of Science.

Assoc. Prof. Dr. Cem KINCAL

Supervisor

Prof. Dr. Ali Bahadır YAVUZ

(Jury Member)

Assoc. Prof. Dr. Alper SEZER

(Jury Member)

Prof. Dr. Özgür ÖZÇELİK

Director

Graduate School of Natural and Applied Sciences

ACKNOWLEDGMENT

I would like to express my endless gratitude to my esteemed teacher, Assoc. Dr. Cem KINCAL, who guides all studies with his knowledge and experience and has great efforts.

I would like to thank S. Deniz KARAGÖZ, a Senior Geology Engineer, who helped us in many areas such as transportation, work permits, equipment support, for his material and moral support within the scope of field studies, and also gave us experience in the field and shared his knowledge and experience.

I would like to thank Prof. Dr. M Yalçın Koca, Dr Tümay Kadakçı KOCA and Lecturer Semih ESKİ, who made valuable contributions to the study with their opinions, advice and resource assistance throughout this study, and to my family and friends who did not withhold their financial and moral support during my study.

I would like to thank Sibelco Turkey for sharing the Sarikisik Feldspar Quarry data and supporting the work within the scope of this thesis.

I would like to thank Melikhan KARAKAŞ, who we worked with during my undergraduate and graduate education and who added value to my thesis with his knowledge in academic and scientific studies.

I would especially like to thank my family for their financial and moral support throughout my education life.

Enes KALHAN

MONITORING AND NUMERICAL ANALYSIS OF OPEN PIT MINE SLOPES IN GNEISSES

ABSTRACT

One of the biggest problems in open pit mining is slope stability. In order to eliminate stability problems, subjects such as geology, climate and production activity should be known and slope geometries should be selected properly against or to eliminate these problems. In this study, the slope stability of a mine opened in rock slopes has been studied. Mine managers stopped production in 2019 due to slope movements in the eastern part of the quarry. In order to continue to production safely, field works have been carried out primarily. During the field works, measurements were taken at the bench slopes and by performing kinematic analyzes, rock mass studies and numerical analyzes, slope geometries that could remain stable according to geological and environmental conditions were tried to be determined. Engineering geology studies such as scanline measurements in steps and investigation of potential failure mechanisms by kinematic analysis technique were carried out. Rock mass classification systems such as SMR and QSlope were used to evaluate slope stability. Based on these classification systems, unstable rock slopes were determined and thematic maps were created using geographic information systems software. The cross-section line was determined with the help of the generated maps and numerical analysis was performed with softwares Swedge v5.013 (2010) and Phase2 v7.013 (2010) from softwares. The compatibility of rock mass classifications with each other was determined by numerical analysis and the factor of safety were calculated by applying the improvement studies suggested by the classification systems in the software.

Keywords: Engineering geology, numerical analysis, QSlope, rock mass classification, slope stability, slope mass rating (SMR)

GNAYSLADA AÇILMIŞ AÇIK MADEN OCAĞI ŞEVLERİNİN SAYISAL ANALİZİ VE İZLENMESİ

ÖZ

Açık ocak madenciliğinde en büyük sorunlardan biri şev stabilitesidir. Stabilite problemlerini ortadan kaldırmak için jeoloji, iklim ve üretim faaliyeti gibi konuların bilinmesi ve bu problemlere karşı veya bu problemlerin giderilmesi için şev geometrilerinin doğru seçilmesi gerekmektedir. Bu çalışmada, kaya şevlerinde açılan bir madenin şev stabilitesi incelenmiştir. Maden yöneticileri, ocağın doğu kesimindeki şev hareketleri nedeniyle 2019 yılında üretimi durdurdu. Güvenli bir şekilde üretime devam edebilmek için öncelikle saha çalışmaları yapılmıştır. Arazi çalışmaları sırasında seki şevlerinde ölçümler yapılmış ve kinematik analizler, kaya kütlesi etütleri ve sayısal analizler yapılarak jeolojik ve çevresel koşullara göre duraylı kalabilecek şev geometrileri belirlenmeye çalışılmıştır. Kademeli tarama çizgisi ölçümleri ve kinematik analiz tekniği ile olası göçme mekanizmalarının araştırılması gibi mühendislik jeolojisi çalışmaları yapılmıştır. Şev stabilitesini değerlendirmek için SMR ve QSlope gibi kaya kütlesi sınıflandırma sistemleri kullanılmıştır. Bu sınıflandırma sistemlerine dayalı olarak duraysız kaya şevleri belirlenmiş ve coğrafi bilgi sistemleri yazılımları kullanılarak tematik haritalar oluşturulmuştur. Oluşturulan haritalar yardımıyla kesit çizgisi belirlenmiş ve yazılımlardan Swedge v5.013 (2010) ve Phase2 v7.013 (2010) yazılımları ile sayısal analiz yapılmıştır. Kaya kütlesi sınıflandırmalarının birbiriyle uyumluluğu sayısal analizlerle belirlenmiş ve yazılımda sınıflandırma sistemlerinin önerdiği iyileştirme çalışmaları uygulanarak güvenlik faktörü hesaplanmıştır.

Anahtar kelimeler: Mühendislik jeolojisi, sayısal analiz, QSlope, kaya kütle sınıflaması, şev stabilitesi, şev kütle puanı (SMR)

CONTENTS

Page

LIST OF FIGURES

Page

LIST OF TABLES

Page

CHAPTER ONE
INTRODUCTION

1.1 Introduction

Slope design is one of the most important works in open pit mining operation. The correct planning in the preliminary preparation part in mining is of great importance in terms of preventing the quarry from encountering problems over a long period of time. The slopes formed in the excavations with the engineering works carried out in open pit mines; It is aimed to remain stable depending on the topography, rock condition, groundwater, precipitation amount, earthquakes or human-induced external factors. Slope stability studies primarily include detailed research such as the structure of the slope, its size, detailed examination of the causes of subsidence and determination of solution methods.

Slope stability studies necessitate many interdepartmental relationships such as Engineering Geology, Geotechnical Engineering, Rock and Soil Mechanics. Along with deaths and injuries caused by mass movements, engineering structures made by human beings are also damaged. Major financial losses occur due to infrastructure problems, property losses, loss of animals and agricultural products, expenses of search and rescue efforts, first aid and temporary accommodation expenses, treatment, feeding and dressing expenses, re-damage and repair expenses of structures and other damages caused by mass movements.

Geological conditions are important especially for mine slopes. For rock slopes, the optimum slope height and accordingly the slope angle are required. At the initial stage, there is a relationship between slope stability and economy. It means that the cost is lower than the less steep slopes that need to be built and steeper slopes (Hoek & Bray, 2004).

In this study, an open pit slope opened in gneisses is considered for the reasons mentioned above. There are many different mining enterprises, large and small, in this

region. Slope movements were determined by authorized engineers while production was continuing in this facility. Production in the eastern part of the quarry was completely stopped due to the instability of the slopes. In order to stabilize these rock slopes opened in gneisses and to continue production, field investigations, engineering geology studies and rock slope stability evaluation were carried out within the scope of this study.

The stability of the slopes was tried to be determined by the measurements made in the summer months. As a result of these studies, the determination of unstable slopes and the improvement and/or strengthening of these slopes have been determined in order for the enterprise to continue its production in the most efficient way. In addition, the steepest slope angles that can remain stable without any strengthening or improvement have been revealed. In addition, these slopes were visualized using geographic information systems in order to evaluate and better understand the classification systems made specifically for rock material. Numerical analyzes were carried out in the regions where instabilities were detected in the rock slopes of the quarry, and the stability was evaluated in more detail.

In order to solve the briefly mentioned problems, in this thesis study; by investigating the factors that cause instability that may occur in step and slope scale in a part of the open pit; A preliminary study was carried out on the slopes in order to make production continuous in the eastern part of the mine. According to the studies carried out, it has been suggested that the necessary arrangements can be made on the slopes. Within the scope of these purposes, the following topics were followed in this thesis study.

1. In the first stage of the study, general geological studies were completed, accompanied by field studies in the region, literature studies, as well as data obtained from the operation manager (previous drillings and outcrops in previously determined road cuts, etc.).
2. In the period between June 2020 and December 2020, field studies were carried out at the mine site during the summer months. The unstable areas

on the slopes of the operation were tried to be determined, and 1619 discontinuity measurements were taken from 119 different points with the line surveys of approximately 1000 m in the eastern part of the quarry, based on the methods suggested by ISRM (2007).

3. Total station prisms and incklometer wells were drilled in areas where instability was previously detected by the business managers and the movement in the eastern part was followed. At the same time, the groundwater level was determined from the previously drilled boreholes in the field.
4. Discontinuities that cause or may cause instability in the study area were measured and kinematic analyzes were made.
5. In the regions that were determined to be kinematically unstable, rock mass classification systems were made using SMR and Q-slope mass classification systems, and the rock mass was more detailed.
6. Numerical analyzes were made in these regions by taking sections from the regions determined according to kinematic analyses, rock mass classification systems analyzes and data obtained from motion monitoring stations.
7. In the light of the data obtained from the numerical analyzes, the improvement processes recommended by the rock mass classification systems were tried to be carried out on the slopes in which the instability was determined in the field and the final slope angle was revealed.

1.2 Location of the Study Area

The Albit Quarry is located approximately 25km southwest of the Cine district of Aydın province (Figure 1.1). Aydın is located within the borders of 1:25,000 scale topographic map with sheet number N19-b1 and is approximately 40 km away from Aydın city center. The closest settlement to the quarry is Karpuzlu, which is the smallest district of the Aegean Region and is connected to Aydın Province.

1.2.1 Geomorphology

The study area is located on a passageway between two hills, with elevations of 570 m at their highest points. The altitude varies between 408-550m The previous topography of the study area (1959) is in the form of a valley at 430-580m elevations. The contour lines produced from the N19-b1 sheet of the region and the previously found stream beds are shown in the map in Figure 1.2.

Figure 1.1 Satellite image of the study area

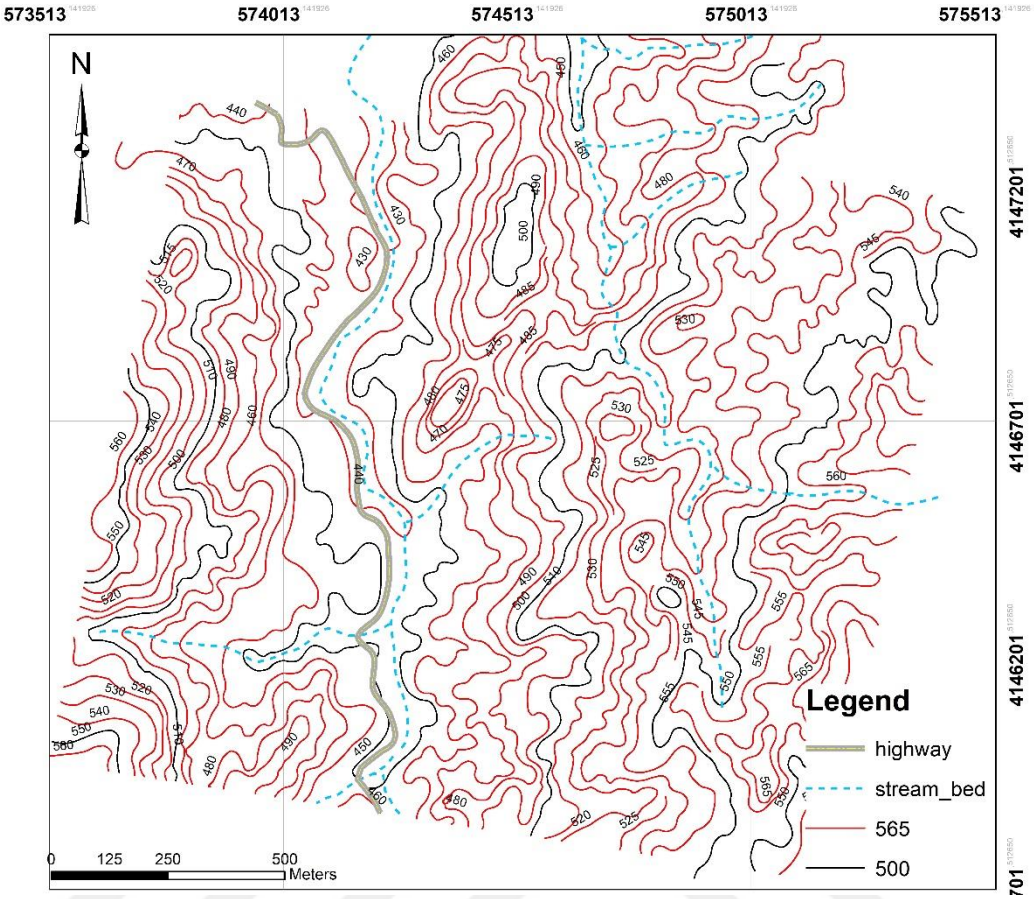

Figure 1.2 N19-b1 topography map

1.2.2 Climate and Precipitation

The Mediterranean climate, which is hot in the summer months and warm and very rainy in the winter months, is effective in the region (Figure 1.3). Due to the topographic structure in this climate type, two different types of plants have been formed in and around Aydın province. These are vegetation in maquis and forest types. Due to the climatic effect in the region, snowfalls are rarely seen. According to the data of the General Directorate of Meteorology and the Ministry of Forestry and Water Affairs (2019), the prevailing wind direction of Aydın in the region is East and depending on seasonal changes, the secondary prevailing wind direction is west-northwest.

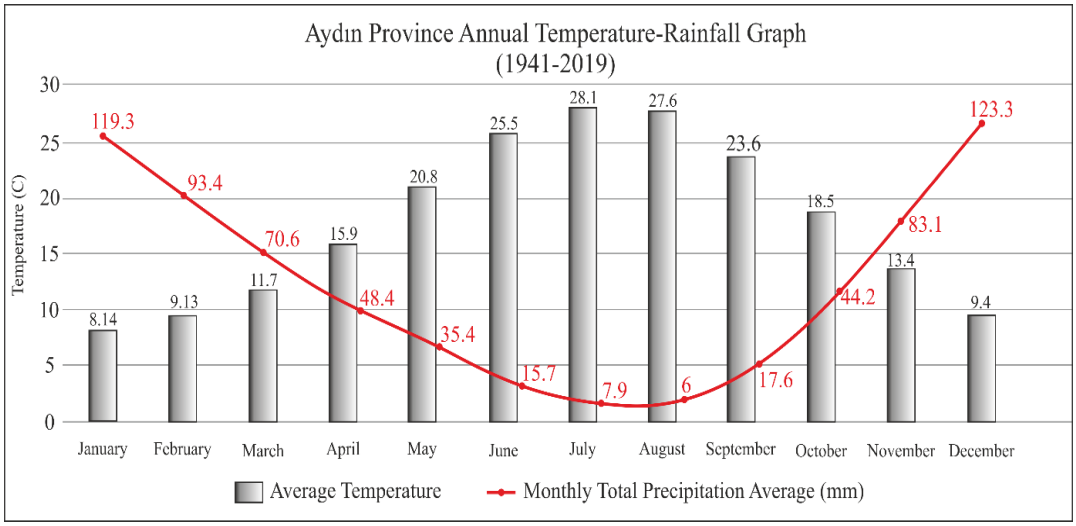

Figure 1.3 Monthly temperature-precipitation graph of the study area (Turkish State Meteorological Service, 2019)

CHAPTER TWO
REGIONAL GEOLOGY AND MINING GEOLOGY OF THE STUDY AREA

The study area is located in the Menderes Massif. which constitutes one of the main tectonic zones of Anatolides that crop out in Western Anatolia (Graciansky, 1965). There are 18 albite open pits of different sizes in this region. The studied mine is one of the most famous albite mining sites in the region (Kıncal, 2014). Leucocratic orthogneisses rich in terms of tourmaline were exposed in the study area. Two types of tourmaline-rich leucocratic orthogneisses were detected in the study area. The first group consists of orthogneisses derived from granoblastic textured coarse granites. The foliation planes of these rocks are defined by the parallel sequence of muscovites. This condition type consists of medium-grained. albite-rich leucocratic orthogneisses (Candan et. al, 2005). All of the geological units in the open pit albite mine have been deformed by a shear zone. The Na-feldspar ore bearing zone with mineralogical composition was developed along the shear zone. The dip directions of foliation planes in orthogneisses are almost perpendicular to this zone. Orthogneisses are characterized by their massive structures. It is seen that the mine site contains gneiss as ore body and wall rock (Figure 2.1). The direction of the ore deposit is N 27 E / 55-60 SE with an approximate length of 660 m developing along the shear zone in the mine. Metaquartzite and rutile lenses are observed. These lenses tend in the NE-SW direction.

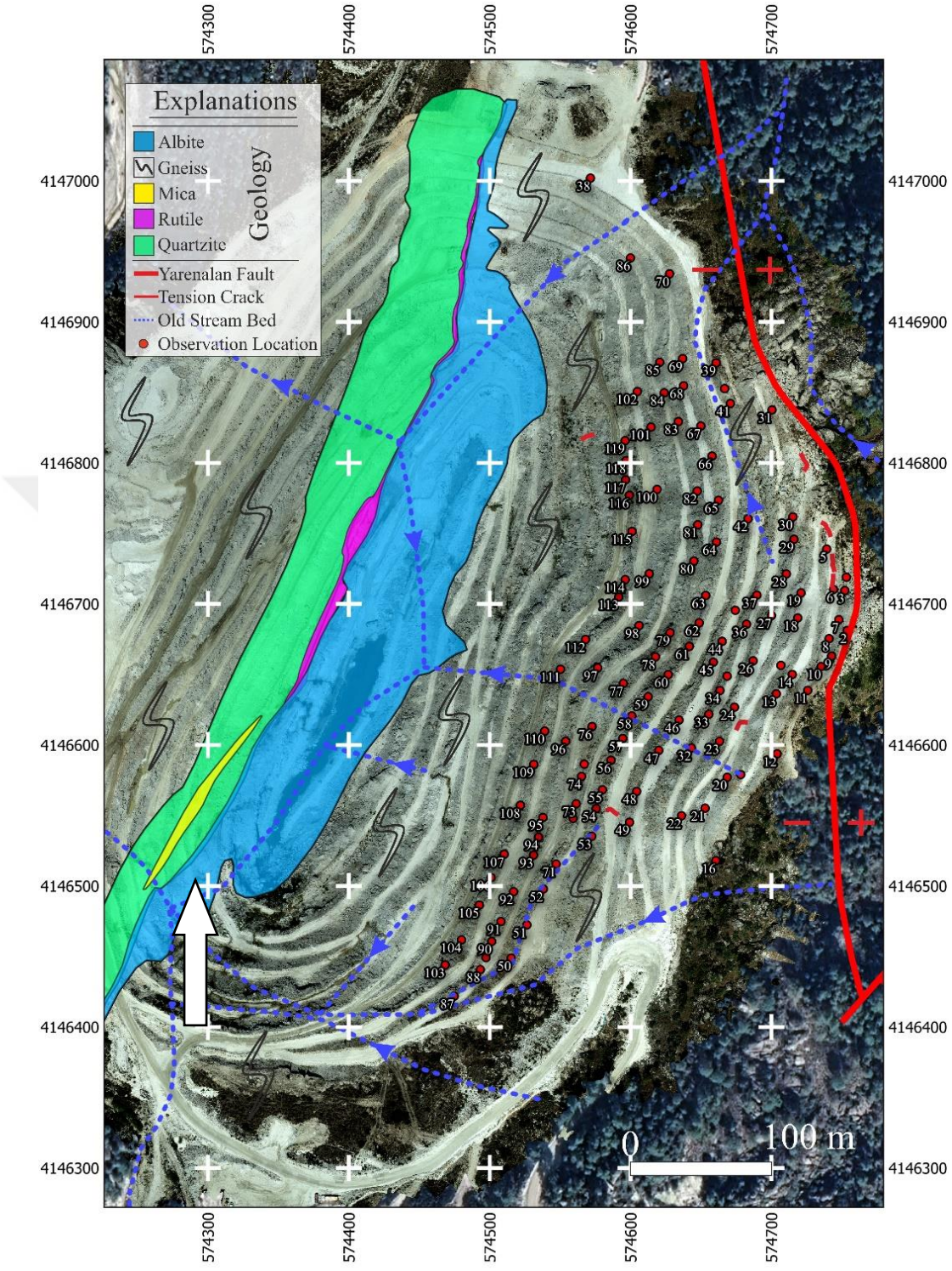

Figure 2.1 Geology map of the study area

CHAPTER THREE
ENGINEERING GEOLOGY

3.1 Introduction

Within the scope of this thesis, some topics of engineering geology were discussed and stability analyzes of the albite mine opened in the gneiss unit were made. For this purpose, discontinuity properties, groundwater conditions, field experiments, geomechanical properties of the rock and kinematically slip types were investigated during field studies. The general view of the eastern slopes studied is given in the Figure 3.1. The slope geometries of the eastern slopes by drone are given in the Figure 3.2. During the studies, previous studies made in the same region and/or made by the company's own resources were also benefited from and used within the scope of this thesis. The details of the above-mentioned engineering geology subjects are also presented in the sub-titles.

Figure 3.1 General view of eastern slopes (Personal archive, 2020)

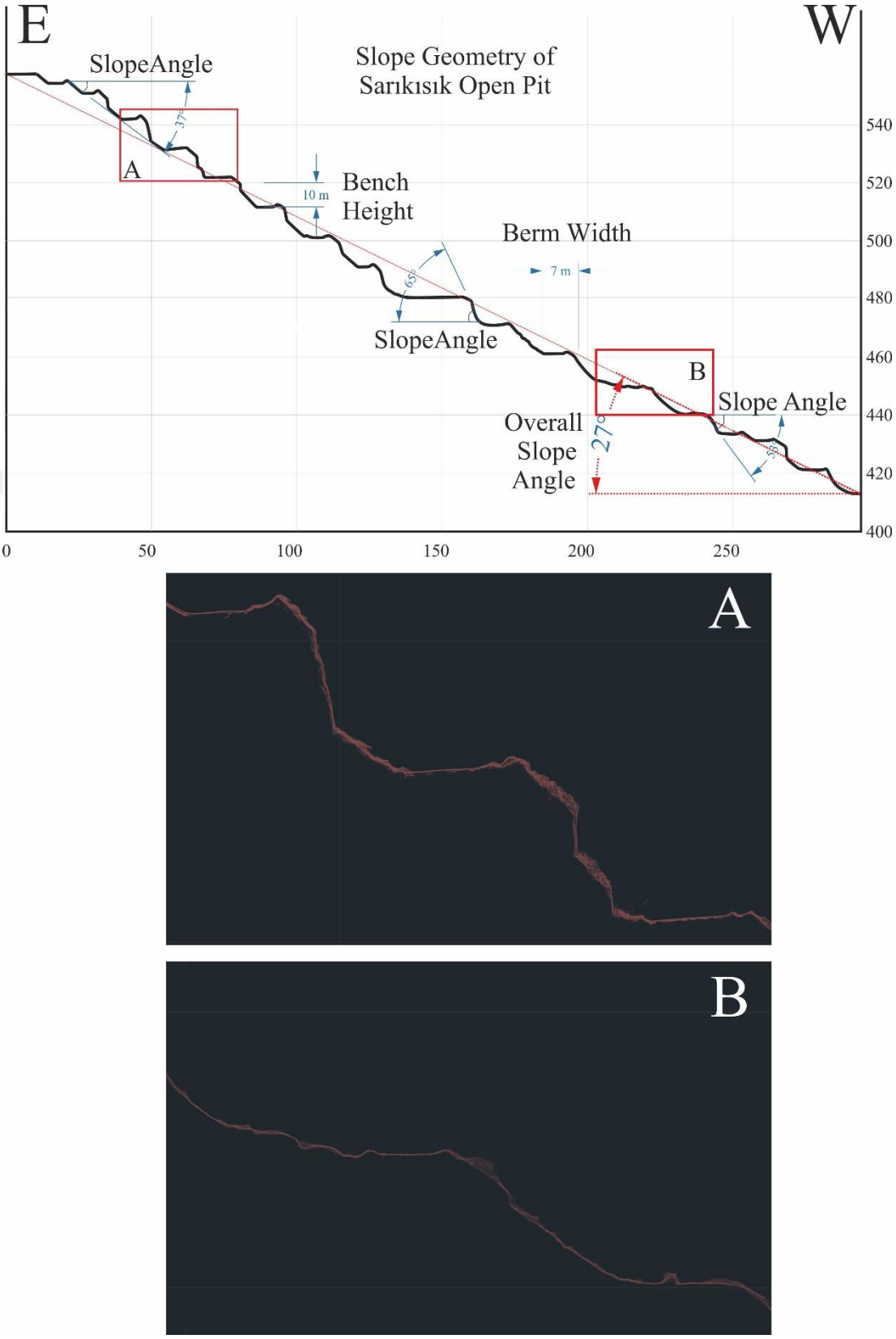

Figure 3.2 Thematic slope geometry of eastern slopes

3.2 Attributes of Discontinuities

The line survey method was used to determine the characteristics of the discontinuities in the slopes located in the eastern part of the mine site. The line survey method is a method that allows examining the rock mass and taking measurements from discontinuities. In this study, the methods recommended by ISRM (2007) were used. For the line study method, which is an effective method in collecting data on the properties of discontinuities, in this study, the properties of discontinuities were revealed by taking 1619 measurements of approximately 1000 m in length. Observations were made only on the eastern slopes of the mine site (Figure 3.3). With the line survey studies, features such as orientation of the discontinuities, spacing, spacing, continuity, surface roughness and waviness, degree of degradation, the characteristics of the filling material and the water state on their surfaces have been determined. The orientation of the discontinuities was determined with the Brunton brand geologist compass, the roughness of the discontinuity surfaces with the Barton roughness comb, the spacing and spacing of the discontinuities were determined with a tape measure and digital caliper.

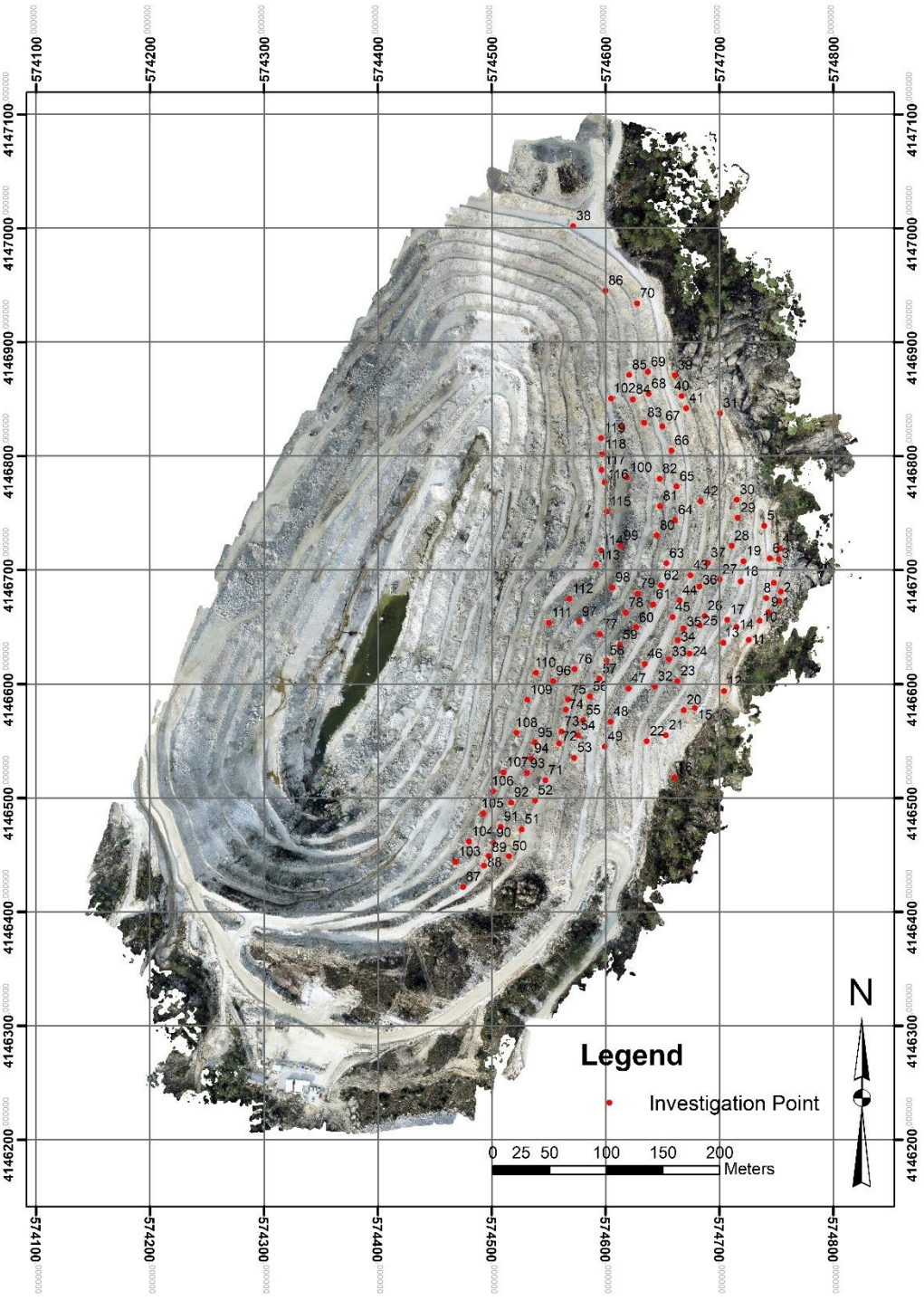

Figure 3.3 Observation points where discontinuity measurements were made on the eastern side of the albite operation

3.2.1 Type of Discontinuity

Discontinuities can be classified according to the way they occur. This is important for geological engineering because discontinuities directly affect the stability conditions in the study area. Discontinuities generally have similar properties in terms of their properties. The following are standard definitions of the most common types of discontinuities. These discontinuities can be briefly described as:

1. *Fault*- If the displacement is visible to the naked eye, such discontinuities can be called faults (Figure 3.4).

Figure 3.4 The fault causing the quartz vein observed in the study area to slip by approximately 10cm (Personal archive, 2020)

2. Bedding—Parallel-surfaced structures that accumulate over geological time with or without a physical formation.

3. Foliation- These are the structures where minerals develop parallel to each other after being exposed to different temperatures and pressures after their formation (Figure 3.5).

Figure 3.5 Foliation planes causing planar shifts in the study area (Personal archive, 2020)

4. Joint—Fractures or cracks in discontinuities where no movement is observed. They are usually cut by other geological structures (flow bands, foliation, etc.). Joints can develop parallel to each other or at an angle to each other (Hoek & Bray, 2004) (Figure 3.6).

Figure 3.6 Joints and joint sets in slope steps (Personal archive, 2020)

3.2.2 Orientation of Discontinuities

The orientation of the discontinuities has a great influence on the potential for the occurrence of instabilities in slopes, in the form of sliding or toppling along the discontinuities. The measurements of the said discontinuities are measured by the geologist with the help of a compass (Figure 3.7). The orientation of the discontinuities and the number of sets formed by these discontinuities are also important input parameters used in rock mass classification. 1613 discontinuity measurements were taken from these observation points and the data were evaluated according to ISRM (2007) standards. According to the 1613 discontinuities obtained from the line survey measurements, 5 dominant discontinuity sets were determined on the east side of the quarry (Figure 3.8). The dip/dip directions of these discontinuity sets are classified according to ISRM (2007) (Table 3.1). All measurements of joint sets on slope surfaces are presented in Appendix-1.

According to this classification, it has been observed that the joint sets generally have high angle slopes. It can be predicted that the reason for this is the high-angle normal fault in the east of the quarry.

Figure 3.7 Taking discontinuity measurements (Personal archive, 2020)

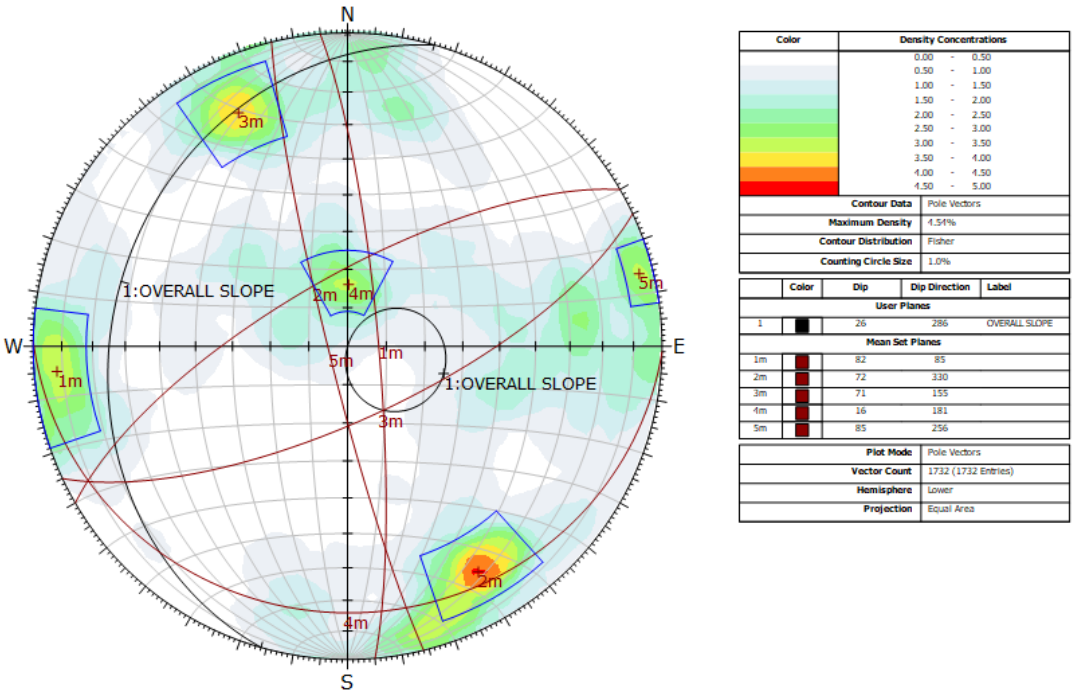

Figure 3.8 Concentration points in the dips program of 1613 discontinuities taken from the field

Table 3.1 Classification of dominant joint sets according to ISRM (2007)

Rock Mass Properties			Discontinuity Sets				
			J1	J2	J3	J4	J5
Orientation of Discontinuity	Min-Max (D/DD):		72-88/072-097	60-82/320-341	59-84/146-164	10-22/153-208	81-89/251-261
	Mean:		81.785/084.99	72.0753/329.93	71.4715/155	16.7429/182.1	84.6739/255.96
	SD	Dip:	3.94	5.94	6.70	4.02	2.29
		Dip Direction:	6.99	5.80	4.68	15.92	3.05

3.2.3 Spacing of Discontinuities

The discontinuity spacing is the perpendicular distance between two discontinuities in a set of discontinuities or parallel joints in rock masses. The discontinuity spacing can be measured from the discontinuities crossing the tape measure along the tape measure laid in a certain direction on the outcrop surface, or it can be determined from drilling cores. However, in practice, since it is not always possible to lay the tape measure perpendicular to the discontinuity sets, two types of spans can be measured.

A scan-line work of approximately 1000 m in length was carried out from the operation site (Figure 3.9). These line studies were taken almost perpendicular to the discontinuities on the slope surfaces, almost perpendicular. Based on these conditions, 1619 discontinuities taken from the eastern slopes of the field were classified according to ISRM (2007). Within the scope of this study, the discontinuous spacing of the dominant joint sets in the eastern part of the quarry was evaluated separately and presented in table 3.2. The discontinuity spacing of the joint sets measured on the slopes is presented in Appendix-2.

According to the results obtained, the distance between the discontinuities of the dominant discontinuity sets in the mining operation was calculated as 2m at most (belonging to the J3 joint set), and the lowest as 0.05m. According to the classification system, all of the joint teams in the field were determined as "modarate spacing" (Table 3.3).

Figure 3.9 Measurement of discontinuity spacing (Personal archive, 2020)

Table 3.2 Classification of discontinuity spacings of dominant joint sets according to ISRM (2007)

Rock Mass Properties		Discontinuity Sets				
		J1	J2	J3	J4	J5
Spacing (m)	Minimum:	0.1	0,10	0.05	0.10	0.10
	Maximum:	1,50	1.20	2.00	1.00	1.80
	Mean:	0.46	0.36	0.37	0.38	0.53
	SD:	0.35	0.27	0.35	0.22	0.32
	Description:	Moderate spacing	Moderate spacing	Moderate spacing	Moderate spacing	Moderate spacing

Table 3.3 Discontinuity spacing descriptions ISRM (2007)

Discontinuity spacing	**Description**
<20 mm	Extremely close
20–60 mm	Very close
60–200 mm	Close
20–60 cm	Moderate
60 cm–2 m	Wide
2–6 m	Very wide
>6 m	Extremely wide

3.2.4 Aperture and Filling of Discontinuities

An aperture is the perpendicular distance between two opposing surfaces of a discontinuity and may be empty or filled by water or any other filling material (Figure 3.10).

Based on the explanations above, the opening and filling of the discontinuities taken from the field are evaluated separately in the table according to ISRM (2007) standards (Table 3.4). Accordingly, the opening of the joint kits is "0.25-0.5 mm: Partly open/Closed Feature and/or 0.5-2.5 mm: Open/Gapped Feature" and the filling is "Geometry: wall roughness, Filling type: weathering grade".

Figure 3.10 Filling material observed in some joint sets (Personal archive, 2020)

Table 3.4 Classification of patency and filling of joint sets according to ISRM (2007) standards

Rock Mass Properties		Discontinuity Sets				
		J1	J2	J3	J4	J5
Aperture	Description:	0.25-0.5 mm: Partly open/Closed Feature and/or 0.5-2.5 mm: Open/Gapped Feature				
Filling	Description:	Geometry: wall roughness, Filling type: weathering grade,				

3.2.5 Persistence of Discontinuities

The continuity of the discontinuities in one plane is an indicator of the propagation in this discontinuity plane and has important effects in terms of stability (Ulusay & Sönmez, 2002) (Figure 3.11).

Continuity class of 5 dominant discontinuity sets according to ISRM (2007) standards for measurements taken from the field is presented in the table 3.5. Accordingly, the continuity of the dominant joint sets was determined in field studies as the shortest 2 and the longest 12m (Table 3.6).

Figure 3.11 Continuity of J1, one of the dominant joint sets observed on the eastern slopes (Personal archive, 2020)

Table 3.5 Continuity class of joint sets according to ISRM (2007)

Rock Mass Properties		**Discontinuity Sets**				
		J1	J2	J3	J4	J5
Persistence (m)	Range	2-8	2-3	1-1.5	5-10	6-12
	Description:	Medium persistence	Low persistence	Low persistence	Medium persistence	High persistence

Table 3.6 Persistence classification according to ISRM (2007)

Description	**Persistence (m)**
Very low	<1
Low	1-3
Medium	3-10
High	10-20
Very High	>20

3.2.6 Roughness of Discontinuities

It is a parameter for determining the planarity of a discontinuity surface. It can be determined as 1st or 2nd in two different ways. While the roughness defines the planarity in the 1st scale, the waviness defines the 2nd scale (Ulusay & Sönmez, 2002) (Figure 3.12).

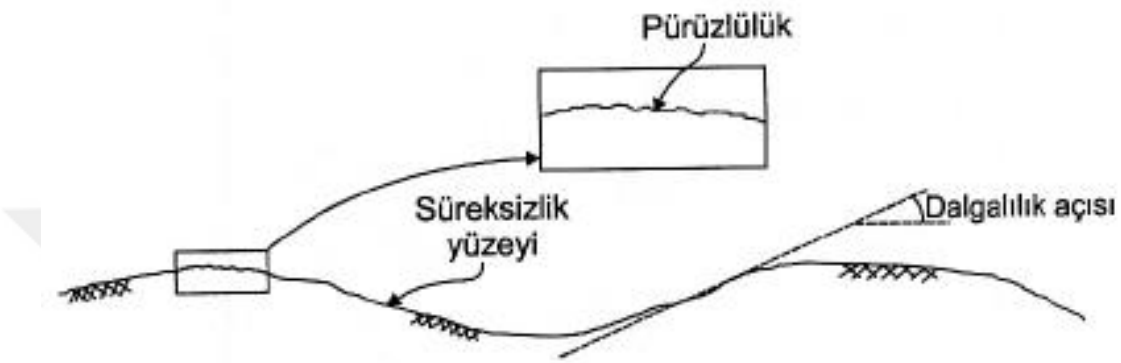

Figure 3.12 Roughness of discontinuity surfaces (Ulusay & Sönmez, 2002)

Within the scope of the study, roughness measurements were taken from the discontinuity surfaces in the field with the help of a comb, as suggested by ISRM (2007) (Figure 3.13). According to these measurements, the roughness classification of the dominant 5 discontinuity sets in the field, again based on the standards developed by ISRM (2007), is given in the table 3.7. Some of these measurements are presented under this topic for illustrative purposes (Figure 3.14).

Figure 3.13 Measurement of roughness in joint sets in gneiss units with a comb (Personal archive, 2020)

Table 3.7 Classification of discontinuities of joint sets according to ISRM (2007) as a result of measurements taken from discontinuity sets on slopes

Rock Mass Properties		Discontinuity Sets				
		J1	J2	J3	J4	J5
Rougness	Description:	Discontinuity surfaces are generally rough-undulating (IV. Class)				

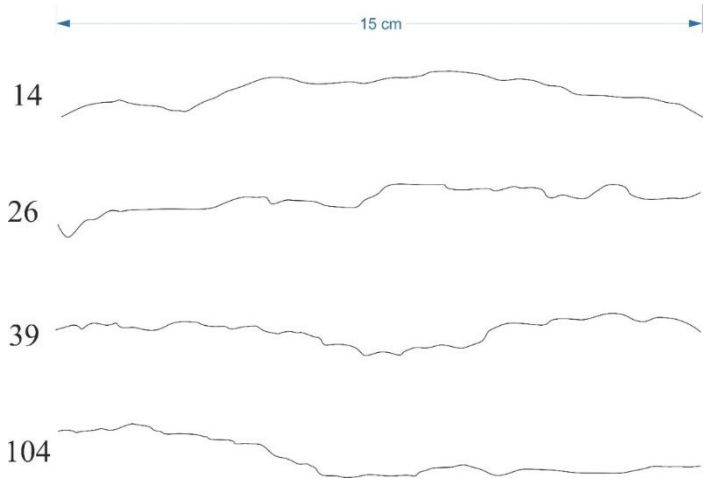

Figure 3.14 The roughness of the discontinuity surfaces at some observation points measured with a comb

3.2.7 Discontinuities Wall Strenght (JCS)

Within the scope of this study, the measurements of the dominant 5 discontinuity sets were carried out by means of a schmidt hammer. Measurements were made according to ISRM (2007) standards for each observation point (Figure 3.15).

Figure 3.15 The schmidt hammer test according to ISRM standards (Personal archive, 2020)

Some experiments and results of rebound values taken from dominant discontinuity surfaces are presented in the table 3.8. All the rebound test results performed in the field are presented in the Appendix-3.

Table 3.8 Sample rebound values of some discontinuities

Location	Rebound Value										Total	Average
8	12	10	14	34	16	28	11	13	10	23	171	17.1
14	15	31	22	21	28	26	15	44	30	34	266	26.6
18	30	22	34	24	21	18	40	32	34	28	283	28.3
29	38	40	34	39	36	28	27	42	37	39	360	36
32	28	22	24	21	26	20	23	25	28	31	248	24.8
34	39	32	25	23	30	24	26	27	34	28	288	28.8
48	28	34	24	40	31	27	25	40	28	33	310	31
52	24	18	19	17	19	21	16	19	20	21	194	19.4
55	14	11	10	10	12	10	12	12	13	10	114	11.4
57	24	28	26	18	20	24	18	20	24	20	222	22.2
61	30	31	36	33	22	23	26	30	32	21	284	28.4
68	50	47	41	40	38	36	44	41	42	40	419	41.9
74	30	37	29	27	30	37	35	27	38	33	323	32.3
75	19	27	25	22	19	20	28	27	22	18	227	22.7
79	29	31	27	36	41	44	27	30	33	41	339	33.9
81	26	19	18	12	17	20	16	16	14	21	179	17.9
88	20	19	14	20	16	14	12	11	20	17	163	16,3
93	22	19	26	28	20	24	24	19	21	20	223	22.3
98	27	30	25	32	34	41	40	37	38	28	332	33.2
105	23	31	21	25	28	29	33	29	35	25	279	27.9
108	32	28	29	30	27	35	33	28	29	22	293	29.3
114	35	41	40	39	35	39	38	22	34	44	367	36.7
119	28	23	30	20	20	35	20	32	33	21	262	26.2

The results of measurements taken from discontinuity surfaces are classified according to ISRM standards. According to the test results taken from the quarry, the lowest bounce value of the discontinuity planes was determined as 10 in the regions where the weathering zones are more intense, and as 56 in the regions with fresh rocks. According to the results obtained and ISRM (2007) standards, the rock class of the slopes in the eastern part of the quarry was determined as “weak-moderate rock” (Table 3.9).

Table 3.9 Classification of field tests results according to ISRM (2007) standards

Rock Mass Properties		Discontinuity Sets				
		J1	J2	J3	J4	J5
Wall Strenght	Highest-lowest Rebound (r):	10-56				
	Mean Rebound:	26.45043				
	SD:	8.872203				
	Grade:	R2-R3				
	Description:	Weak rock-Medium strong rock				

3.3 Groundwater Situation

No significant groundwater level could be recorded in the mine site. However, groundwater has been detected at -80 m levels in extremely cracked and fractured fault zones in deep water drillings. Although it is not considered as a groundwater level, there is water accumulating in the cracks. Crack waters are observed at -2 to -3m depths in rainy periods.

3.4 Geomechanical Properties of Intack Rock

The properties of the rock material in the rock mass can be made in the laboratory with a sample that will represent the rock mass. For example, sending only the "best" core samples to the laboratory for uniaxial compression testing is not a situation that can lead to an overestimation of rock strength. When testing a rock material taken from a rock mass, a distinction must be made between "index" and "mechanical" properties.

1. Index properties: Conditions that can mechanically determine the behavior of a rock and assist in determining the qualitative properties of the rock can be called index features. For example, if the porosity in the rock material increases, the strength will decrease.
2. Mechanical properties: They are properties that help to quantify changes in the shape of rock material. One of the most known and used by most engineers or industries is the "uniaxial compressive strength" test.

These two parameters are the most used parameters in stability analysis in open pits, road cuts and similar engineering applications (Read & Stacey, 2010).

Within the scope of this study, it was deemed appropriate to perform the unit weight test from the above-mentioned index tests and the UCS test from the mechanical properties. The UCS value was previously determined by different researchers in the same region, by laboratory experiments. In this article, it is aimed to determine the UCS value indirectly by using an empirical method in addition to laboratory experiments. For this, the JCS value mentioned in the previous sections was used. Details will be detailed in the sub-topic.

3.4.1 Index properties (Unit weight)

They take different values according to the unit volume weight, the space in the rock, the crack and the amount of water contained therein. The unit volume weight is found by dividing the weight of the sample by the total rock volume. The volume filled by water and air is expressed as “void volume” (Erdoğan & Yavuz, 2004). The unit volume weights of the rocks when they are found in nature are called the "natural unit volume weight", the unit volume weights when all the cavities are filled with water are called the "saturated unit volume weight" and the unit volume weights when the hollow parts are filled with air are called the "dry unit weight" (Erdoğan & Yavuz, 2004).

Unit volume weight is an important parameter in the physical properties of rocks. Unit volume weight is one of the physical properties that are also examined in terms of durability and durability of natural stones. Because rocks with high unit volume weights generally have low porosity and with low water absorption capacity, they are generally among the rock groups with high durability and strength (Erdoğan & Yavuz, 2004).

Unit weight of gneiss unit was determined as approximately 26 in field studies conducted in the same region. The laboratory results of Kadakçı & Koca (2014) are presented in the table 3.10.

Table 3.10 Test results of orthogneiss mass (Kadakçı & Koca, 2014)

Physico-Mechanical Parameters (n=Test Number)	**Experiment results**
ɣ (kN/m^3) n:18	25.9±0.01

3.4.2 Mechanical properties (Uniaxial Compressive Strenght Test)

The most common test performed on cores from drilling or cylindrical rock samples prepared in the laboratory is the uniaxial compressive strength test. As mentioned in the introduction, the Schmidt hammer test was deemed appropriate for the determination of the UCS value within the scope of this thesis (Figure 3.16). The purpose of this is to obtain approximately the same results in laboratory experiments that were previously carried out in different studies in the same region. For this reason, in this study, it was preferred to determine the UCS value indirectly with the Schmidt Hammer from the field instead of the laboratory experiment. With this experiment, it has also been tested whether the same result can be found with laboratory experiments in a shorter time and with less cost.

Schmidt hammer test was performed to measure the uniaxial compressive strength (UCS) of discontinuity planes proposed by Barton & Choubey (1973). Experiments were carried out with L-type Schmidt hammer at a total of 119 different points. As a result of the laboratory studies conducted by Kadakçı & Koca (2014) belonging to the same region, the unit volume weights values of orthogneisses were used (Table 12). UCS values were calculated by using the following equation 3.1 suggested by Barton & Choubey (1977). Orthogneiss rock slopes were determined to be "Moderately Strong" according to the Anon (1977) classification (Table 3.11).

$$LogJCS = 0.00088\gamma R + 1.01 \qquad (3.1)$$

In the above equation;

JCS: Strength of the discontinuity surface (MPa)

ɣ*:* Unit volume weight (kN/m^3)

R: Schmidt rebound value.

Table 3.11 Test results of orthogneiss mass (Kadakçı & Koca, 2014)

Physico-Mechanical Parameters (n=Test Number)	**Experiment results**
ɣ (kN/m^3) n: 18	25.9±0.01
σ_{ci} (MPa) n: 12	27.34±5.30

As a result of the experiments, the UCS value of the rock mass was determined indirectly, according to the equation. The UCS value is similar to laboratory experiments in the same region. According to the results of the experiment performed by Kadakçı (2014), the UCS value of the rock mass in the region was approximately 27 MPa, while the result obtained as a result of the experiments conducted within the scope of this article was determined as approximately 32 (Table 3.12).

Table 3.12 Classification of experimental results according to Anon (1977)

Number of Test	Highest-lowest Rebound	Mean Rebound	Standard Deviation	Mean log(JCS)	Mean UCS (MPa)	Grade	Description
119	10-56	26.45043	8.872203	1.497	32.9	R3	Medium Strong Rock

Figure 3.16 The construction of the swirl hammer test to determine the UCS value from the slope steps (Personal archive, 2020)

Another determination of the UCS value belongs to Deere & Miller (1966), first and most comprehensively. For this purpose, the chart in the Figure 3.17 was developed by the researchers for the estimation of the uniaxial pressure value. According to this chart, when the rebound values obtained from the shim hammer and the unit volume weight of the rock material are combined at one point, it is possible to estimate the UCS value. According to this chart, the results obtained are similar to the results obtained within the scope of the article. The UCS value was found to be approximately 32+-5 in the results obtained by both the chart and the formula.

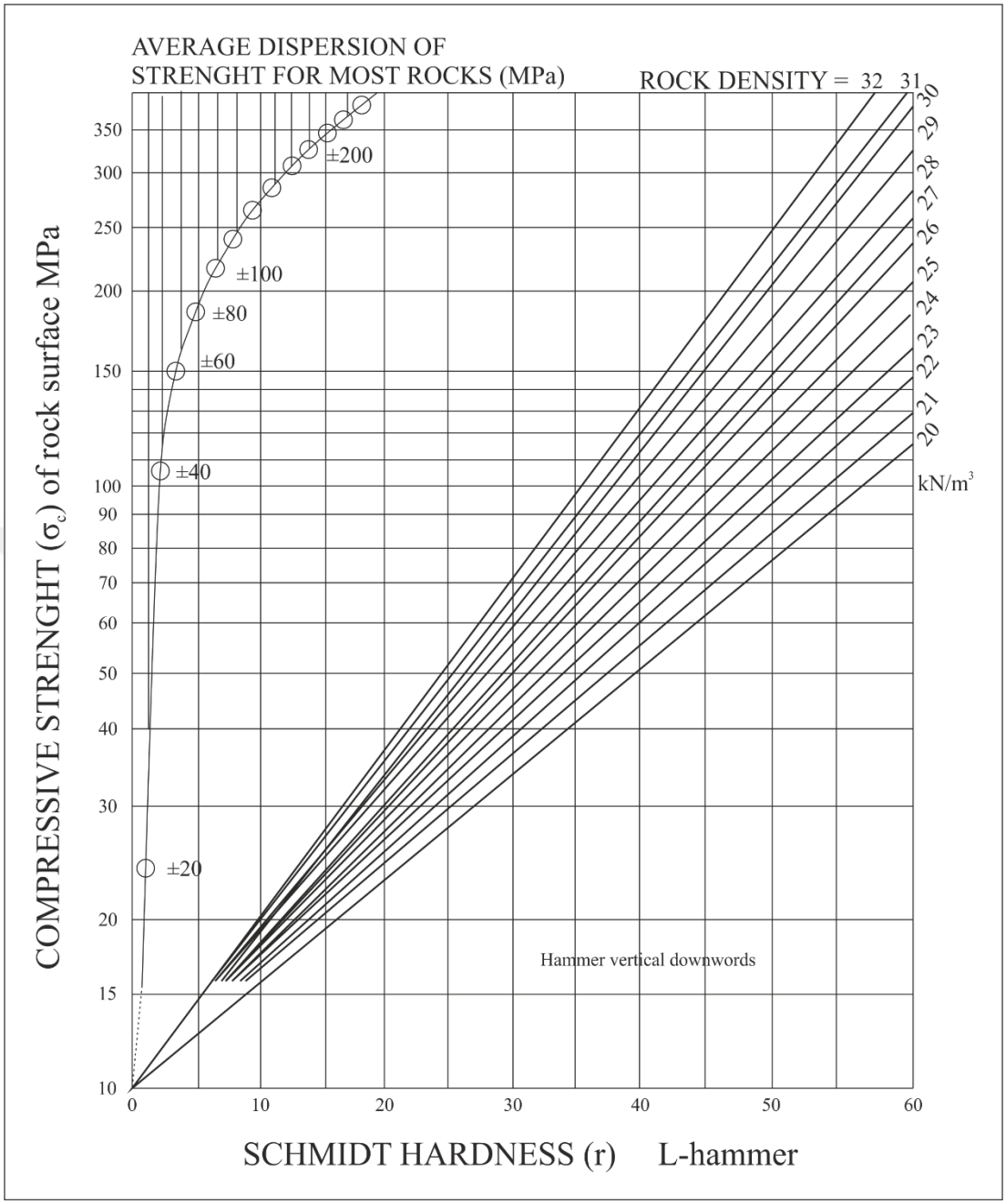

Figure 3.17 The relationship between the Schmidt rebound hardness value and the compressive strength of the rock surface

3.5 Weathering and Alteration

Observations were made at 141 points in order to determine the weathering and alteration developed on the slopes on the eastern side of the mining operation. Weathering was detected at 27 points out of 141 points and lost its rock feature in some slopes (Figure 3.18). Although some observation points show rock features, these points are included in the "weathering points" because they do not have a discontinuity plane.

3.5.1 Weathering Condition

Weathering can be defined as the change in the appearance and/or structure of a rock by exposure to physical or chemical effects. There are serious changes in the strength of the rock mass, which undergoes weathering under the influence of various environmental factors, and this change may result in instability problems. Various parameters such as climate, groundwater level and chemistry are the parameters that cause weathering. With the effect of these environmental factors, the open pit has decreased the strength of the rock mass and caused stability problems. The location of the enterprise in many creek bed regions and the excessive rainfall in winter due to the climate effect reduced the strength of these rocks and adversely affected them. Likewise, due to the excavations made due to production and the corrections made in the stages during the slope design stage, as a result of the pressure release, the rocks underwent physical weathering and reduced their mechanical properties and lost their rock properties. The impact areas of these observed weathering states were determined and the map in Figure 3.18 is shown. Due to the decreasing rock strength due to weathering, block debris and slips of different sizes can be seen clearly in the quarry (Figure 3.19 and 3.20).

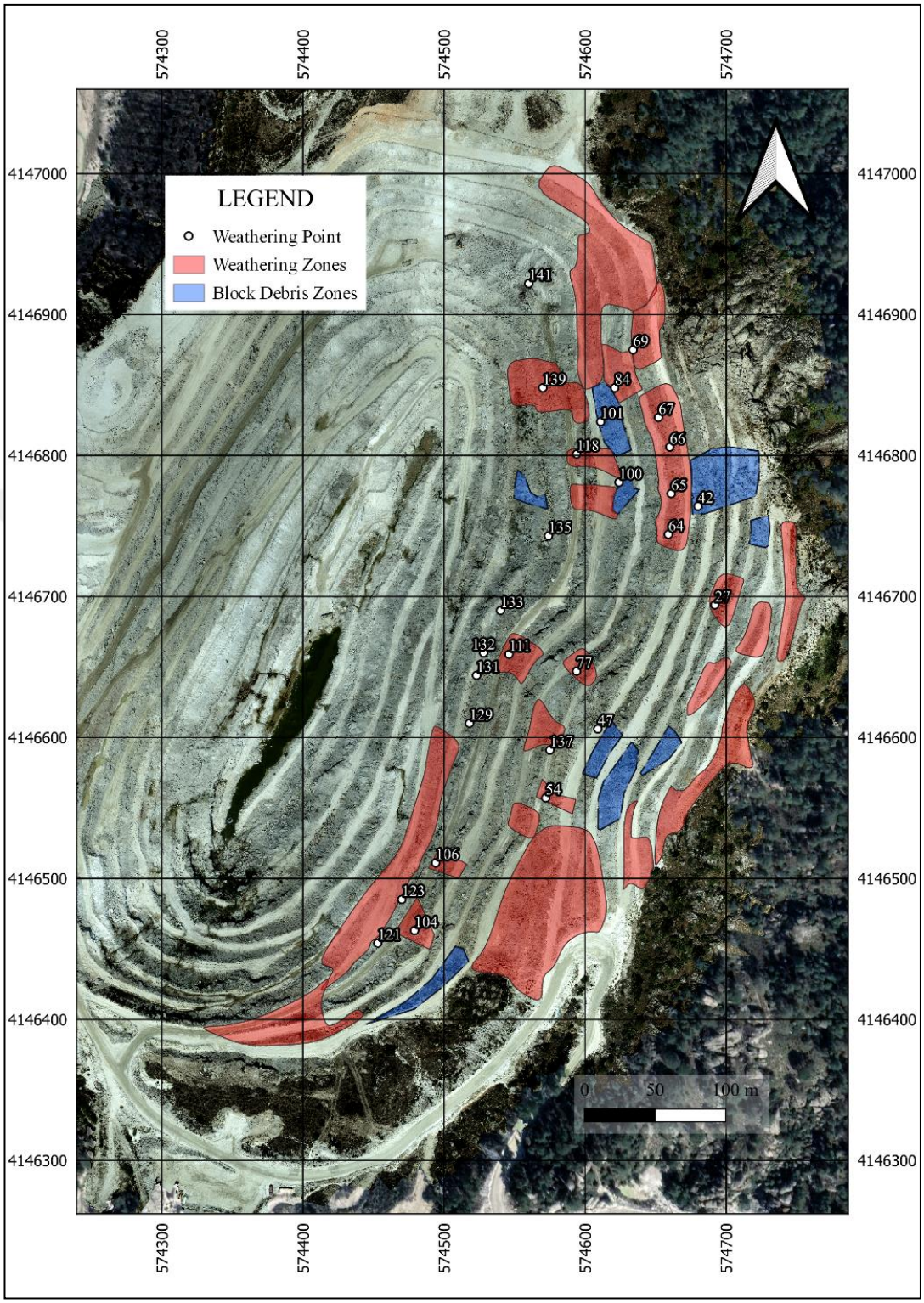

Figure 3.18 Map of the study area showing the weathering zones and block debris

Figure 3.19 The weathering and loss of rock feature observed on the slope at the 111th Observation Point (Personal archive, 2020)

Figure 3.20 Block debris due to weathering seen at observation points 47 and 101 (Personal archive, 2020)

3.5.2 Alteration

It is known that the strength of the rock mass will decrease due to weathering and it may cause problems on the slopes. Although weathering generally reduces the strength of the rock, in some cases it can increase the strength of the rock.

In the mine in this study, the effects of physical weathering can be clearly seen, and alterations due to chemical weathering processes can easily be seen. As a result of the interaction of hydrothermal fluids with the rock mass, which developed due to faulting, oxidation occurred on the rock surface and it was observed that the strength of the rock increased. The fact that the UCS values obtained from the Schmidt hammer experiments in these regions are also high supports this statement. The presence of hydrothermal fluids released due to faulting is supported by the dendritic structure formed in the rock wall in the image in figure 3.21.

Figure 3.21 Dendritic traces formed by the hydrothermal fluid located in the alteration zone and exposed due to faulting (Personal archive, 2020)

Drone images were used to determine the weathering zones in the quarry. By means of these images, weathering zones on the eastern slopes were determined and engineering geology studies could not be carried out in these regions (Figure 3.22). As mentioned in the previous section, it has almost lost its rock mass feature in these zones and has been classified as HW-EW in field observations.

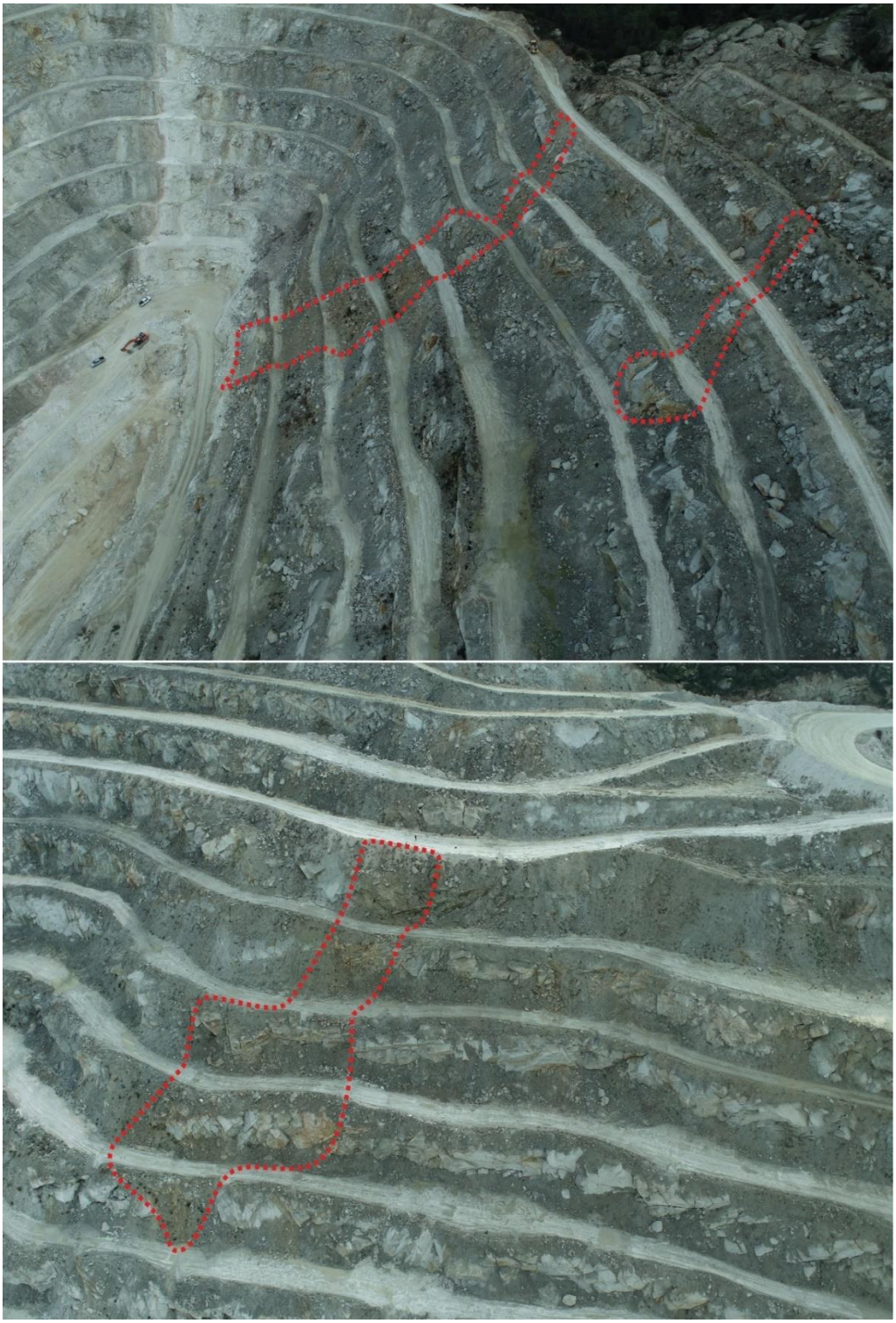

Figure 3.22 Some weathering zones on the eastern slopes (Personal archive, 2020)

3.6 Kinematic Analysis of Pit Slope

Rock slopes often failure along existing geological structures. Therefore. most rock slope problems require consideration of geometric relationships between discontinuity planes slope. and related force vectors. One of the most important requirements for rock slopes is to determine the correct failure mechanism (Bell, 1992). Within the scope of this study scan-line work proposed by ISRM (2007) was conducted at 119 different observation point in the eastern part of the open pit mine opened in gneisses.

1613 discontinuity measurements were taken from these observation points and the data were evaluated according to ISRM (2007) standards. The orientations of the discontinuity planes were transferred to the stereographic projection with Dips 7.016 (RocScience, 2019) software and the type of failures at each observation point were evaluated kinematically and expressed as a percentage in the pie chart (Figure 3.23) (Table 3.13) (Figure 3.24).

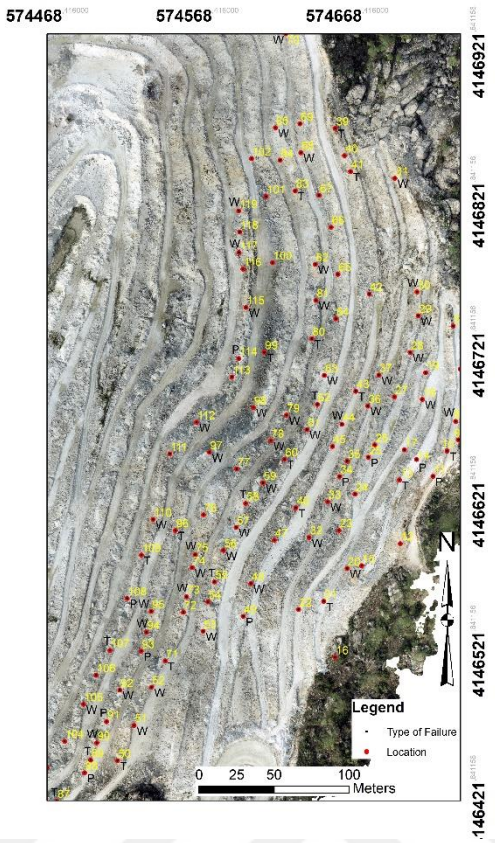

Figure 3.23 Observation points where eastern slopes have kinematic failure potential

Table 3.13 Types of failure kinematically at observation point

Location	Slope dip/dip direction	Failure Type	Potential of failure mechanism	Location	Slope dip/dip direction	Failure Type	Potential of failure mechanism
1	38/284	Kinematically Stable	-	31	44/245	W	Structurally controlled
2	38/286	Kinematically Stable	-	32	55/290	W	Structurally controlled
3	43/272	Kinematically Stable	-	33	50/295	W	Structurally controlled
4	39/275	Kinematically Stable	-	34	57/295	P	Structurally controlled
5	40/267	Kinematically Stable	-	35	58/290	Kinematically Stable	-
6	41/274	T	Structurally controlled	36	58/296	W	Structurally controlled
7	48/285	Kinematically Stable	-	37	58/288	W	Structurally controlled
8	58/281	W	Structurally controlled	38	50/190	Kinematically Stable	-
9	56/273	Kinematically Stable	-	39	74/248	T	Structurally controlled
10	56/270	T	Structurally controlled	40	60/243	Kinematically Stable	-

Table 3.13 continues

11	48/309	P	Structurally controlled	41	54/253	T	Structurally controlled
12	47/277	Kinematically Stable	-	42		Kinematically Stable	-
13	50/291	T	Structurally controlled	43	54/296	T	Structurally controlled
14	48/286	P	Structurally controlled	44	73/294	W	Structurally controlled
15		Kinematically Stable	-	45	59/300	Kinematically Stable	-
16		Kinematically Stable	-	46	47/301	T	Structurally controlled
17		Kinematically Stable	-	47	35/310	Kinematically Stable	-
18	48/279	W	Structurally controlled	48	40/299	W	Structurally controlled
19	48/298	Kinematically Stable	-	49	44/282	P	Structurally controlled
20	45/286	W	Structurally controlled	50	47/282	T	Structurally controlled
21	47/288	T	Structurally controlled	51	51/287	W	Structurally controlled
22	38/298	Kinematically Stable	-	52	53/295	W	Structurally controlled
23	62/297	Kinematically Stable	-	53	43/278	W	Structurally controlled
24	59/296	Kinematically Stable	-	54		-	-
25	59/295	P	Structurally controlled	55	45/296	T	Structurally controlled
26	62/287	Kinematically Stable	-	56	41/302	W	Structurally controlled
27		Kinematically Stable	-	57	42/305	W	Structurally controlled
28	50/295	W	Structurally controlled	58	35/317	T	Structurally controlled
29	53/286	W	Structurally controlled	59	39/291	W	Structurally controlled
30	56/269	W	Structurally controlled	60	46/297	T	Structurally controlled
61	73/297	W	Structurally controlled	91	47/292	P	Structurally controlled
62	55/285	T	Structurally controlled	92	54/289	W	Structurally controlled
63	45/278	W	Structurally controlled	93	60/308	P	Structurally controlled
64		Kinematically Stable	-	94	52/285	W	Structurally controlled
65		Kinematically Stable	-	95	45/282	W	Structurally controlled
66		Kinematically Stable	-	96	56/286	T	Structurally controlled
67		Kinematically Stable	-	97	55/315	W	Structurally controlled
68	44/257	W	Structurally controlled	98	55/298	W	Structurally controlled
69		Kinematically Stable	-	99	60/285	T	Structurally controlled
70	39/231	W	Structurally controlled	100		Kinematically Stable	-
71	81/304	T	Structurally controlled	101		Kinematically Stable	-
72		Kinematically Stable	-	102	48/268	Kinematically Stable	-
73	51/288	W	Structurally controlled	103	45/315	W	Structurally controlled
74	55/288	W	Structurally controlled	104		Kinematically Stable	-
75	63/294	W	Structurally controlled	105	54/298	W	Structurally controlled
76	38/290	Kinematically Stable	-	106		Kinematically Stable	-
77		Kinematically Stable	-	107	63/293	T	Structurally controlled
78	57/308	W	Structurally controlled	108	60/278	P	Structurally controlled
79	60/291	W	Structurally controlled	109	60/285	T	Structurally controlled

Table 3.13 continues

80	50/284	T	Structurally controlled	110	60/276	W	Structurally controlled
81	48/276	W	Structurally controlled	111		Kinematically Stable	-
82	50/261	W	Structurally controlled	112	58/310	W	Structurally controlled
83	45/260	T	Structurally controlled	113	50/286	Kinematically Stable	-
84		Kinematically Stable	-	114		P	Structurally controlled
85	42/270	W	Structurally controlled	115	68/272	W	Structurally controlled
86	65/215	-	-	116		Kinematically Stable	-
87	43/323	T	Structurally controlled	117	44/265	W	Structurally controlled
88	57/291	P	Structurally controlled	118		Kinematically Stable	-
89	58/298	T	Structurally controlled	119	60/266	W	Structurally controlled
90	54/316	W	Structurally controlled				

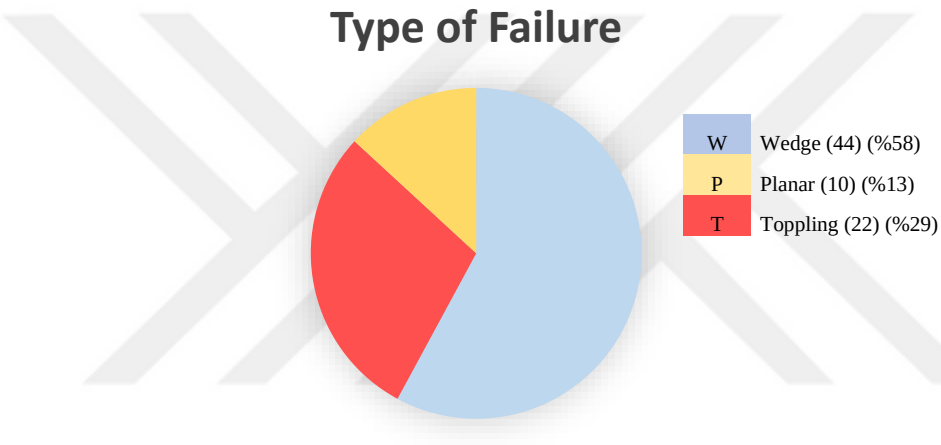

Figure 3.24 Pie chart of kinematic failures at observation points

3.6.1 Planar Failure

Planar failure is a type of failure that occurs when a discontinuity plane whose direction is approximately parallel to the slope surface is shifted in the direction of the slope. In order for this slip failure to occur or to pose a potential hazard, certain geometric conditions must be met. These conditions are according to Hoek & Bray (1981) and Norrich & Wyllie (1996);

1. The angle of inclination of the plane of discontinuity must be smaller than the angle of inclination of the slope, that is, the plane of discontinuity must intersect the slope ($\alpha_{discontinuity} < \alpha_{slope}$).
2. The angle of inclination of the discontinuity plane must be greater than the internal friction of the rock material ($\alpha_{discontinuity} > \phi$).
3. The direction of the slope and the direction of the discontinuity plane must be approximately parallel to each other or approximately ± 20 different from each other.

In the kinematic analyzes made with the discontinuities taken in the eastern part of the study area, a total of 45 planar failure potentials were determined. The mean orientation of these discontinuity planes, which cause planar failure, was determined as 41/285. The field view of these planar slips caused by the joints and their kinematic analysis using the lower hemisphere projection are given in Figure 3.25.

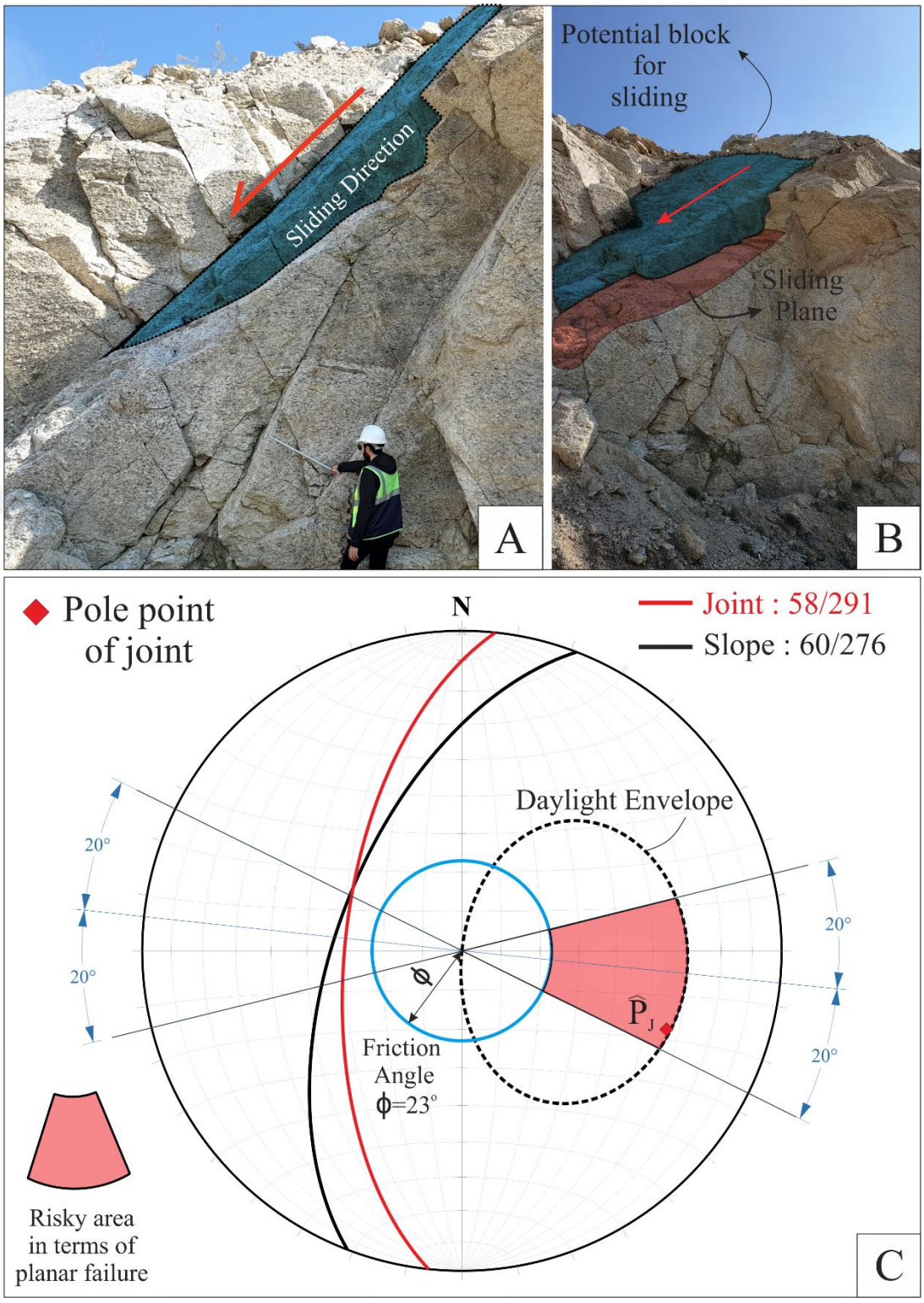

Figure 3.25 Planar sliding failure caused by joints; (a) The view of the sliding in the field and the direction of the sliding, (b) The block and sliding plane that is likely to sliding, (c) Kinematic analysis of the planar failure

3.6.2 Wedge Failure

Wedge failure is characterized as a special type of planar slip. In fact, 39 of the slopes with 72 wedge failure potential also have planar slip potential. This type of slip is a type of failure that occurs when the wedge block slips along the cross-section line formed by two intersecting discontinuity planes on the slope. As with planar shear, certain geometric conditions must be met for this type of failure to pose a potential hazard. These conditions are;

1. The slope angle of the slope must be greater than the dip angle of the line of intersection of the planes forming the wedge ($\alpha_{slope} > \psi_{intersection}$).
2. The plunge angle of the wedge cross-section line must be greater than the average of the internal friction angles of the planes forming the wedge ($\psi_{intersection} > \phi$).

According to the discontinuity measurements taken from the slopes in the eastern part of the mine, 72 wedge failures were determined. The field view and kinematic analysis of an example of 74 wedge-type failures seen in the study area are given in Figure 3.26.

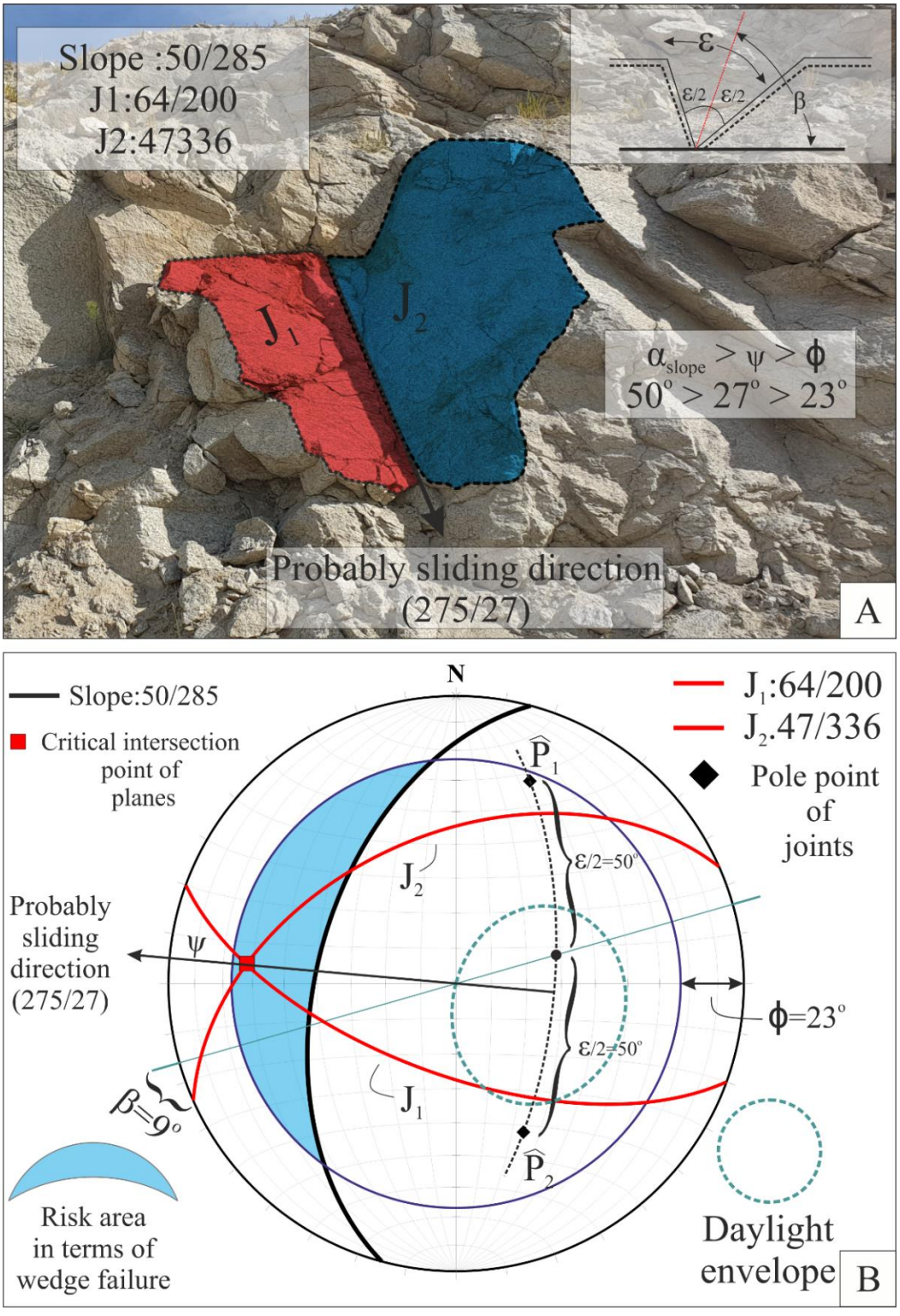

Figure 3.26 Wedge type sliding failure, (a) View of planes forming the wedge in the field, (b) Kinematic analysis of wedge type sliding failure

3.6.3 Toppling Failure

The first step in the analysis of rollover failures is to identify potential rollover conditions (Hoek & Bray, 2004). If the discontinuities are at a high angle and these discontinuity planes are inclined into the slope, this type of failure is called a toppling failure (Goodman & Bray, 1976).

It also proved that the discontinuity angles in the cluster analysis made with the discontinuity measurements taken in the study area are mostly high-angle and the overturn failures with a 45% slice determined by the kinematic analysis technique (a total of 98, 54 flexural and 44 direct toppling) are high. The thematic map showing the types of rollover failures observed in the study area and their distribution in the field is presented in Figure 3.27.

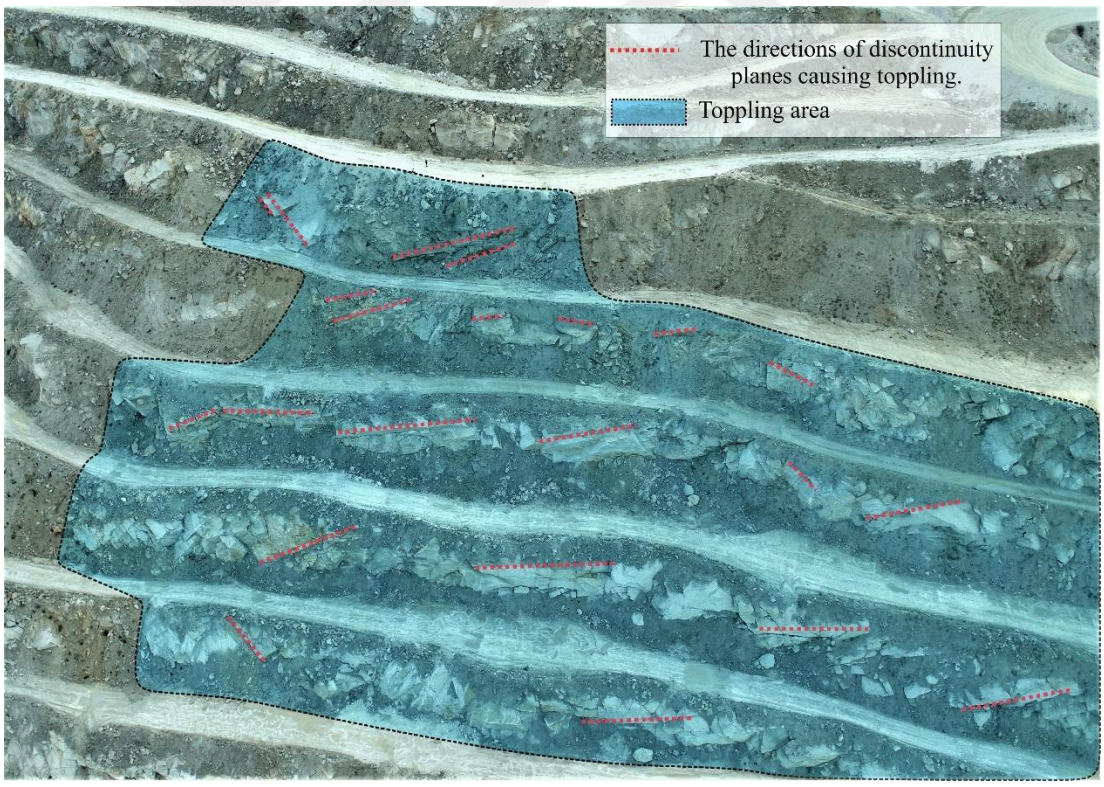

Figure 3.27 Generally the directions of high persistence and high angle discontinuity planes that caused toppling failures

With the measurements taken from the eastern slopes of the mining operation, the slopes with potential overturn failure were determined. The kinematic analyzes and related figures of these slopes are shown in 3.28, 3.29 and 3.30.

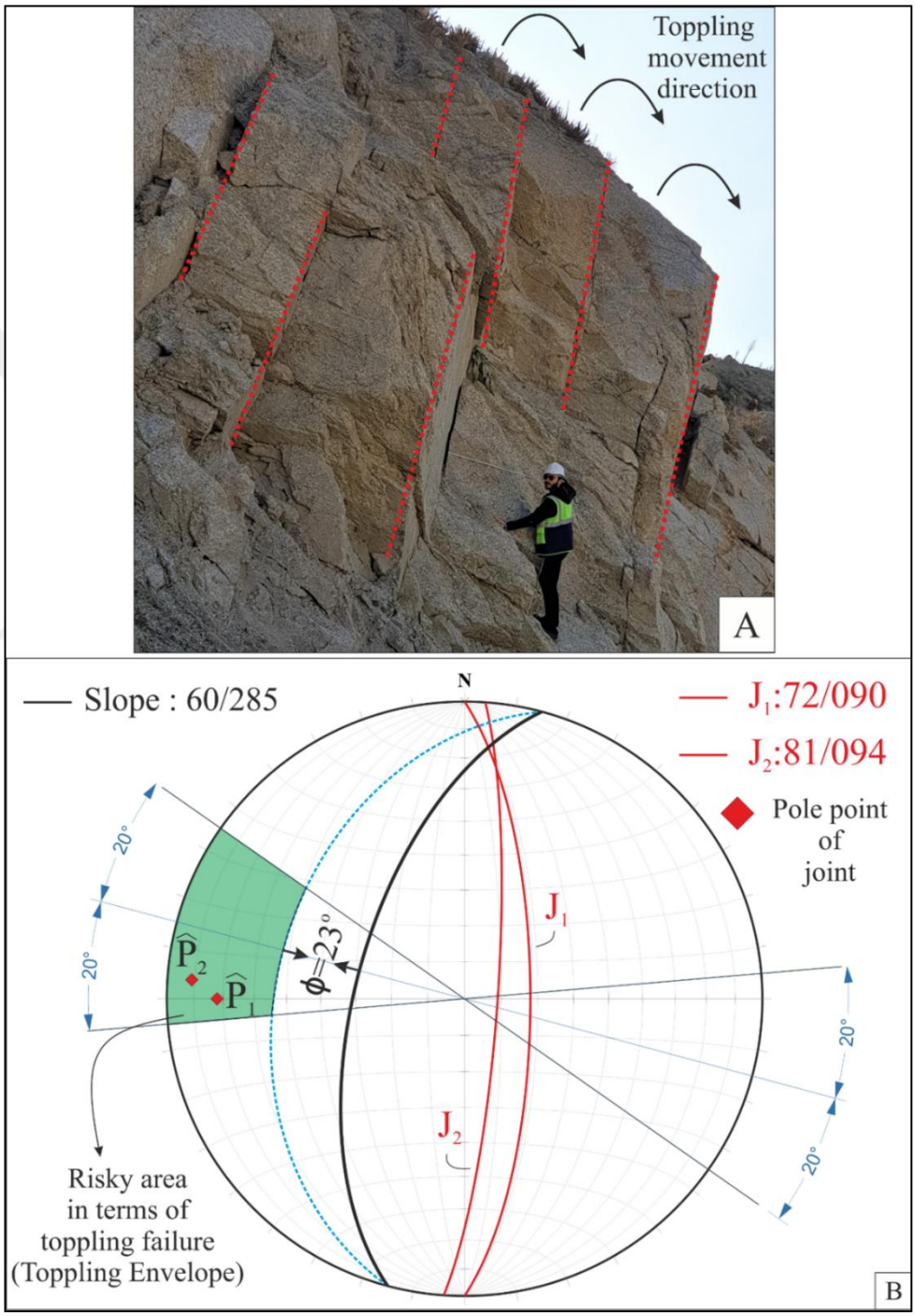

Figure 3.28 Flexural toppling failure; (a) High angle discontinuities and possible toppling blocks in the field view, (b) Kinematic analysis of flexural toppling failure

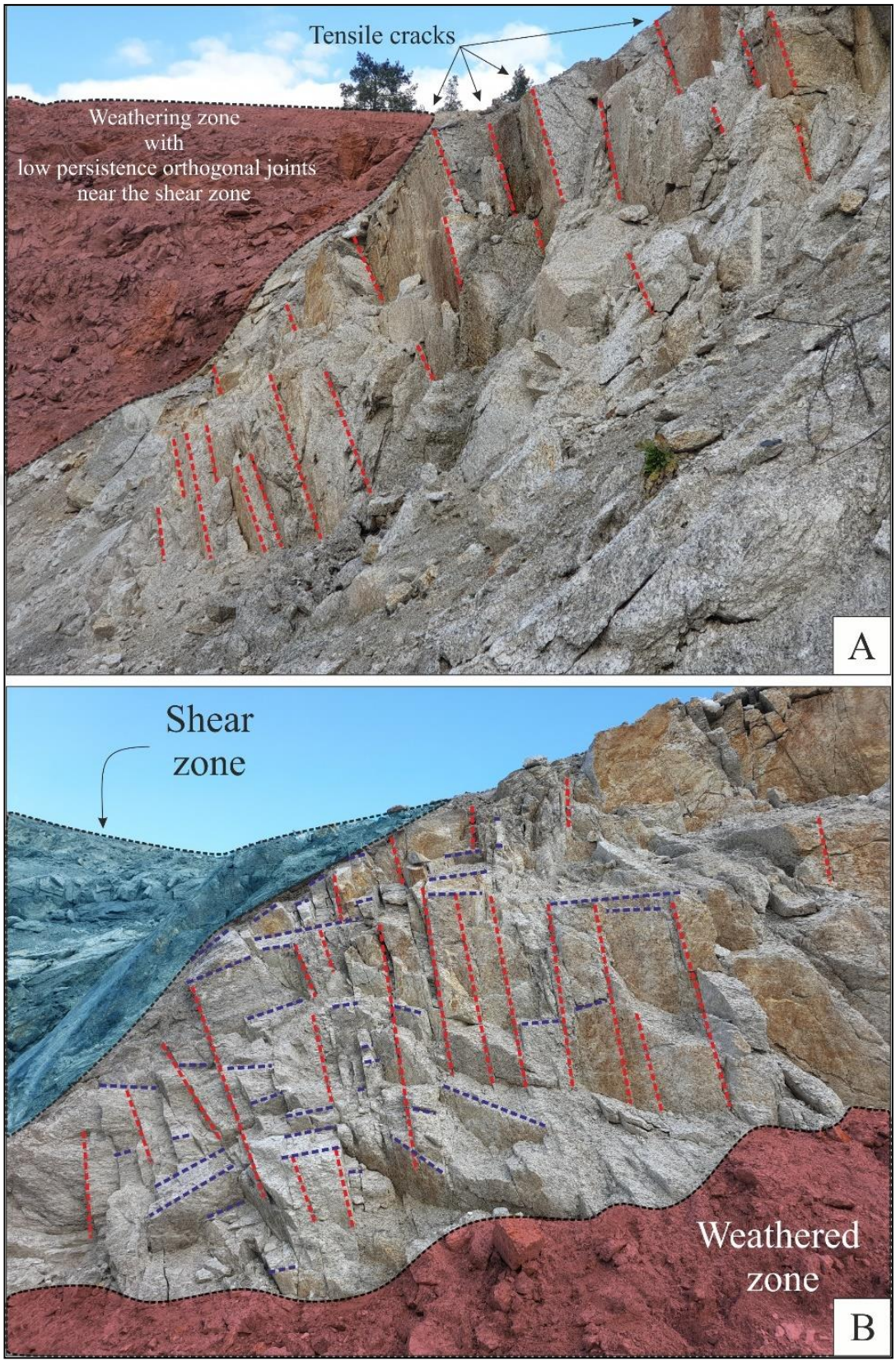

Figure 3.29 Direct toppling field view; (a) High angle discontinuity planes, (b) Sets of discontinuities perpendicular to each other (front view of a)

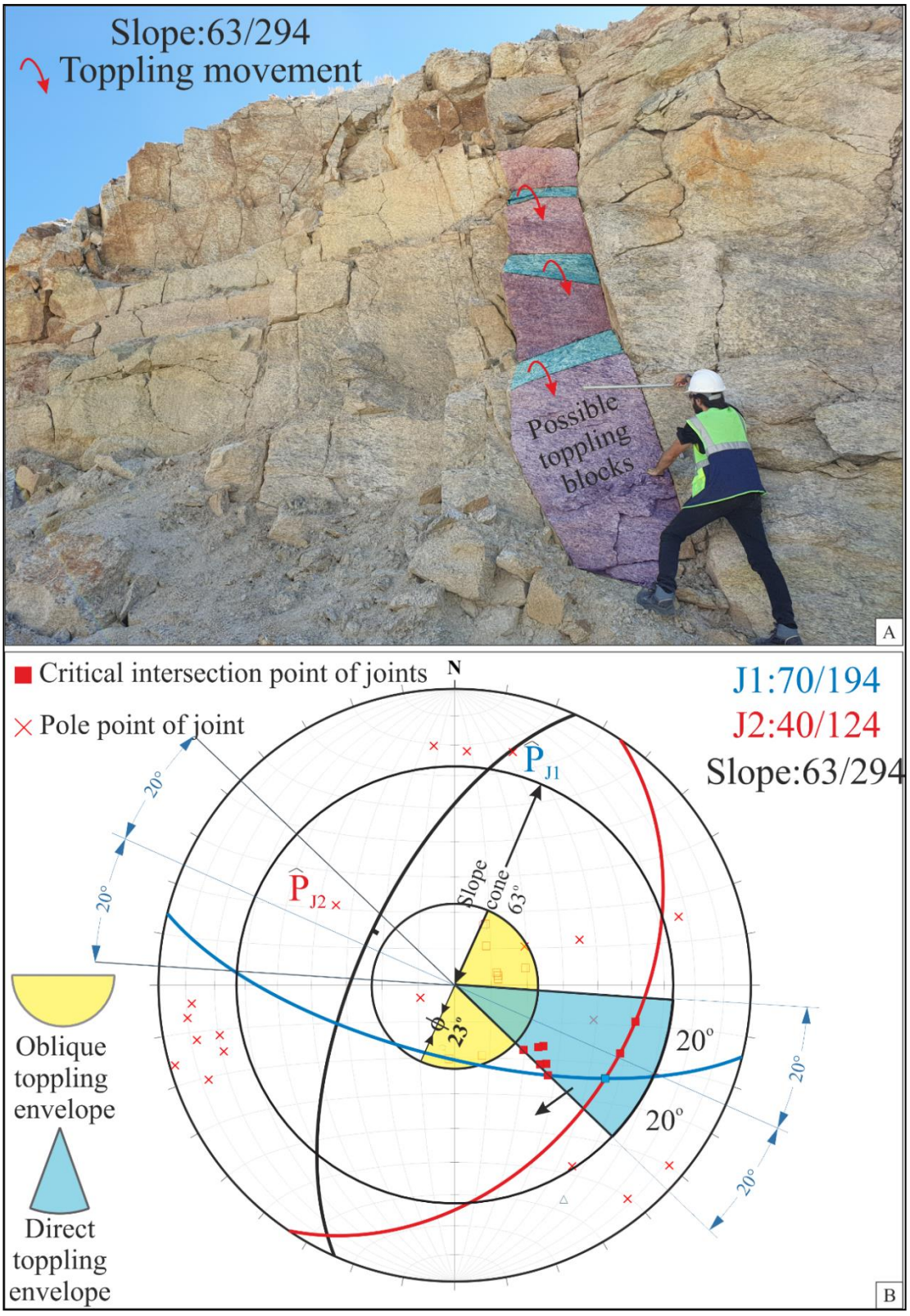

Figure 3.30 Direct toppling type failure; (a) Blocks formed by sets of joints perpendicular to each other, (b) Kinematic analysis of direct (block) toppling type failure

CHAPTER FOUR
ROCK CLASSIFICATION SYSTEMS

4.1 Slope Mass Rating (SMR) System

SMR is a geotechnical classification system developed by Romana (1985) for rock slopes and which obtained from basic RMR. It is calculated by adding a few adjustment factors to the basic RMR system. These adjustment factors are directly related to the relationship between the joints in the rock slope and the slope geometry. However, it also takes into account the excavation or blasting method. The SMR score calculated by subtracting from the RMR system is obtained with the given expression Equation 4.1.

$$SMR=RMR_{basic} + (F1xF2xF3) +F4 \quad (4.1)$$

Where RMR is a system developed by Bieniawski (1973,1989) to evaluate the quality of rock masses in engineering projects. The RMR system is calculated according to the proposal of Bieniawski (1989) and for this who has developed 5 different parameters that represent the discontinuity conditions in the rock mass. These parameters are UCS of intact rock, %RQD, spacing between discontinuities, condition of discontinuities and groundwater, respectively. Detailed scoring of these parameters is given in the table 4.1. 4th parameter of RMR was detailed by Bieniawski (1989) in order to define the discontinuity conditions of rock mass in more detail (table 4.2). The RMR system takes values ranging from 0 to 100 (Bieniawski, 1973) (Table 4.3).

Table 4.1 Rock rating system (Bieniawski, 1989)

Parameter			Range of values						
1	Strength of intact rock material	Is50 (MPa)	> 10	4-10	2-4	1-2	For the low range, σ_c is preferred		
		σ_c (MPa)	> 250	100-250	50-100	25-50	5-25	1-5	<1
	RATING		15	12	7	4	2	1	0
2	%RQD		90-100	75-90	50-75	25-50	<25		
	RATING		20	17	13	8	3		
3	Spacing of discontinuities		> 2m	0.6-2m	20-60cm	20-6cm	<6cm		
	RATING		20	15	10	8	5		
4*	Condition of discontinuities		Very rough surfaces, Not continuous, No separation, Unweathered wall rock	Slightly rough surfaces, Separation <1 mm, Slightly weathered walls	Slightly rough surfaces, Separation <1 mm, Highly weathered walls	Slickensided surfaces, Gouge <5 mm thick, Separation 1-5 mm (Continuous)	Soft gouge >5 mm thick, Separation >5 mm (Continuous)		
	RATING		30	25	20	10	0		
5	Ground water	Inflow per 10 m tunnel length	none	<10 l/min	10-25 l/min	25-125 l/min	> 125 l/min		
		pw / σ_1	0	0-0.1	0.1-0.2	0.2-0.5	> 0.5		
		General conditions	completely dry	damp	wet	dripping	flowing		
	RATING		15	10	7	4	0		

Table 4.2 Guidelines for classifying the conditions of discontinuity in RMR

Discontinuity length (persistence)		Separation (aperture)		Roughness		Infilling (gouge)		Weathering	
Value (m)	Rating	Value (mm)	Rating	Description	Rating	Description	Rating	Description	Rating
<1	6	None	6	Very rough	6	None	6	Unweathered	6
1-3	4	<0.1	5	Rough	5	Hard filling <5mm	4	Slightly weathered	5
3-10	2	0.1-1.0	4	Slightly rough	3	Hard filling >5mm	2	Moderately weathered	3
10-20	1	1-5	1	Smooth	1	Soft filling <5mm	2	Highly weathered	1
>20	0	>5	0	Slickensided	0	Soft filling >5mm	0	Decomposed	0

Table 4.3 Definition classification according on RMR

Rating	Class	Description
100-81	I	Very good rock
80-61	II	Good rock
60-41	III	Fair rock
40-21	IV	Poor rock
<20	V	Very poor rock

Other parameters given in the equation can be explained as follows. F1 is a parameter related to the dip direction of the discontinuity (or the plunge direction of the intersection line of two planes (a_i)) and slope in the rock mass., α_j and α_s respectively (Anbalagan et al. 1992). F2 is explained as a parameter related to the dip of the discontinuity (β_j) (or the angle of plunge of two discontinuities (β_i) in the case of a wedge) that causes failure in the rock slope. This parameter is taken as 1.0 for toppling type failure (Romana 1985). Both F1 and F2 can be calculated from the table as well as approximately calculated in the with an Equation 4.2 and 4.3 developed by Romana (1993) as an alternatively.

$$F1 = (1-\sin \left| A \right|)^2 \tag{4.2}$$

$$F2 = \tan^2 B \tag{4.3}$$

Another parameter, F3 is a parameter depend on the dips relationships between the joints and the slope surface, in fact, which the adjustment factor range between 0 and -60 developed by Bieniawski (Romana, 1993) (Table 4.4). F4, which is the final correction factor, is an adjustment factor depending on the method of excavation or blasting in the rock slope (Romana, 1985) (Table 4.5). In addition to planar and toppling failure modes, wedge type failure was also described by Anbalagan et al. (1992) added and take into account for in the SMR system. In this article, 3 types of failure types namely planar, wedge and toppling were used as developed by Angalabad et al. (1992).

Table 4.4 Adjustment ratings for F1, F2, and F3 (Romana, 1985, modified by (Anbalagan, 1992)

Type of failure			Very favourable	Favourable	Normal	Unfavourable	Very unfavourable
P T W	A=	$\lvert\alpha_j-\alpha_s\rvert$ $\lvert\alpha_j-\alpha_s-180\rvert$ $\lvert\alpha_i-\alpha_s\rvert$	$>30^0$	$30\text{-}20^0$	$20\text{-}10^0$	$10\text{-}5^0$	$<5^0$
P/T/W	F_1		0.15	0.40	0.70	0.85	1.00
P W	B=	β_j β_i	$<20^0$	$20\text{-}30^0$	$30\text{-}35^0$	$35\text{-}45^0$	$>45^0$
P/W	F_2		0.15	0.40	0.70	0.85	1.00
T	F_2		1.00	1.00	1.00	1.00	1.00
P	C=	$\beta_j-\beta_s$	$>10^0$	$10\text{-}0^0$	0^0	$0\text{-}(-10^0)$	$<(-10^0)$
W		$\beta_i-\beta_s$	$<110^0$	$110\text{-}120^0$	$>120^0$	-	-
T		$\beta_j+\beta_s$					
P/T/W	F_3		0	-6	-25	-50	-60

FAILURE: P planar; W wedge; T toppling. DIP DIRECTION: αj discontinuity; αs slope. DIP: βj discontinuity; βs: slope

Table 4.5 Adjustment factor F4 for the method of excavation (Romana, 1985)

Excavation method (F4)			
Presplitting	+10	Blasting or mechanical	0
Smooth blasting	+8	Natural slope	+15
Natural slope	+15		

Different classes for rock slopes from very bad to very good according to the SMR score were defined by Romana (1985). After SMR scoring, definitions such as slope stability condition, failure type and failure probability can be made. It was developed to guide the front end of planning for rock slope (Table 4.6). Also prepared the improvement guide by Romana (2003) according to the classed described (Figure 4.1).

Table 4.6 Description of SMR classes (Romana, 1985)

Class	SMR	Description	Stability	Failures	Failure probability
I	81-100	Very good	Completely unstable	None	0
II	61-80	Good	Unstable	Some blocks	0.2
III	41-60	Normal	Partially stable	Some joints or many wedges	0.4
IV	21-40	Bad	Stable	Planar or big wedges	0.6
V	0-20	Very bad	Completely stable	Big planar or soil-like	0.9

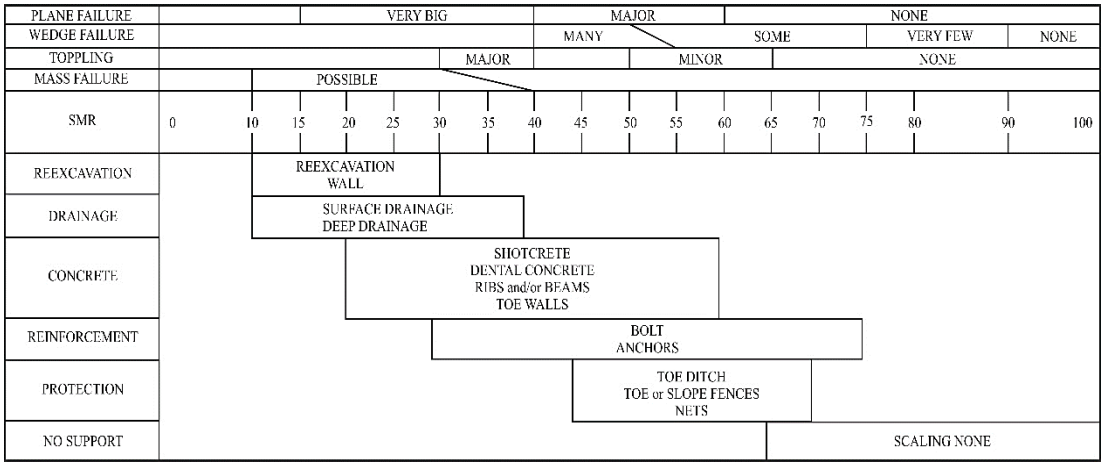

Figure 4.1 Slope support guidelines based on SMR (Romana, 1985)

4.2 Application of SMR

In order to make SMR classification, it is necessary to know the failure mechanism in the rock slope. The discontinuities taken from the 119 slopes in the eastern part of the open pit were transferred to the Dips V.7.016 (2019) software and the potential failure mechanism at each observation location was determined.

Type of failure kinematically failures were detected in 76 of 119 rock slopes at the observation points. It was not included in the SMR system due to the loss of rock feature because of its high weathering in other slopes or kinematically failure was not observed. After determining the failure mechanisms, RMR rock mass classification was made on all slopes. The first 5 parameters used as input parameters in RMR classification were obtained from scanline measurements. Again, as mentioned in the previous sections, the UCS value was obtained by the Schmidt hammer experiment and the RQD value was obtained according to Priest & Hudson (1976) suggestion. In order to calculate the RQD value within the scope of this study, vertical or near-vertical measurements were taken from the discontinuities. RQD values were obtained by using the equation suggested by Priest & Hudson (1976) from the scanline measurements taken. The RQD values obtained according to the scan-line measurements made on some slopes are presented in the table 4.7.

Table 4.7 RQD values of some slopes used in the RMR scoring system

Location		DS (Discontinuity spacing)		1/λ (m^{-1})		FORMULA ($RQD\%=100e^{-0.1\lambda}(0.1\lambda+1)$)					RQD
8	DS=	0.15	λ=	6.67		RQD=	100	0.51	6.67	1.67	85.57
14	DS=	0.20	λ=	5		RQD=	100	0.61	5.00	1.50	90.98
18	DS=	0.08	λ=	12.5		RQD=	100	0.29	12.50	2.25	64.46
29	DS=	0.14	λ=	7.14		RQD=	100	0.49	714	1.71	83.92
32	DS=	0.12	λ=	8.33		RQD=	100	0.43	8,.33	1.83	79.68
34	DS=	0.08	λ=	12.5		RQD=	100	0.29	12.50	2.25	64.46
39	DS=	0.08	λ=	12.5		RQD=	100	0.29	12.50	2.25	64.46
48	DS=	0.10	λ=	10		RQD=	100	0.37	10.00	2.00	73.58
52	DS=	0.09	λ=	11.1		RQD=	100	0.33	11.11	2.11	69.50
55	DS=	0.10	λ=	10		RQD=	100	0.37	10.00	2.00	73.58
57	DS=	0.17	λ=	5.88		RQD=	100	0.56	5.88	1.59	88.20
61	DS=	0.20	λ=	5		RQD=	100	0.61	5.00	1.50	90.98
68	DS=	0.14	λ=	7.14		RQD=	100	0.49	7.14	1.71	83.92
74	DS=	0.15	λ=	6.67		RQD=	100	0.51	6.67	1.67	85.57
75	DS=	0.06	λ=	16.7		RQD=	100	0.19	16.67	2.67	50.37
79	DS=	0.13	λ=	7.69		RQD=	100	0.46	7.69	1.77	81.98
81	DS=	0.10	λ=	10		RQD=	100	0.37	10.00	2.00	73.58
88	DS=	0.22	λ=	4.63		RQD=	100	0.63	4.63	1.46	92.08
93	DS=	0.11	λ=	9.17		RQD=	100	0.40	9.17	1.92	76.61
98	DS=	0.21	λ=	4.76		RQD=	100	0.62	4.76	1.48	91.69
105	DS=	0.05	λ=	20		RQD=	100	0.14	20.00	3.00	40.60
108	DS=	0.11	λ=	8.93		RQD=	100	0.41	8.93	1.89	77.51
114	DS=	0.05	λ=	20		RQD=	100	0.14	20.00	3.00	40.60
119	DS=	0.05	λ=	20		RQD=	100	0.14	20.00	3.00	40.60

As a result of the calculations, the RQD class empirically calculated in the study area according to ISRM standards was determined as “Good” according to the Deere (1964) classification (Table 4.8).

Table 4.8 RQD classification according to Deere (1964)

RQD (%)	Rock Mass Quality
0-25	Very poor
25-50	Poor
50-75	Fair
75-90	Good
90-100	Excellent

The RMR inputs and their scores of some slopes are presented in the table 4.9 to serve as an example, but the RMR scoring was also applied at 76 observation points.

Table 4.9 RMR input parameters and RMR score for some slopes

Slope	UCS Rating	RQD% Rating	Spacing Rating	Discontinuities condition Rating						GW Rating	RMR Rating
				P	A	R	I	W	Total		
8	3	17	6	4	1	5	6	3	19	15	60
14	4	18	7	2	6	3	6	5	22	15	66
18	4	12	6	4	4	5	6	5	24	15	61
29	5	16	6	4	0	5	6	5	20	15	62
32	3	15	6	2	0	5	2	3	12	15	51
34	3	12	5	2	0	2	0	3	7	15	42
39	4	13	5	2	0	5	6	5	18	15	55
48	4	15	6	2	0	5	6	3	16	15	56
52	3	14	5	2	0	5	6	3	16	15	53
55	2	14	6	4	0	5	6	3	18	15	55
57	4	17	7	4	0	5	6	3	18	15	61
61	5	18	7	4	5	5	6	5	25	15	70
68	6	17	7	6	6	5	6	5	28	15	73
74	5	17	6	2	0	5	6	3	16	15	59
75	4	10	6	2	0	5	6	3	16	15	51
79	5	16	6	4	0	5	6	3	18	15	60
81	3	15	6	4	0	5	6	3	18	15	57
88	3	18	7	4	1	5	6	5	21	15	64
93	3	15	6	4	0	5	6	3	18	15	57
98	5	18	7	2	0	5	6	5	18	15	63
105	4	9	5	2	0	5	6	3	16	15	49
108	4	15	6	2	0	5	6	5	18	15	58
114	6	9	5	4	0	3	6	3	16	15	51
119	4	5	8	4	0	5	6	1	16	15	48

P: Persistence, A: Aperture, R: Roughness, I: Infilling, W: Weathering

After the types of failure kinematically and RMR scores of 76 observation points were calculated, the input parameters required for SMR calculation were also collected from the field. In this process, joint and / or joint set and slope dip angle / dip direction measurements were taken for each slope. In other words, each slope has been evaluated separately, independently from each other. SMR scoring, failure mechanisms and class of the mentioned slopes are presented in the table 4.10.

Table 4.10 SMR scoring and adjustment factors for slopes

L	F.Type	RMR	F1	F2	F3	F4	SMR	Class	L	F.Type	RMR	F1	F2	F3	F4	SMR	Class
6	T	70	0.96	1	-25	8	54	III	63	W	63	0.19	0.7	-60	8	63.02	II
8	W	60	0.524	0.7	-60	8	46	III	68	W	73	0.85	0.85	-50	8	44.88	III
10	T	52	0.4	1	-25	8	50	III	70	W	50	0.23	0.4	-50	8	53.4	III
11	P	66	0.96	0.85	-50	8	33.2	IV	71	T	55	0.7	1	0	8	63	II
13	T	64	0.65	1	-25	8	55.8	III	73	W	55	0.15	0.4	-60	8	59.4	III
14	P	66	0.43	1.07	-50	8	51	III	74	W	59	0.83	0.7	-60	8	32.14	IV
18	W	61	0.127	0.21	-60	8	67.4	II	75	W	51	0.4	0.7	-60	8	42.2	III
20	W	66	0.771	0.39	-60	8	56	III	78	W	69	0.86	1	-50	8	34	IV
21	T	68	0.931	1	-6	8	70.4	II	79	W	60	0.809	0.4	-60	8	48.58	III
25	P	67	0.54	0.704	-60	8	52.2	III	80	T	63	0.85	1	-25	8	49.75	III
28	W	62	0.371	0.421	-60	8	60.6	III	81	W	57	0.7	0.85	-50	8	35.25	IV
29	W	62	0.85	0.61	-60	8	38.9	IV	82	W	59	0.85	0.85	-60	8	23.65	IV
30	W	60	0.771	0.259	-60	8	56	III	83	T	57	0.86	1	-25	8	43.5	III
31	W	58	0.158	0.23	-60	8	63.8	II	85	W	51	0.7	0.85	-50	8	29.25	IV
32	W	51	0.235	0.7	-60	8	49.1	III	87	T	57	0.93	1	-25	8	41.75	III
33	W	56	0.15	0.4	-60	8	60.4	III	88	P	64	0.93	1	-50	8	25.5	IV
34	P	42	0.28	1	-50	8	36	IV	89	T	52	0.28	1	-25	8	53	III
36	W	54	0.265	0.75	-60	8	50.1	III	90	W	50	0.72	0.45	-60	8	38.56	IV
37	W	60	0.7	0.4	-60	8	51.2	III	91	P	53	0.7	0.7	-50	8	36.5	IV
39	T	55	0.65	1	-6	8	59.1	III	92	W	62	0.68	0.45	-60	8	51.64	III
41	T	43	0.5	1	-25	8	38.5	IV	93	P	57	0.7	0.85	-60	8	29.3	IV
43	T	56	0.627	1	-25	8	48.3	III	94	W	51	0.7	0.85	-60	8	23.3	IV
44	W	62	0.101	1	-50	8	65	II	95	W	66	0.85	0.85	-50	8	37.88	IV
46	T	55	0.477	1	-25	8	51.1	III	96	T	48	0.7	1	-25	8	38.5	IV
48	W	56	0.109	0.39	-50	8	61.9	II	97	W	54	0.16	1	-60	8	52.4	III
49	P	56	0.19	0.85	-50	8	55.9	III	98	W	63	0.9	0.86	-60	8	24.56	IV
50	T	60	0.281	1	-6	8	66.3	II	99	T	63	1	1	-25	8	46	III
51	W	53	0.15	0.7	-60	8	54.7	III	103	W	52	0.47	0.56	-50	8	46.84	III
52	W	53	0.15	0.655	-60	8	55.1	III	105	W	49	0.23	0.85	-60	8	45.27	III
53	W	61	0.71	0.31	-60	8	55.8	III	107	T	48	0.43	1	-25	8	45.25	III
55	T	55	0.801	1	-25	8	4	III	108	P	58	0.7	1	-60	8	24	IV
56	W	65	0.74	0.2	-60	8	64.1	II	109	T	61	0.7	1	-25	8	51.5	III
57	W	61	0.13	0.198	-60	8	67.5	II	110	W	57	0.7	0.85	-60	8	29.3	IV
58	T	52	0.35	1	-6	8	57.9	III	112	W	50	0.1	0.4	-60	8	55.6	III
59	W	57	0.93	0,56	-50	8	39	IV	114	P	51	0.7	1	-50	8	24	IV
60	T	62	0.86	1	-25	8	48.5	III	115	W	54	0.16	1	-60	8	52.4	III
61	W	70	0.2	1	-50	8	68	II	117	W	51	0.85	0.85	-50	8	22.88	IV

Table 4.10 continues

62	T	70	0.4	1	-25	8	68	II	119	W	48	0.7	1	-60	8	14	V

L: Observation Location of Slopes

In the study area, 4 different classes were identified, including 1 very bad, 22 bad, 41 normal and 12 good. An SMR value that falls within the very good range was not detected on any slope. The very bad rock slope, as you can see from the table, is the slope number 119. Although these studies were carried out in the summer, the algae and rust traces observed in the discontinuity planes at the 119th observation point are an indication that there may be water outflow on the slope during rainy periods. This caused the 119th Observation location to be classified as "very bad" due to the separating effect of water. However, the reason why none of the slopes are included in the “very good” class can be interpreted as the fact that the region is under tectonic regime and again, the groundwater in the region is at very high levels and the weathering effect is highly effective. Kinematically major type of failure mechanism in rock slopes in the study area is wedge type failure with 58% (44 pieces) as mentioned in previous sections. According to the classification system developed by Romana (1985) in the slopes in this study area, III. The rate of those entering the class is 54% (41 pieces) (Figure 4.2).

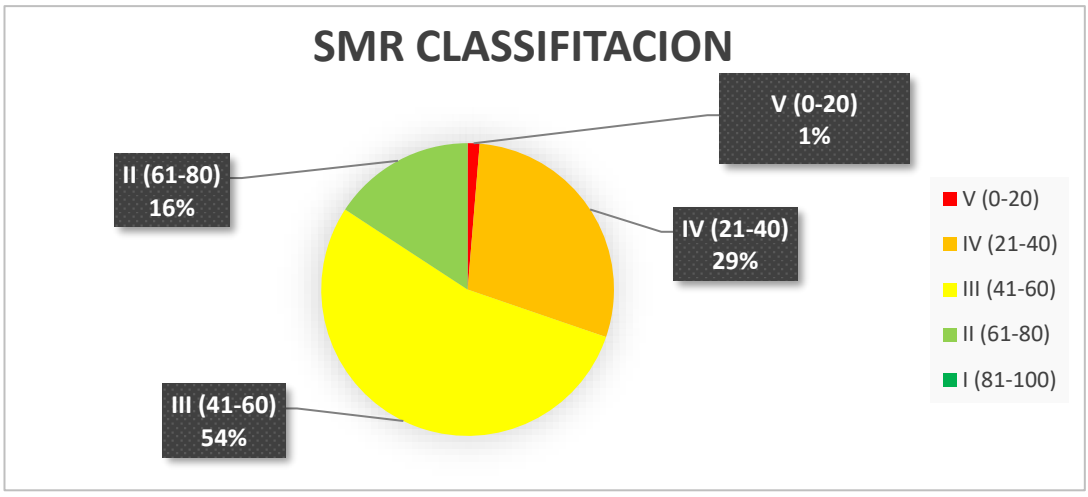

Figure 4.2 Pie chart of SMR classification system on slopes

This ratio also belongs to the class most observed in slopes at observation points. In this classification system, the possible failure modes specified in the table, namely "planar or big wedge", are kinematically compatible with the major failure mechanism in the open pit mine. This harmony can be easily observed on the slope number 32 (Figure 4.3). SMR class in the 32th slope is III and its kinematic failure mechanism is Wedge. As seen in the figure, the failure mechanism determined by Romana (1985) and the failure mechanism determined kinematically of a rock slope of SMR class III are similar. However, it can be observed in the stereographic projection that there may be a few planar failures at the same locations.

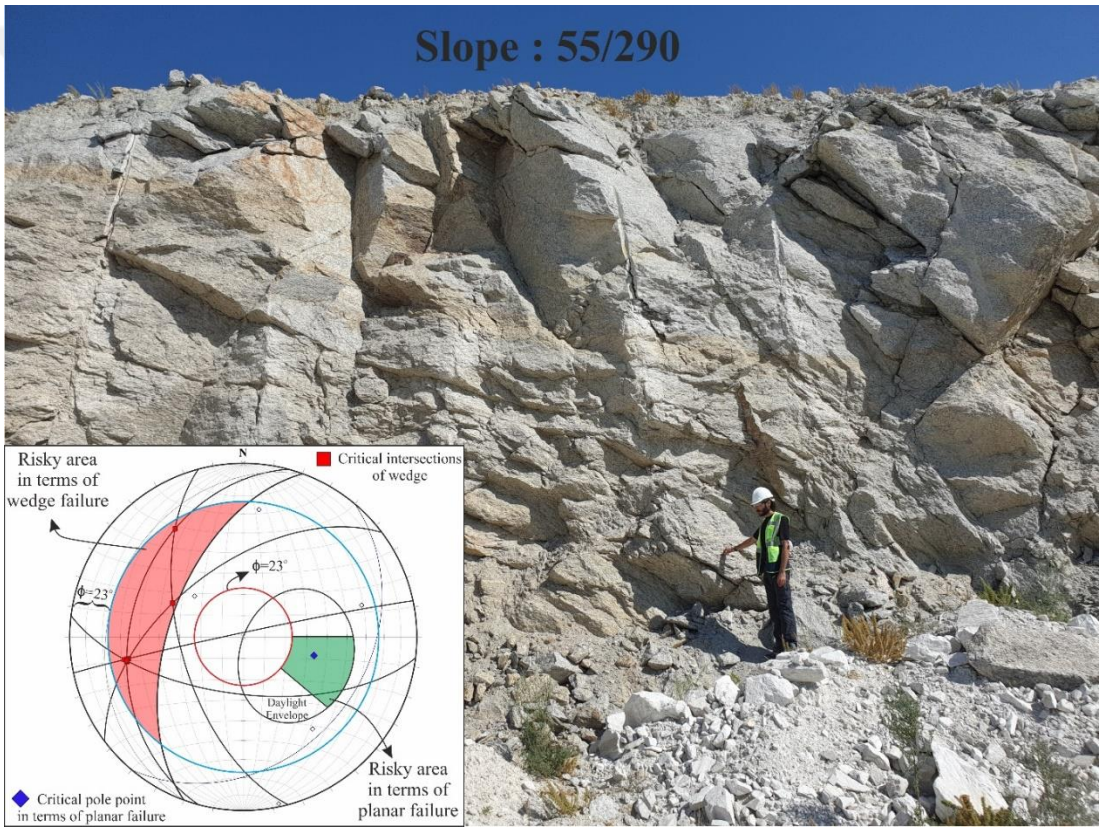

Figure 4.3 View of slope number 32 from the field and its kinematic analysis

RMR scores in the studied rock slopes range between 42 and 73. SMR scores range between 14 and 70.41. In other words, it is seen that the SMR decreases the RMR score in the rock slopes in this study. As an exception, SMR score is higher than RMR score in 18 slopes (Figure 4.4).

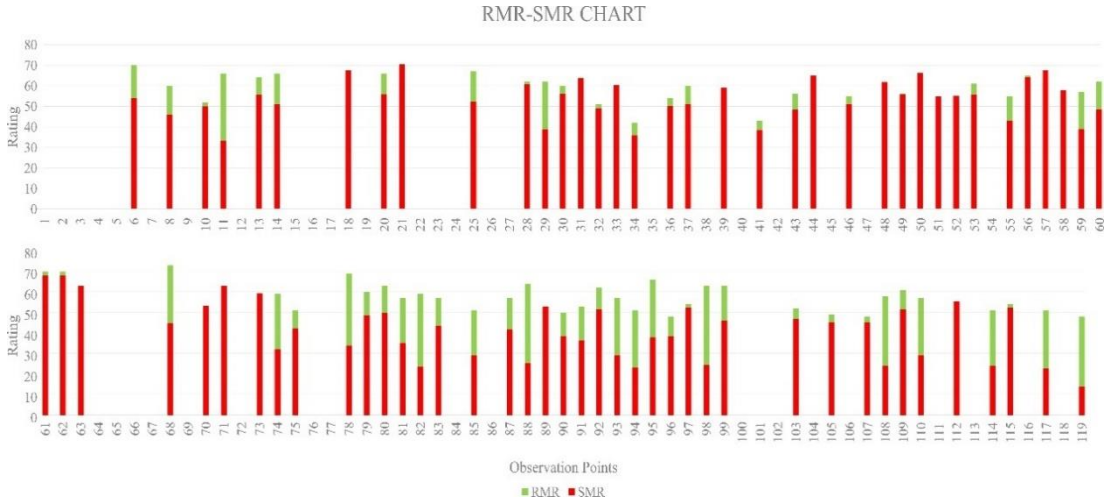

Figure 4.4 SMR-RMR chart

As can be seen from this graph, the slopes numbered 18, 21, 31, 33, 39, 44, 48, 50, 51, 52, 57, 58, 63, 70, 71, 73, 89 and 112 are more than SMR points. This is because it can be said that the relationship between discontinuity and slope angles in the SMR system is more favorable than other rock slopes. This caused the SMR to be higher than RMR. In order to better interpret the SMR and RMR scoring made in the open pit and to evaluate the scores in the individual slope scale, the scoring has been depicted by using the IDW method via ArcMap 10.8 software (Figure 4.5).

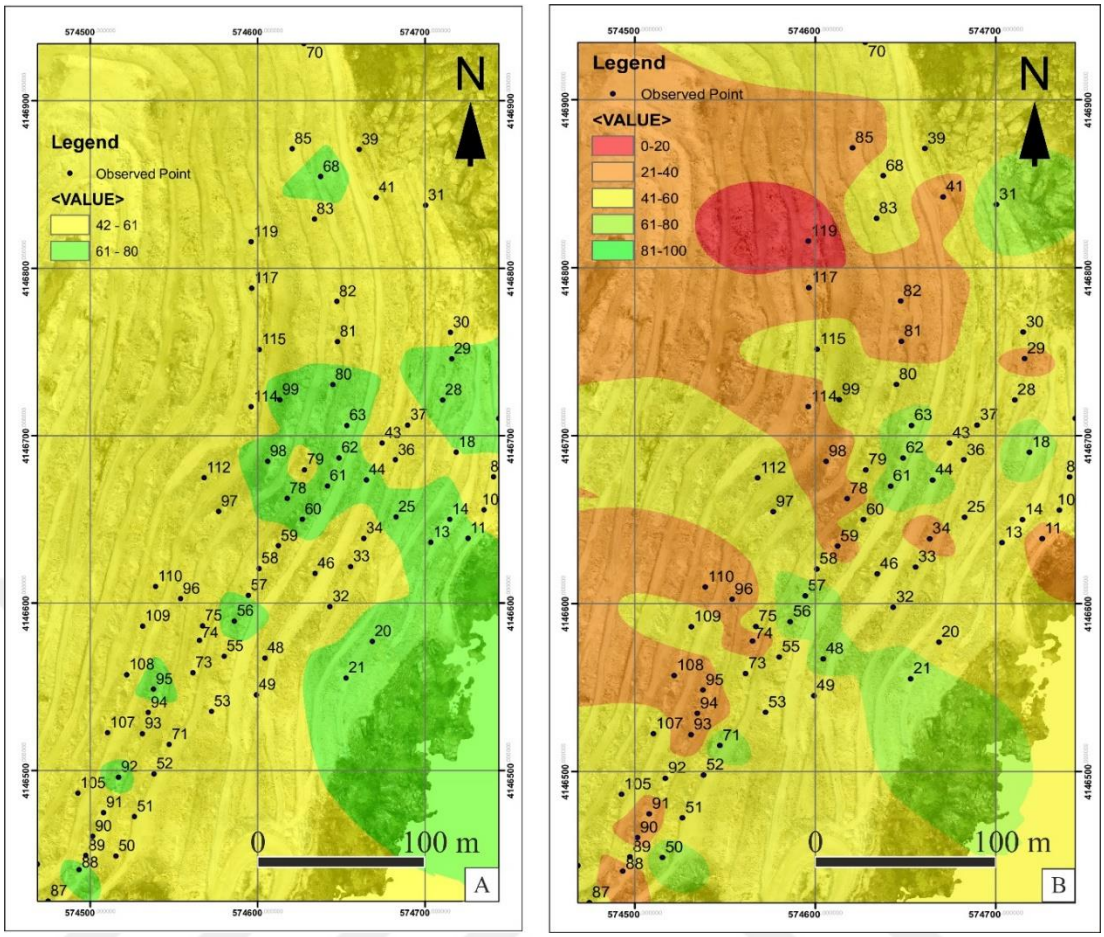

Figure 4.5 Thematic map of the scores in the study area created with the IDW method; (a) RMR map, (b) SMR map

As can be seen in the figures, it is clearly observed that the adjustment factors in SMR scoring decrease the RMR score. According to the RMR scores given in the table, in any of the 76 rock slopes, it was not classified as "very bad rock" and "bad rock". Percentage expression of this for 76 slopes is presented in the pie chart (Figure 4.6). In the classifications made on 76 rock slopes in SMR class, 1 of them were classified as very bad and 22 of them were bad. To be expressed as a percentage, the sum of slopes included in the very bad and bad rock class was determined as 30% in the SMR classification system, while this rate is 0% in the RMR system. Again, in the SMR system, rock slope in the normal class (III) is 54%, while this rate is 64% in the RMR class. The most significant percentage difference belonging to the same rock slopes was determined in the rock class belonging to the "Good" class. While the rate

of slopes in the "good rock (II)" class in SMR system is 16%, this rate is calculated as more than twice in the RMR system, that is, 36%.

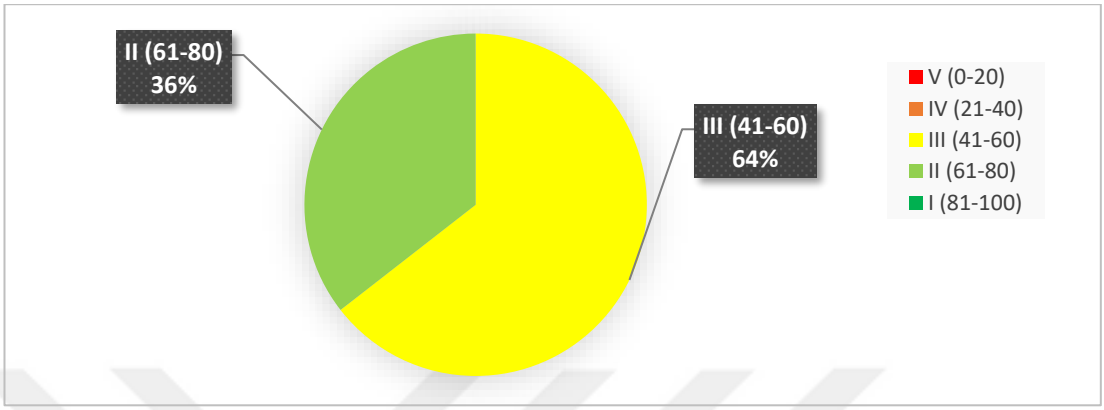

Figure 4.6 Classification of RMR systems as a percentage

However, using Inverse Distance Weighted (IDW) analysis, in the "Linear Interpolation" method, the "Distance Coefficient Power" value was selected as 2 in the "Continous Mode" range. The visualization process of the classification system, which was interpolated with the IDW method, was transferred to the image obtained from the drone with the 3DSurvey program (Figure 4.7).

Thanks to this imaging process, the SMR score of each slope at the observation points was evaluated both on the step scale and throughout the pit. As seen in the figure, the SMR score is in the low range at many observation points of the east slopes.

In addition, it is possible to evaluate the classification system for each slope. Within the scope of this study, some of the points that were observed to be renewed kinematically were closely examined. According to this classification system, adjacent slopes 61 and 59 are considered in this study (Figure 4.8).

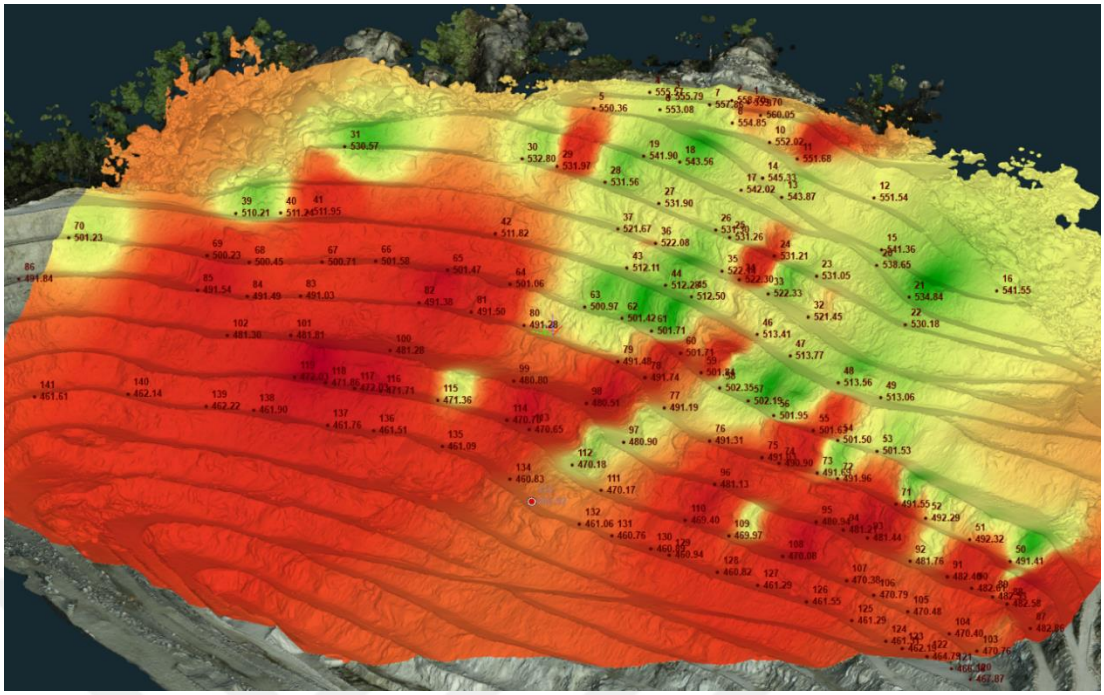

Figure 4.7 3D view of the SMR score on the slopes

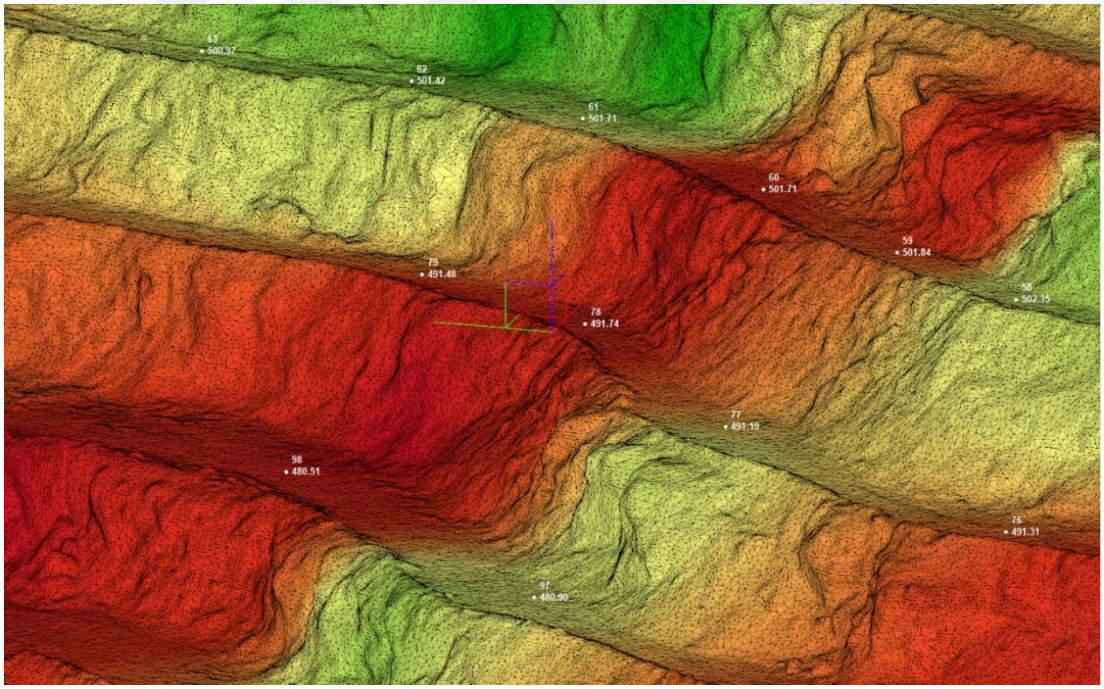

Figure 4.8 3D view of slopes 59 and 61

The features of the above-mentioned slopes such as discontinuity features (discontinuity spacing, orientation and wall strenght), kinematic failure potential, UCS value, %RQD value are given in detail in the subtitles.

4.2.1 Details of slope number 59

4.2.1.1 Attributes of Discontinuities

The photograph of the observation point number 59 taken from the field is given in figure 4.9.

Figure 4.9 Field view of 59. Observation point

As can be seen in the figure, it contains many discontinuity and discontinuity sets. According to the scan-line measurements made at this observation point, the orientation of the discontinuities is given table 4.11.

Table 4.11 Orientations of discontinuity sets at the observation point

Location	J1	J2	J3	J4
59	42/261	44/327	62/154	82/65

The discontinuity spacing of the dominant joint sets at this observation point was determined as 0.15m. According to this data, the discontinuity frequency ($\lambda=m^{-1}$) was found to be 6.67 ($\lambda=m^{-1}$) the %RQD value was 85.57. The schmidt hammer rebound numbers on the rock slope were found to be 16, 26, 18, 44, 22, 18, 20, 16, 36 and 28. Accordingly, the JCS value was determined as 1.46 and the UCS value as 28.77 (MPa). Kinematic failure type obtained from dominant discontinuity joints is given in figure 4.10. In this analysis performed according to the Dips program, wedge-type failure was determined kinematically at this observation point.

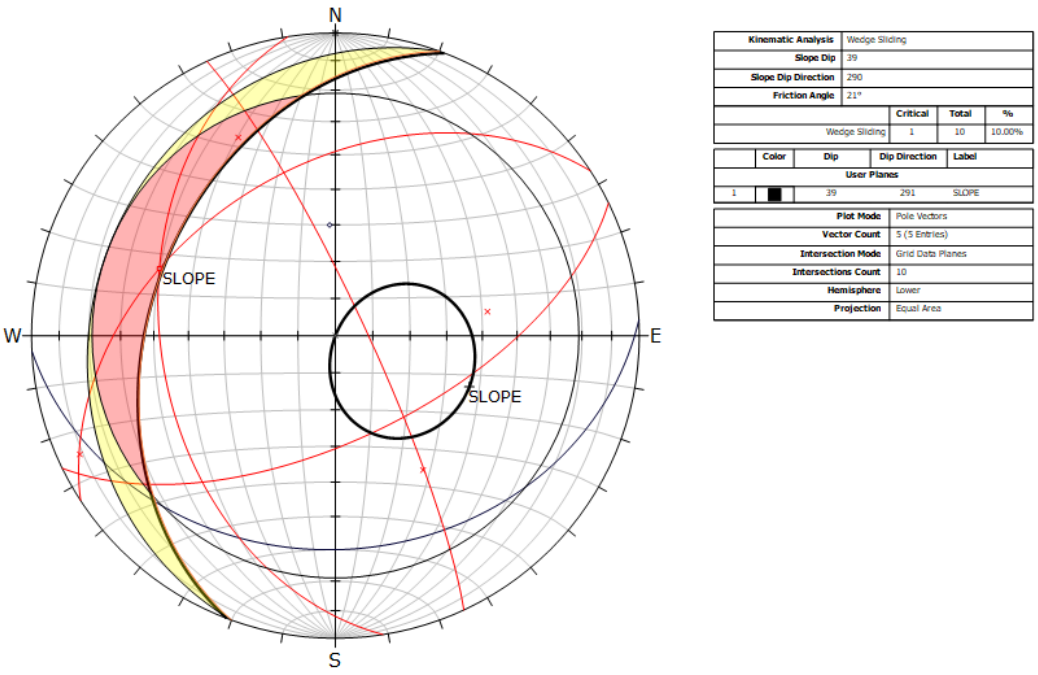

Figure 4.10 Kinematic failure type of 59. observation point

4.2.2 Details of Slope Number 61

4.2.2.1 Attributes of Discontinuities

The photograph of the observation point number 61 taken from the field is given in figure 4.11. As seen in the figure, although there is a discontinuity at the observation

point 61, the slope angle is approximately 75-80 degrees. The orientations of the discontinuities at this observation point are given in Table 4.12.

Figure 4.11 Field view of 61. observation point

Table 4.12 Orientations of discontinuity sets at the observation point

Location	J1	J2	J3	J4	J5	J6	J7
61	46/143	64/320	86/251	65/321	84/157	47/141	17/203

The discontinuity spacing of the dominant joint sets at this observation point was determined as 0.2m. According to this data, the discontinuity frequency ($\lambda=m^{-1}$) was found to be 5 ($\lambda=m^{-1}$) the %RQD value was 90. The schmidt hammer rebound numbers on the rock slope were found to be 30, 31, 36, 33, 22, 23, 26, 30, 32 and 21. Accordingly, the JCS value was determined as 1.53 and the UCS value as 34.1 (MPa). Kinematic failure type obtained from dominant discontinuity joints is given in figure

4.12. In this analysis performed according to the Dips program, wedge-type failure was determined kinematically at this observation point.

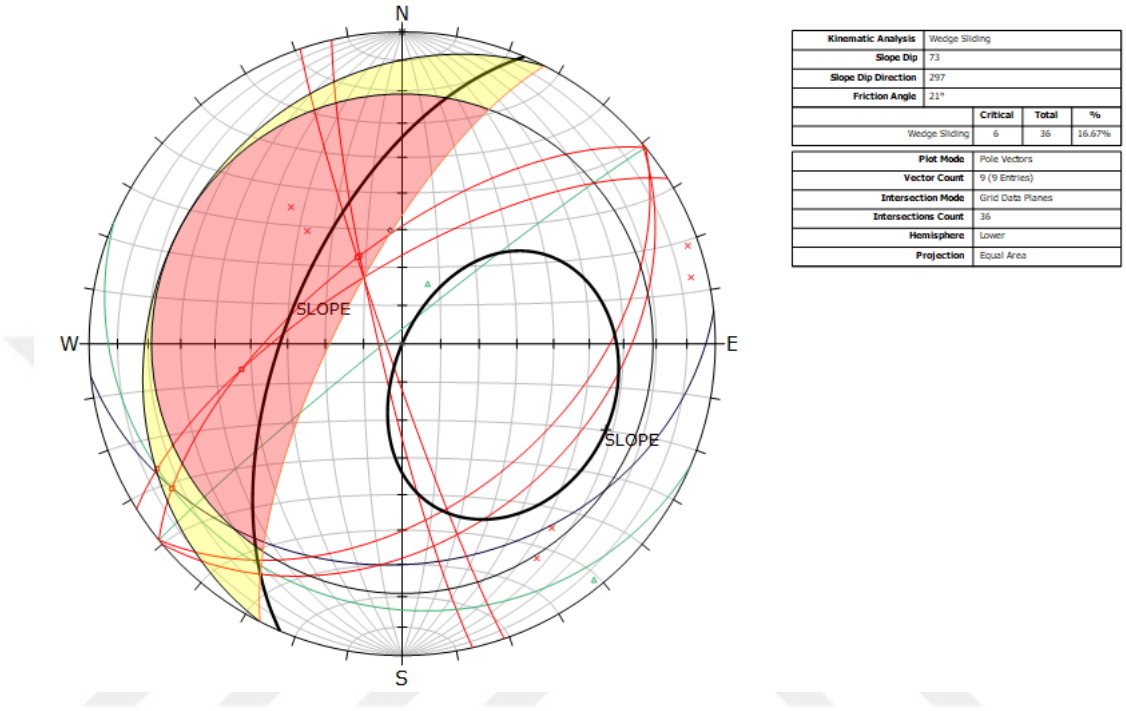

Kinematic Analysis	Wedge Sliding		
Slope Dip	73		
Slope Dip Direction	297		
Friction Angle	21°		
	Critical	Total	%
Wedge Sliding	6	36	16.67%

Plot Mode	Pole Vectors
Vector Count	9 (9 Entries)
Intersection Mode	Grid Data Planes
Intersections Count	36
Hemisphere	Lower
Projection	Equal Area

Figure 4.12 Kinematic failure type of 61. observation point

4.2.3 Comparison of The Slopes

As seen in the above section, the mentioned slopes 59 and 61 are different from each other. In slope number 59, the number of discontinuities is lower, but the discontinuity spacing is lower too. Accordingly, it was observed that the %RQD value was fewer. Again, due to the low JCS value in the 59 numbered slope, the UCS value was also lower than the 61 numbered slope. Considering all of these data and the parameters in the SMR system, the SMR score of the observation point 59 was lower than the observation point 61.

4.3 Strengthening Processes According to The SMR System

In addition to the SMR classification system, some improvement and support systems have also been proposed by Romana (2003). Each of the 76 rock slopes studied on this figure developed by Romana (2003) is shown separately (Figure 4.13).

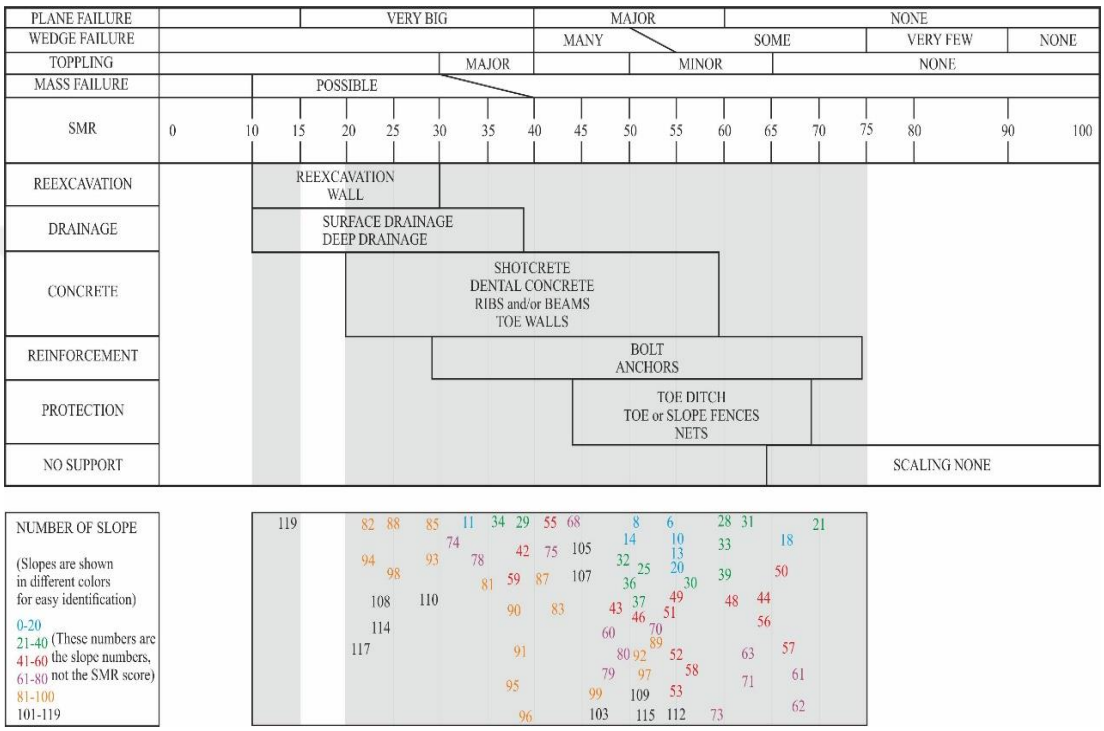

Figure 4.13 Showing the slopes in the study area in the support system

As can be seen from the figure, in the improvement diagram made according to the SMR score, all slopes can suggest one or more improvement or strengthening. As stated before, the rock slopes in 3rd class are in density as can be seen in this diagram (Figure 4.14). The classification table determined according to the classification system is given in appendix-4.

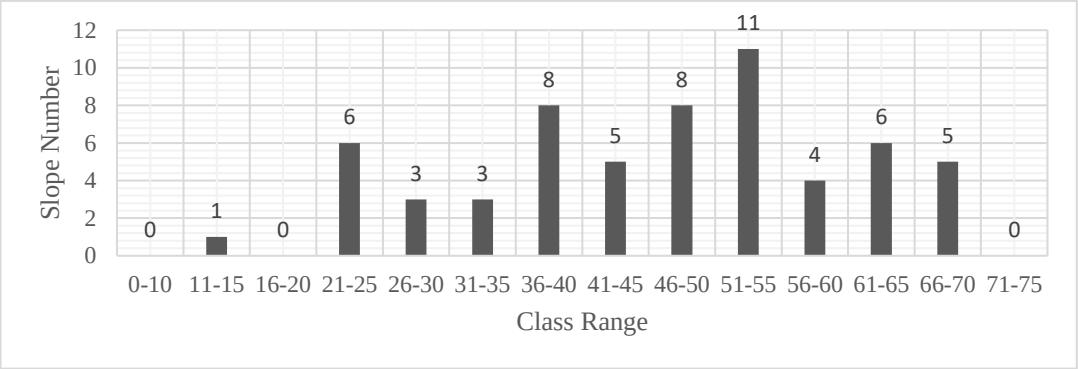

Figure 4.14 Graph of the number of slopes falling in SMR class intervals

For example, slope number 46 has a score of 51.1. According to the improvements suggested by Romana, many different improvements can be made on this slope such as shotcrete, bolt anchors and toe ditch. Another example can be given to slopes 119, 82, 98, 110. Improvement works for these slopes should be different than others. Improvement works such as re-excavation or surface drainage should be done on these slopes. The different comments that can be made for other slopes can be easily examined in the diagram developed by Romana (2003). It should not be forgotten that these reinforcement or support systems are only a guide. Different systems can be developed according to the production activity or the expenses of the contractor company.

4.4 Q-Slope

Qslope is a geotechnical classification system developed by Barton & Bar (2015) for engineering studies such as slope and road cuts that using 6 different parameters, such as RQD, Jn, Jr, Ja, Jw and SRF, as in the Q system. However, unlike the Q-system, several parameters have been updated and they proposed the following Equation 4.4 to estimate the Qslope value (Barton & Bar, 2017).

$$\text{Qslope} = \frac{RQD}{J_n}\left(\frac{J_r}{J_a}\right)_0 \frac{J_{wice}}{SRF_{slope}} \tag{4.4}$$

The first 4 parameters in this equation are as in QSystem (Barton et. al. 1974) and remained unchanged. Namely, rock quality definition, RQD (Deere, 1963) joint set number (Jn), joint roughness number (Jr), and joint alteration number (Ja) (Barton & Bar, 2017). RQD / Jn represents the block size (Table 4.13 and 4.14). Jr / Ja is known as a friction resistance pair and can be applied to joints on either side of the wedge as needed (Table 4.15 and 4.16) (Barton, 2018). However, the adjustment factor for discontinuities in the rock slopes, that called the O-factor (Table 4.17), has been developed by Barton & Bar (2015) and it is not available in the Q system. Another parameter is the Environmental and geological condition number, which is used in this system as J_{wice} (Table 4.18). This is different from Q-system in that the slopes are exposed to external factors (such as climate, wind and freezing) for a very long time and Qslope has also gained a new structure (Barton & Bar, 2015). Due to the slopes are exposed to external factors (such as climate, wind and freezing) for a very long time, they are scored differently than in the Q-system and therefore the Qslope has also gained a new structure (Barton & Bar, 2015). A table is also provided by the developers for Jwice's evaluation. In case of slope reinforcement or drainage measures, adjustment factors are also included and calculations of these adjustments are presented in tables. SRF slope is the stress reduction factor for the slope. SRFa has been developed to determine the physical conditions of the slope surface and can be scored from the given table 4.19. SRFb is similarly used in the Q-index and is a parameter developed for the stress-strength on the slope (Table 4.20). SRFb is a very considerable parameter for highly weathearing, weak and low strength materials in rock slope. However, it becomes more important as the slope and height of the slope increase (Barton & Bar, 2017). SRFc was developed for planes of weakness that adversely affect rock slopes in many aspect (Table 4.21). SRFslope uses the maximum value between SRFa, SRFb and SRFc. Tables are given to estimate SRFa, SRFb, SRFc values, respectively (Barton & Bar, 2015). In other words, Jwice / Srf_{slope} is external factors and stress. The shear resistance, τ, can be approximated using Equation 4.5.

$$\tau = \sigma_n \, tan^{-1}\left(\frac{J_r}{J_a}\right) \tag{4.5}$$

Table 4.13 The RQD factor description (Barton & Bar, 2017)

RQD (%)	Description*	RQD
A	Very poor	0-25
B	Poor	25-50
C	Fair	50-75
D	Good	75-90
E	Excellent	90-100

* A nominal value of 10 is used to evaluate Q-slope

Table 4.14 The Jn factor description (Barton & Bar, 2017)

Joint Set Number	Description	Jn
A	Massive, no or few joints	0.5-1
B	One joint set	2
C	One joint set + random joints	3
D	Two joint sets	4
E	Two joint sets + random joints	6
F	Three joint sets	9
G	Three joint sets + random joints	12
H	Four or more joint sets, random, heavily jointed.	15
J	Crushed rock, earthlike	20

* The description is used for small-scale and intermediate-scale features, 1.0 is added when the joint set mean spacing is greater than 3m.

Table 4.15 The Jr factor description (Barton & Bar, 2017)

Joint Roughness Number	Description	Jr
a) Rock wall contact, b) contact after shearing		
A	Discontinuous joints	4
B	Rough or irregular, undulating	3
C	Smooth, undulating	2
D	Slickensided, undulating	1.5

Table 4.15 Continuies

E	Rough or irregular, planar	1.5
F	Smooth, planar	1
G	Slickensided, planar	0.5
c) No rock-wall contact when sheared		
H	Zone containing clay minerals thick enough to prevent rock-wall contact.	1
J	Sandy, gravely or crushed zone thick enough to prevent rock-wall contact.	1

* The A to G classes for rock-wall contact and contact after shearing, and H-J classes for no rock-wall contact for shearing condition.

Table 4.16 The Ja factor description (Barton & Bar, 2017)

Joint Alteration Number Description	Ja
a) Rock-wall contact (no clay fillings, only coatings)	
Tightly healed, hard non-softening, impermeable filling, i.e. quartz or epidote.	0.75
Unaltered joint walls, surface staining only.	1
Slightly altered joint walls. Non-softening mineral coatings, sandy particles, clay-free disintegrated rock, etc.	2
Silty- or sandy-clay coatings, small clay disintegrated rock, etc.	3
Softening or low friction clay mineral coatings, i.e., kaolinite or mica. Also, chlorite, talc, gypsum, graphite, etc., and small quantities of swelling clays.	4
b) Rock-wall contact after some shearing (thin clay fillings, probable thickness ≈ 1-5mm)	
Sandy particles, clay-free disintegrated rock, etc.	4
Strongly over-consolidated non-softening clay mineral fillings.	6
Medium or low over-consolidation, softening, clay mineral fillings.	8
Swelling-clay fillings, i.e., montmorillonite. Value of Ja depends on per cent of swelling clay-size particles, and access to water.	8-12
c) No rock-wall contact when sheared (thick clay/crushed rock fillings)	
Zones or bands of disintegrated or crushed rock & clay (see G, H, J for descriptions)	6, 8, 8-12
Zones of bands of silty- or sandy-clay, small clay fraction (non-softening).	5
Thick, continuous zones or bands of clay (see G, H, J for descriptions)	10, 13, 13-20

A to E classes for rock-wall contact (no clay infillings, only coatings), F to J classes for rock-wall contact after some shearing (thin clay infillings, probable thickness ≈1-5 mm), M to OPR classes for no rock-wall contact when sheared (thick clay/crushed rock infillings).

Table 4.17 Discontinuity orientation (O-) factor

O-factor Description	Set A	Set B
Very favorably oriented	2	1.5
Quite favorable	1	1
Unfavorable	0.75	0.9
Very unfavorable	0.5	0.8
Causing failure if unsupported	0.25	0.5

Table 4.18 Environmental and geological condition number, Jwice

Jwice*	Desert Environment	Wet Environment	Tropical Storms	Ice Wedging
Stable structure, competent rock:	1	0.7	0.5	0.9
Stable structure, incompetent rock:	0.7	0.6	0.3	0.5
Unstable structure, competent rock:	0.8	0.5	0.1	0.3
Unstable structure, incompetent rock:	0.5	0.3	0.05	0.2

* Note: When drainage measures are installed, apply Jwice x1.5.
When slope reinforcement measures are installed, apply Jwice x1.3.
When drainage and reinforcement are installed, apply both factors Jwice x1.5 x 1.3.

Table 4.19 SRFa: Physical condition

Description	SRFa
Slight loosening due to surface location, disturbance from blasting or excavation.	2.5
Loose blocks, signs of tension cracks and joint shearing, susceptibility to weathering.	5
As above, but strong susceptibility to weathering.	10
Slope in advanced stage of erosion & loosening due to periodic water erosion/ice-wedging effects.	15
Residual slope with significant transport of material down-slope.	20

Table 4.20 SRFb: Stress and strength

Description	σ_c/σ_1*	SRFb
Moderate stress-strength range.	50-200	2.5-1
High stress-strength range.	10-50	5-2.5
Localized intact rock failure.	5-10	10-5
Crushing or plastic yield.	2.5-5	15-10
Plastic flow of strain softened material.	1-2.5	20-15

** Note: σc = unconfined compressive strength (MPa);*
σ_1= *maximum principal stress (MPa).*

Table 4.21 SRFc: Major discontinuity

Description*	SRFc
Major discontinuity with little or no clay, and orientation is:	
favorable	1
unfavorable	2
very unfavorable	4
causing failure if unsupported	8
Major discontinuity with RQD100=0 due to clay and crushed rock, and orientation is:	
favorable	2
unfavorable	4
very unfavorable	8
causing failure if unsupported	16
Major discontinuity with RQD300=0 due to clay and crushed rock, and orientation is:	
favorable	4
unfavorable	8
very unfavorable	12
causing failure if unsupported	24

* Note: RQD100=1m & R QD300=3m perpendicular sample of discontinuity, respectively.

However, thanks to an equation developed by Barton & Bar (2015), the steepest slope slope that can remain stable without reinforcement and improvement can be calculated simply with the help of the following equation 4.6 and can read in the figure 4.15.

$$\beta=20log_{10}Q_{slope}+65^{o} \quad (4.6)$$

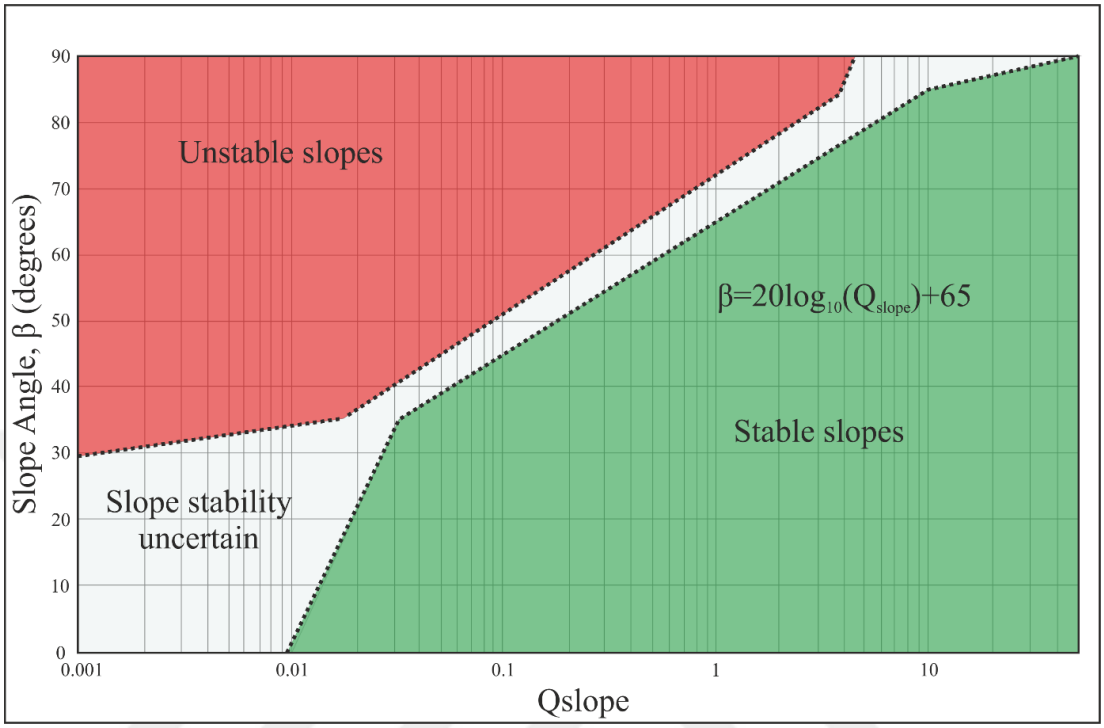

Figure 4.15 Q-slope stability chart

The equation matches the central data for tilt angles between 35 and 85. For different Qslope grades, the angles shown below can be considered fixed (Barton & Bar, 2015).

Q-slope = 10 - slope angle 85°.
Q-slope = 1 - slope angle 65°.
Q-slope = 0.1 - slope angle 45°.
Q-slope = 0.01 - slope angle 25°.

4.5 Application of Q-Slope

Qslope is another classification system used in this article to better examine and evaluate the slope stability. As mentioned in the slope stability assessment section, it is an empirical system developed by Qslope Barton & Bar (2015) in order to evaluate the rock slopes with different parameters and to determine the steepest slope angle that

can remain stable without any reinforcement at the first stage of the project (Barton & Bar, 2017). Within the scope of this study, the slopes at 76 observation points in the open pit mine were scored based on the tables and formulas suggested by Barton & Bar (2017). In the mining operation, all slopes were realized in orthogneiss mass and all of the slopes have a height of less than 30 meters (average heights of the slopes of 10-12 meters). This exemplary embodiment also Barton & Bar (2015) developed by the present duplicate existing literature data of this system and opened in a mine in Turkey gneiss is intended to show how to use properly. RQD value, which is one of the first 6 parameters of the formula developed specifically for this system, is a parameter used in the RMR system, which is necessary for calculating SMR, it was used as calculated in the RMR system shown in the previous section. Another parameter of the formula, Jn (Number of Discontinuous Sets) was determined as a result of scanline measurements. It should be noted here that the measurements taken for each slope are unique and have been considered independently of other slopes. Jr / Ja is evaluated differently for each slope step. Here, it was scored for the most unfavorable joint set as suggested for the O factor developed by Barton & Bar (2015). In wedge-type failures, the secondary joint set that causes failure was given appropriate scores, also developed by Barton & Bar (2015). In order to calculate Jwice, which is another parameter developed differently from the Q system, the amount of precipitation and temperature that the region falls according to months by using the local meteorological resources of the country (Figure 4.16).

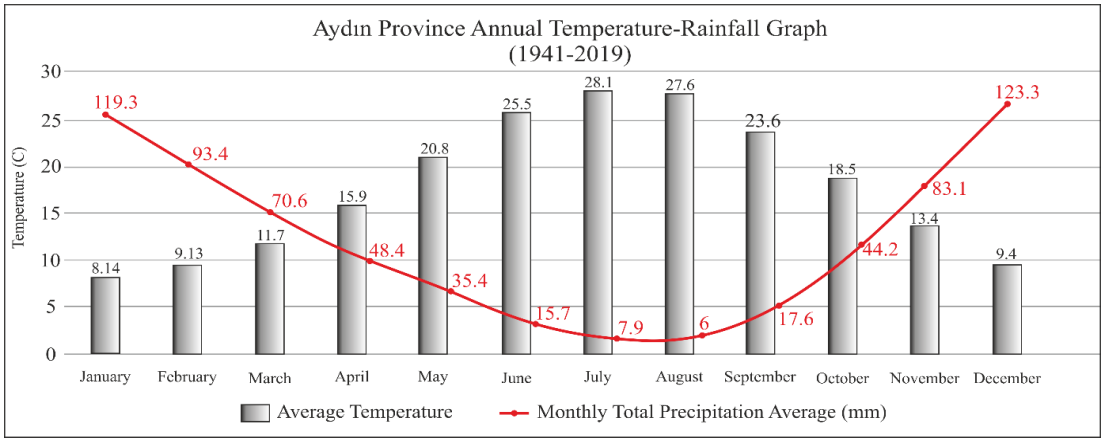

Figure 4.16 Monthly temperature-precipitation graph of the study area (Turkish State Meteorological Service, 2019)

According to these data, the “Wet Environment” class was chosen as one of the classes recommended by Barton & Bar (2015) should be chosen. The reason for this is that, as can be seen from the data, the region receives heavy rainfall, especially in winter, and the average temperature is low during these rainy periods. During the investigations carried out in the summer periods, it was determined that the slope steps were stable (production stopped), but because of the characteristics of the discontinuity planes on the slopes (orientation, roughness, spacing, etc.) it was found to be "incompetent" rock. In other words, for this study, the Jwice value of each slope was determined as 0.6. In addition, when there was no drainage and / or reinforcement system in the proposed graph in any step of the pit slopes, it was not multiplied by any coefficient. Observation points for the SRFa parameter were evaluated separately. As a result of these observations, it was thought that there were large block falls on the slopes due to blasting and there was a rock slope to weathering conditions. Considering these situations, the B Description class suggested in the scoring system for the rock slope is given, namely “Loose blocks, signs of tension cracks and joint shearing, susceptibility to weathering, severe disturbance from blasting”. One of the parameters required to define the SRFb parameter is UCS, and this parameter was determined empirically by using Schmidt hammer in the field. The second parameter is the maximum principal stress. This parameter is calculated by RocLab V.0.1 software by following Generalized Hoek & Brown failure criterion for jointed rock mass (RocScience, 2007). As a result of these operations, σ_c / σ_1 value was calculated and SRFb score was found. The SRFc value, which is the last denominator of the system, was again realized by defining the main discontinuity sets from the observation points. A different SRFc score was found for each slope. According to Barton & Bar (2015), the highest value of SRF a, b, c, values was included in the calculation. At the end of all these processes, after the necessary calculations were made at 76 observation points, the Qslope score of each slope was revealed (Table 4.22).

Table 4.22 Q slope values of slopes at observation locations

Location	RQD/Jn	(Jr/Ja)*(O-fac)	(Jr/Ja)*(O-fac)	Jwice/SRF(a,b,c)	QSlope VALUE	Location	RQD/Jn	(Jr/Ja)*(O-fac)	(Jr/Ja)*(O-fac)	Jwice/SRF(a,b,c)	QSlope VALUE
6	15.5	1.125	1	0.12	2.092	63	5.666	2.25	2.7	0.12	4.131
8	7.083	1.125	1.35	0.12	1.290	68	6.916	0.375	0.45	0.12	0.1400
10	12.166	1.125	1	0.12	1.642	70	4.866	0.25	0.4	0.12	0.0584
11	30	1	1	0.12	3.6	71	3.92	0.562	0.675	0.12	0.178
13	6	0.375	1	0.12	0.27	73	5.066	0.525	0.675	0.12	0.2308
14	15	1.5	1	0.12	2.7	74	5.666	0.281	0.337	0.12	0.0645
18	5.333	0.75	1.2	0.12	0.576	75	3.333	0.562	0.675	0.12	0.151
20	14.166	0.75	1.2	0.06	0.765	78	5.266	0.562	0.675	0.12	0.239
21	10.33	0.1875	0.8	0.12	0.186	79	5.4	1.125	0.675	0.12	0.492
25	7.083	1.5	0.8	0.12	1.02	80	3.866	0.375	1	0.12	0.174
28	5.666	0.375	0.6	0.12	0.153	81	4.866	0.187	0.3	0.12	0.0328
29	5.533	0.375	0.6	0.12	0.149	82	5.127	0.281	0.337	0.12	0.058
30	4.6	0.75	1.2	0.12	0.496	83	4.905	0.375	1	0.12	0.2207
31	6.333	0.562	1.35	0.12	0.577	85	5.791	0.093	0.337	0.12	0.0219
32	5.266	0.562	0.67	0.12	0.239	87	5.594	0.187	1	0.12	0.125
33	5.4	0.375	0.6	0.12	0.145	88	15.346	0.187	1	0.07	0.215
34	5.333	0.187	1	0.12	0.12	89	4.297	0.562	1	0.12	0.290
36	4.266	0.562	0.67	0.12	0.194	90	4.905	0.375	0.6	0.12	0.132
37	6.583	0.375	0.6	0.12	0.177	91	5.127	0.125	1	0.12	0.076
39	4.266	0.375	0.8	0.12	0.153	92	5.704	1.125	1.35	0.12	1.039
41	2.666	0.375	0.8	0.12	0.096	93	4.952	0.562	1	0.12	0.334
43	6.333	0.375	1	0.12	0.285	94	3.471	0.375	0.75	0.12	0.117
44	7.083	1.125	1.35	0.12	1.290	95	5.879	0.187	0.6	0.12	0.079
46	5.4	0.375	1	0.12	0.243	96	2.706	0.375	1	0.12	0.121
48	6.083	0.375	0.6	0.12	0.164	97	5.790	0.56	0.675	0.12	0.263
49	10.666	0.125	1	0.12	0.16	98	6.066	0.375	0.6	0.12	0.163
50	6.583	0.562	1	0.12	0.444	99	6	0.75	1	0.12	0.54
51	4.166	0.562	0.67	0.12	0.189	103	4.266	0.187	1	0.12	0.096
52	4.6	1.125	0.75	0.12	0.465	105	2.666	0.75	1.2	0.12	0.288
53	7.083	0.375	0.6	0.12	0.191	107	4	0.375	1	0.12	0.18
55	4.866	0.187	1	0.12	0.109	108	5.133	0.375	1	0.12	0.231
56	6.133	0.75	1.2	0.12	0.662	109	5.4	0.375	1	0.12	0.243
57	7.333	1.125	1.35	0.12	1.336	110	5.266	0.375	0.6	0.12	0.142
58	8.777	0.562	1	0.12	0.592	112	5.666	0.375	0.6	0.12	0.153
59	7.083	0.562	0.67	0.12	0.322	114	6.666	0.375	1	0.12	0.3
60	6	0.75	1	0.12	0.54	115	4.662	0.375	0.6	0.12	0.125
61	6	2.25	2.7	0.12	4.374	117	3.114	0.187	0.3	0.12	0.021
62	6.133	1.125	1	0.12	0.828	119	2.66	0.375	0.6	0.12	0.072

After the Qslope scores were calculated, they were placed in the semi-logarithmic table proposed by Barton & Bar (2015) (Figure 4.17). All rock slopes are indicated by yellow circles outside black.

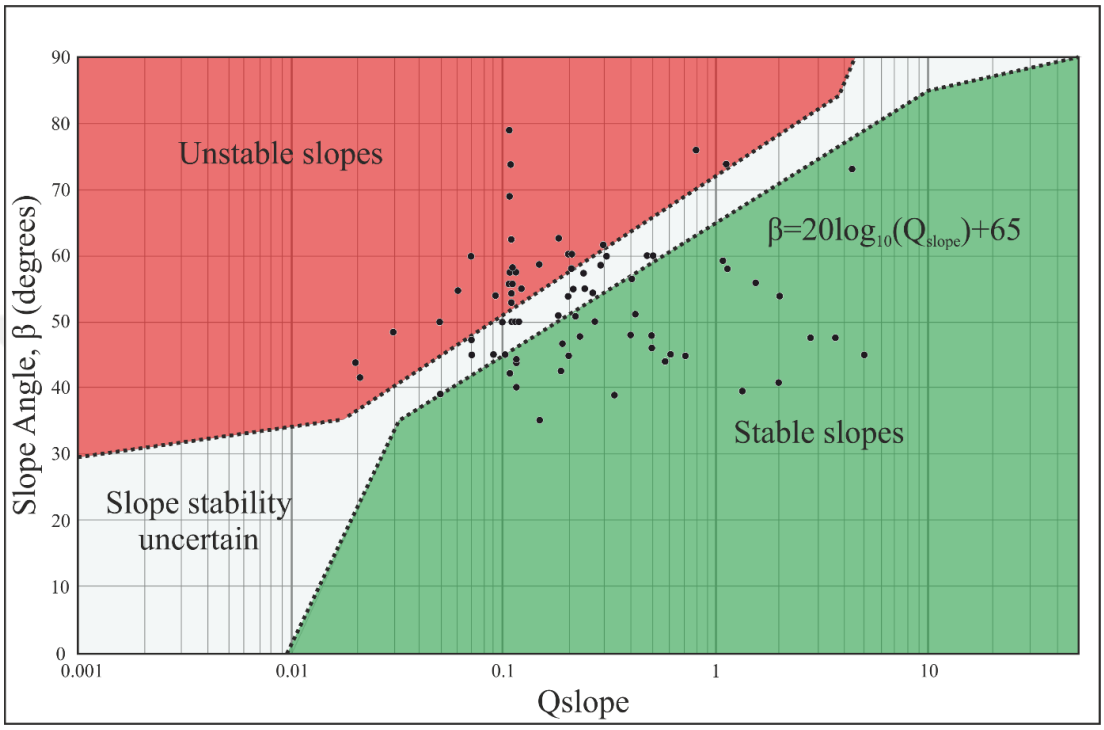

Figure 4.17 Classification of slopes in Qslope

According to this classification system 31 stable, 27 unstable and 18 uncertain classes were determined as a result of the analyzes performed on a total of 76 slopes. The proportional values of these classes were determined as 41%, 35% and 24%, respectively (Figure 4.18).

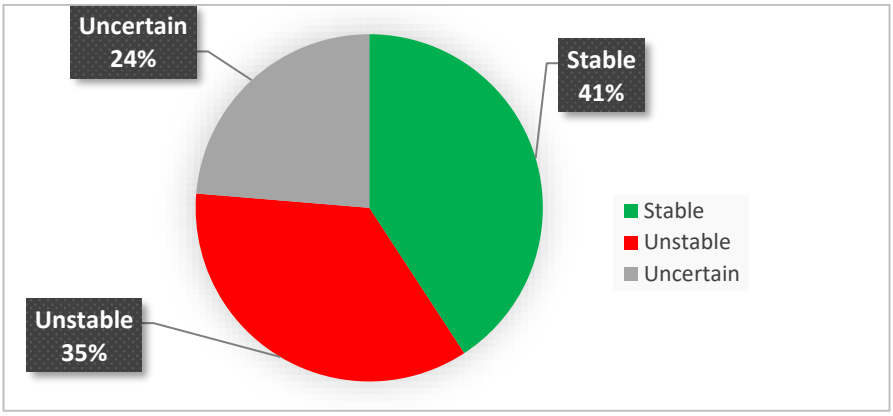

Figure 4.18 Pie chart of Q slope classes

Barton & Bar (2015) stated that in addition to the diagram above, the steepest slope angle that can remain stable without reinforcement and support system can be found with a simple Equation 4.6.

It is possible to classify the rock slope by comparing the current slope angles of the aforementioned slopes and the steepest slope angles produced by the formula developed by Barton & Bar (2015). In the analysis made within the scope of this study, the steepest slope angle was determined by both methods (Table 4.23). In addition, the relationship between the existing slope angles and the slope angles that can remain stable is presented graphically (Figure 4.19). The classification table determined according to the classification system is given in appendix-5.

Table 4.23 Classification of the steepest slopes compared to existing slopes according to the proposed equation

Location	Current slope angle	Steepest slope angle	Qslope Class	Location	Current slope angle	Steepest slope angle	Qslope Class
6	41	71.413309	Stable	39	74	48.727824	Unstable
8	58	67.218104	Stable	41	54	44.645425	Unstable
10	56	69.310108	Stable	43	54	54.096897	Uncertain
11	48	76.12605	Stable	44	73	67.218104	Unstable
13	50	53.627275	Stable	46	47	52.712125	Stable
14	48	73.627275	Stable	48	40	49.310108	Stable
18	48	60.20845	Stable	49	44	49.0824	Stable
20	45	62.673229	Stable	50	47	57.954992	Stable
21	47	50.390259	Stable	51	51	50.567926	Uncertain
25	59	65.172003	Stable	52	53	58.363057	Stable
28	50	48.693829	Uncertain	53	43	50.632029	Stable
29	53	48.487012	Unstable	55	45	45.788282	Stable
30	56	58.923632	Stable	56	41	61.422406	Stable
31	44	60.225398	Stable	57	39	67.519379	Stable
32	55	52.602868	Uncertain	58	35	60.453767	Stable
33	50	48.27515	Uncertain	59	39	55.176905	Stable
34	57	46.583625	Unstable	60	46	59.647875	Stable
36	57	50.773925	Unstable	61	73	77.817576	Stable
37	58	49.996192	Unstable	62	76	63.360607	Unstable
63	45	77.321104	Stable	92	54	65.336941	Stable
68	44	47.926437	Stable	93	60	55.482857	Uncertain
70	39	40.328257	Uncertain	94	50	46.37657	Uncertain
71	79	50.037872	Unstable	95	45	42.993729	Uncertain
73	51	52.266598	Stable	96	56	46.712946	Unstable
74	55	41.197504	Unstable	97	55	53.426972	Uncertain
75	63	48.629726	Unstable	98	55	49.286278	Unstable
78	57	52.602868	Uncertain	99	60	59.647875	Uncertain
79	60	58.840626	Uncertain	103	45	44.645425	Uncertain
80	50	49.810985	Uncertain	105	54	54.18785	Uncertain
81	48	35.330707	Unstable	107	63	50.10545	Unstable
82	50	40.329347	Unstable	108	60	52.27224	Unstable
83	45	51.877149	Stable	109	60	52.712125	Unstable
85	42	31.844097	Unstable	110	56	48.057992	Unstable
87	43	46.999238	Stable	112	58	48.693829	Unstable
88	57	51.681626	Unstable	114	62	54.542425	Unstable
89	58	54.250595	Uncertain	115	68	46.999963	Unstable
90	54	47.440056	Unstable	117	44	31.452448	Unstable
91	47	42.720266	Uncertain	119	60	42.14665	Unstable

Figure 4.19 The relationship between the current slope angles and maximum slope angles at the observation points

According to the results of Qslope on 76 slopes, 18 uncertain classes were determined. These slopes can become stable in the classification system empirically made even by only reducing the slope angles by a few degrees. To give an example, the slope number 51 is included in the stable class only by reducing the angle with a difference of 0.43 degrees. In other words, the slope can become stable in relation to the material properties with the necessary slope angle reduction process that can be made on slopes. However, the openings of several slopes that appear to be "stable" in the table were reduced more than necessary. This increases the cost of excavation and causes loss of time. Some of the mentioned slopes can be given as 18, 31, 48, 56, 57 and 63. Classes were depict by IDW method using ArcMap 10.8 program to show the spread of Qslope classification in the field and slope scale. During this digitization process, the classification developed by Barton & Bar (2015) was used. Since the program uses the IDW method only as a numerical value, stable slopes are given 1, uncertain slopes 0, and unstable slopes -1 values. After this coding process was completed, its distribution was depict on the mining working on the slope of 76 with the IDW method (Figure 4.20). After visualization with the IDW method, the Qslope values were transferred onto the 3D image to better evaluate them (Figure 4.21). In

addition, the slopes at observation points 59 and 61 were also visualized at the slope scale to be evaluated in more detail (Figure 4.22).

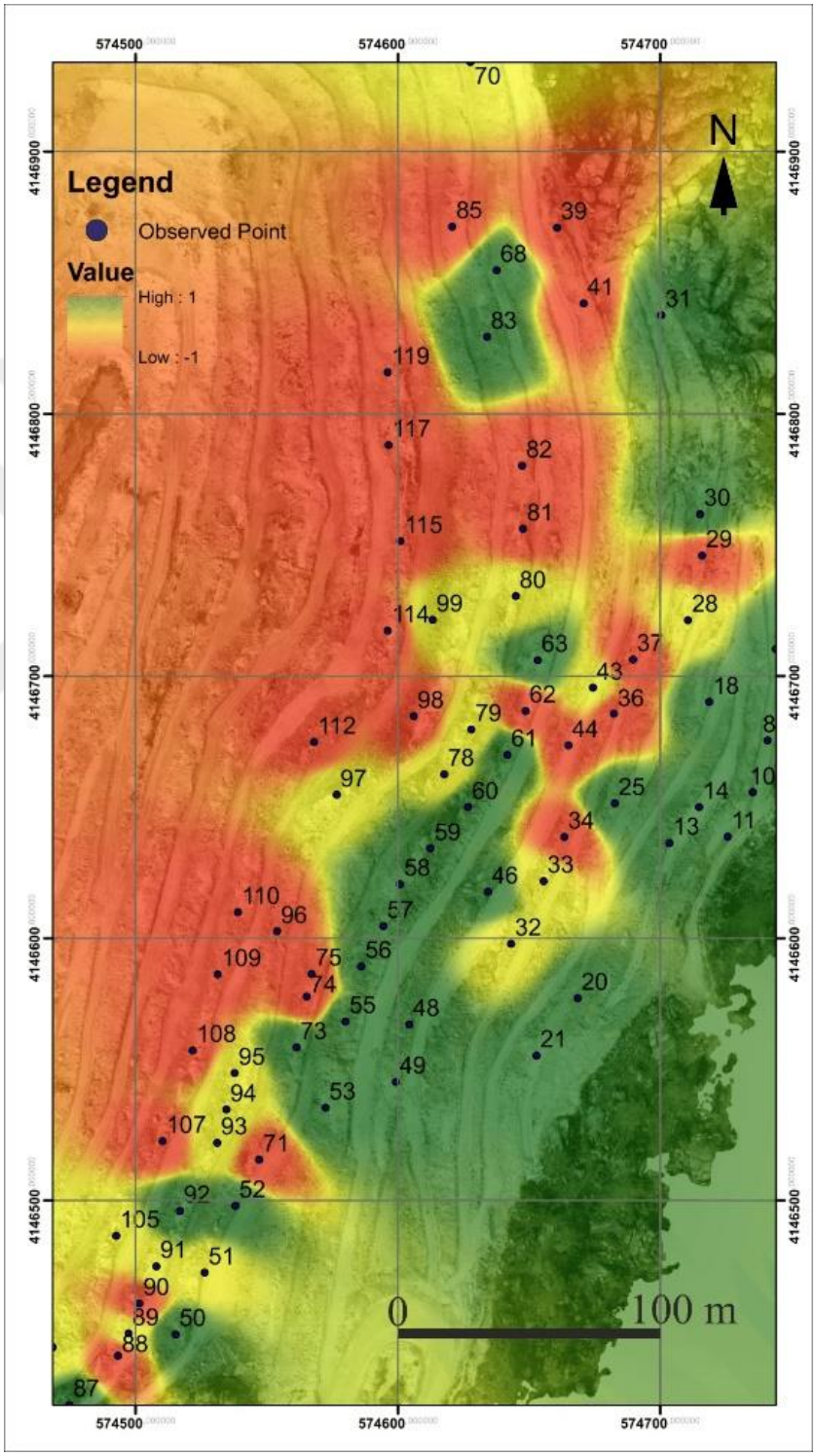

Figure 4.20 Depict of Qslope scores by IDW method

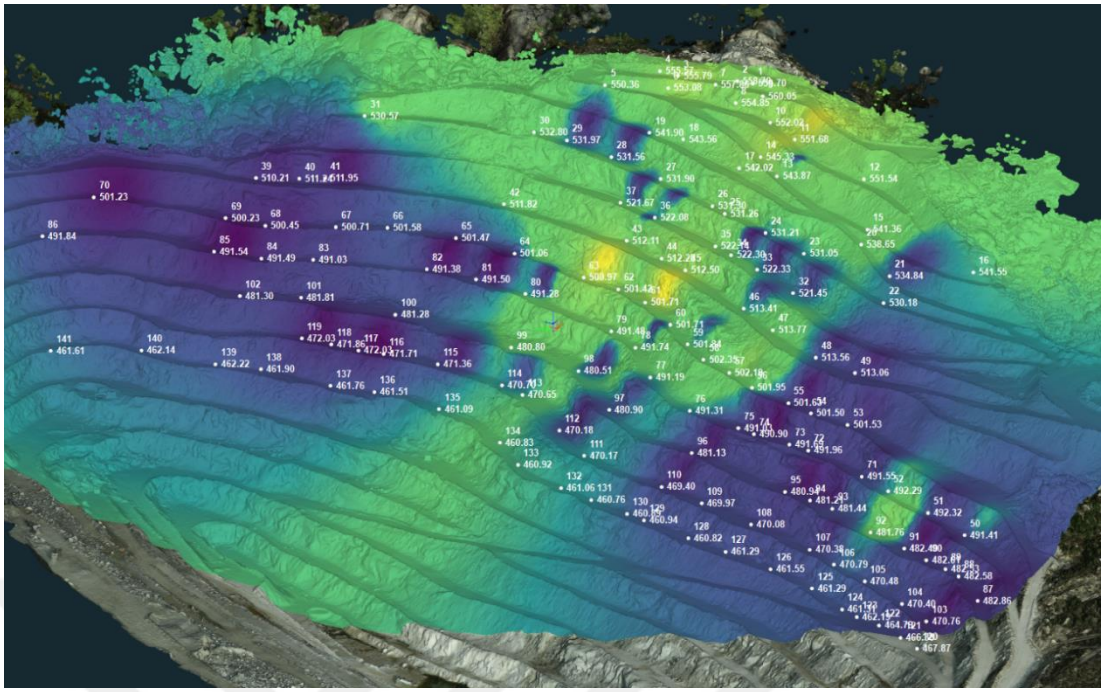

Figure 4.21 Representation of the Qslope classification system on slopes in 3D after visualization with the IDW method

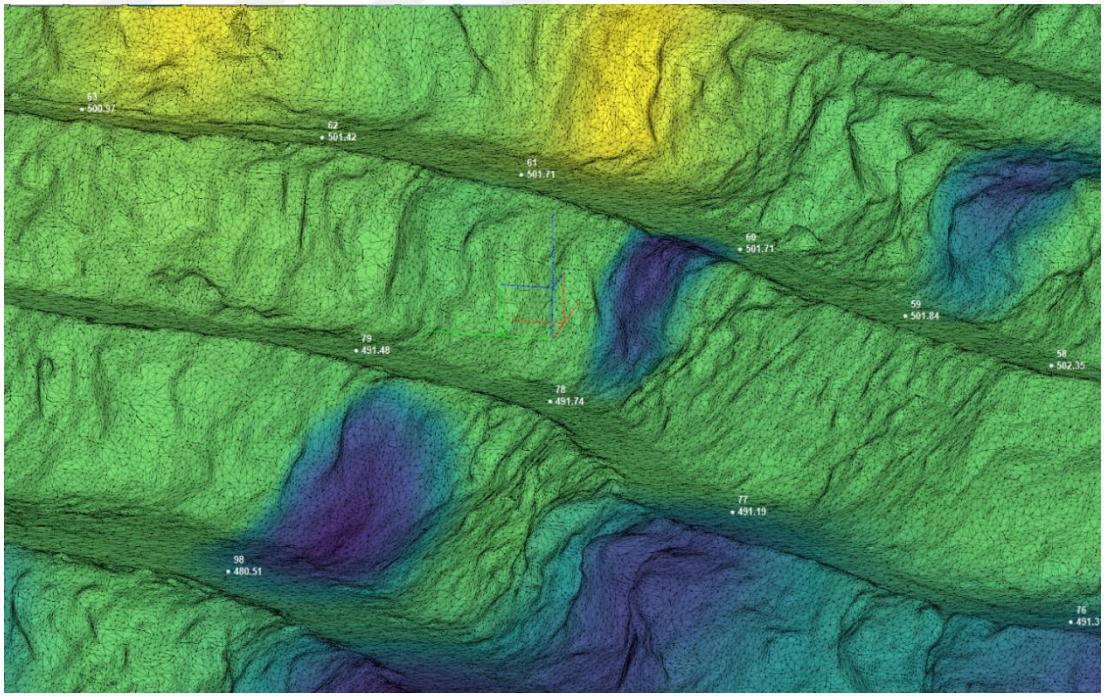

Figure 4.22 Close examination of the Qslope score of slopes 59-61

Since the discontinuity features and the mechanical properties of the rock mass at these observation points are detailed in the SMR system, they are not repeated in this section. However, as seen in the visualization processes, the Qslope score was low in slope 59. According to these results, although the Qslope value was 0.32 in the slope numbered 59, this value was determined as 4.37 in the slope numbered 61. According to the Qslope system, both slopes are classified as "stable", although there are very high differences in value between the two slopes. The reason for this is that the slope angle at the observation point 59 is approximately 39^0. For this reason, the slope angles at both observation points did not reach the maximum slope angle.

CHAPTER FIVE
MONITORING

Slopes lose their stability for a certain period of time. These movements indicate that the rock slopes are unstable. However, this situation can continue for years without any defeat. However, some slopes can accelerate as a result of a small movement and cause collapses by moving more. Slope monitoring programs should be implemented to detect such slope movements at the outset.

Open pit mines are at the top of the places where slope movements are most common. It is necessary to constantly monitor the movement of existing slopes in such enterprises. The reason for this is to continue production safely.

While activities such as production blasting and excavation in mining accelerate this situation, external forces such as climate, precipitation and earthquake also have an accelerating effect on the movements on the slopes. In addition, although there are many reasons for slope activity in open pits, one of them is uncontrolled excavations at the base of the slope (Hoek & Bray, 2004).

Within the scope of this study, the total station data placed in the eastern part of the mining operation and made only in the summer periods and the measurements made with the UAV were compared. The data of field measurements will be detailed in sub-titles.

5.1 Unmanned Aerial Vehicle (UAV)

Remote sensing; It can be defined as the technique of examining, evaluating and recording the earth, the objects on the earth and earth resources without physical connection. In this section, the remote sensing study carried out within the scope of the thesis is mentioned. Although there are many branches of remote sensing, unmanned aerial vehicle and photogrammetry technique will be mentioned under this main title and sub-titles.

5.1.1 UAV Study

Before carrying out geological observations and field studies in the study area, a specially produced unmanned aerial vehicle was used for mapping with rotary wing RTK (Real Time Kinematic) system. With this UAV used, aerial photographs were taken with a camera angle of -90 degrees (rare) at the borders of the work area from a height of 100 meters with 70%/80% overlaps. The flight plan of this measurement made in the study area is given in Figure 5.1 and the flight parameter details are given in table 5.1.

Figure 5.1 Flight plan of the worksite in the GS RTK app on the Phantom 4 RTK's onboard display controller

Table 5.1 Parameters and details used in measurements made with the Phantom 4 RTK

UAV Type	Rotary Wing (Drone)
Flight Plan	Autonomus
Camera Resolution	20 Mgpx
Overlapping*	%70-%80
Flight Height (AGL)**	100 m
Camera Angle	-90 Degree (Nadir)
Flight Mode	2D Photogrammetry
Position System	RTK
Solution	Fixed

**: Horizontal and Vertical Overlap, respectivetely.*
***: Above Ground Level*

The fact that the system is equipped with RTK ensures that the coordinates at the midpoints of the aerial photographs are more accurate and precise. By using 3D Survey photogrammetry software with these aerial photographs; dense point cloud, textured mesh model, digital elevation model and orthophoto were created. These data were used throughout the study. The production of these data is explained in detail under the title of Photogrammetry.

5.1.2.1 Photogrammetry and Process

If we explain the term photogrammetry in general; It can be defined as the method of measuring objects over photographs (terrestrial or aerial photogrammetry) and the metric interpretation of the data in the image. As a technical term; It is the measurement of two- or three-dimensional objects through photographs. In this study, many data types were obtained from aerial photographs obtained with coordinates. In this study, these data were produced by SfM photogrammetry technique. SfM; It is a photogrammetry technique that produces a new type of data with a stereo image technique, which aims to create 3D images and various models in images taken in 2D, called Strate from Motion (Çelik, 2020). The use of 3D Survey software to create the data types described above and the process steps are given below.

1. Uploading Photos

2. Alignment Photos

3. Balancing

4. Sparse Point Cloud

5. Hotspot Cloud

6. Textured Mesh Pattern

7. Orthophoto

8. Export Transactions

While the UAV with RTK is measuring in the air (horizontal and vertical overlay photo taking stage), it is connected to the internet with the M2M type data sim card modem in the remote. This internet connection receives location correction information by connecting to fixed GNSS stations in TUSAGA AKTİF CORS center. These received location (coordinate) corrections are instantly transferred to the UAV using a 2.4GHz connection with OcuSync technology. Thus, the drone writes these coordinates in EXIF format with high accuracy and precision to the midpoints of the aerial photographs during the measurement. Afterwards, EXIF information is read from the photos transferred to the 3D Survey program and it aligns (merges) the photos taken with overlay. After the photos are transferred, it is important to choose the coordinate system where the project will be resolved. The modem in the control connected to the TUSAGA CORS system receives the correction information over the 3-degree ITRF 96 (International Terrestrial Reference Frame, GRS 1980 Ellipsoid) coordinate system. Therefore, in order not to increase the margin of error due to transformations between coordinate systems and not to cause irregularities, the coordinate system that the project will be analyzed should be chosen accordingly. While the project is being resolved; (for this study) TUREF/TM27 (EPSG Code:5253) was chosen. TUREF system; (Turkish National Reference Frame, GRS 1980 Ellipsoid) It is a coordinate system that works on the basis of 3-degree slice (Gauss Kruger) and TM (Transverse Mercator) projection. After these processes, the Ground Control Point, which is determined in the field before, is included in the balancing process in order to increase the accuracy and precision of the solution. The coordinates of these GCPs are taken from the GNSS receiver in the above-mentioned system, and

then the average of these coordinates is taken and evaluated as a control point. The margins of error of these GCPs are given in Table 5.2.

Table 5.2 GCP margins of error

GCPs	Accuracy
GCP-1	0.003 m
GCP -2	0.011 m
GCP -3	0.029 m
GCP -4	0.027 m
GCP -5	0.023 m
GCP -6	0.009 m
GCP -7	0.019 m

The sparse point cloud that occurs after the balancing process is completed indicates that the operations made up to this step are error-free. Then, it is passed to the step of creating a dense point cloud, and in this step, the density of this point cloud is selected according to the purpose of the study (Low, Very Low, Medium, High and Very High). After the point cloud is formed, data in raster or vector data types containing geographic information such as digital elevation model, textured mesh model, contour and orthophoto are created. The characteristics of these data produced for this study are presented in Table 5.3 and their images are presented separately with figure 5.2, 5.3 and 5.4.

Table 5.3 Details of data generated during and/or after the photogrammetric process

Coordinate System	TUREF/TM27 (EPSG :5253)
Number of Photos	365 image
Number of Point (Point Cloud)	144.786.888 points
Grid Cell Size (DEM)*	0.15 m
Number of Triangle (Textured Mesh Model)	7.000.000 triangles
Resolution (Orthophoto)	20061x26379 pixels
GSD**	2.7cm (for AGL:100 m)

*Digital Elevation Model

**Ground Sampling Distance; It shows the area that a pixel on the orthophoto represents on the earth. The higher the GSD value, the higher the resolution.

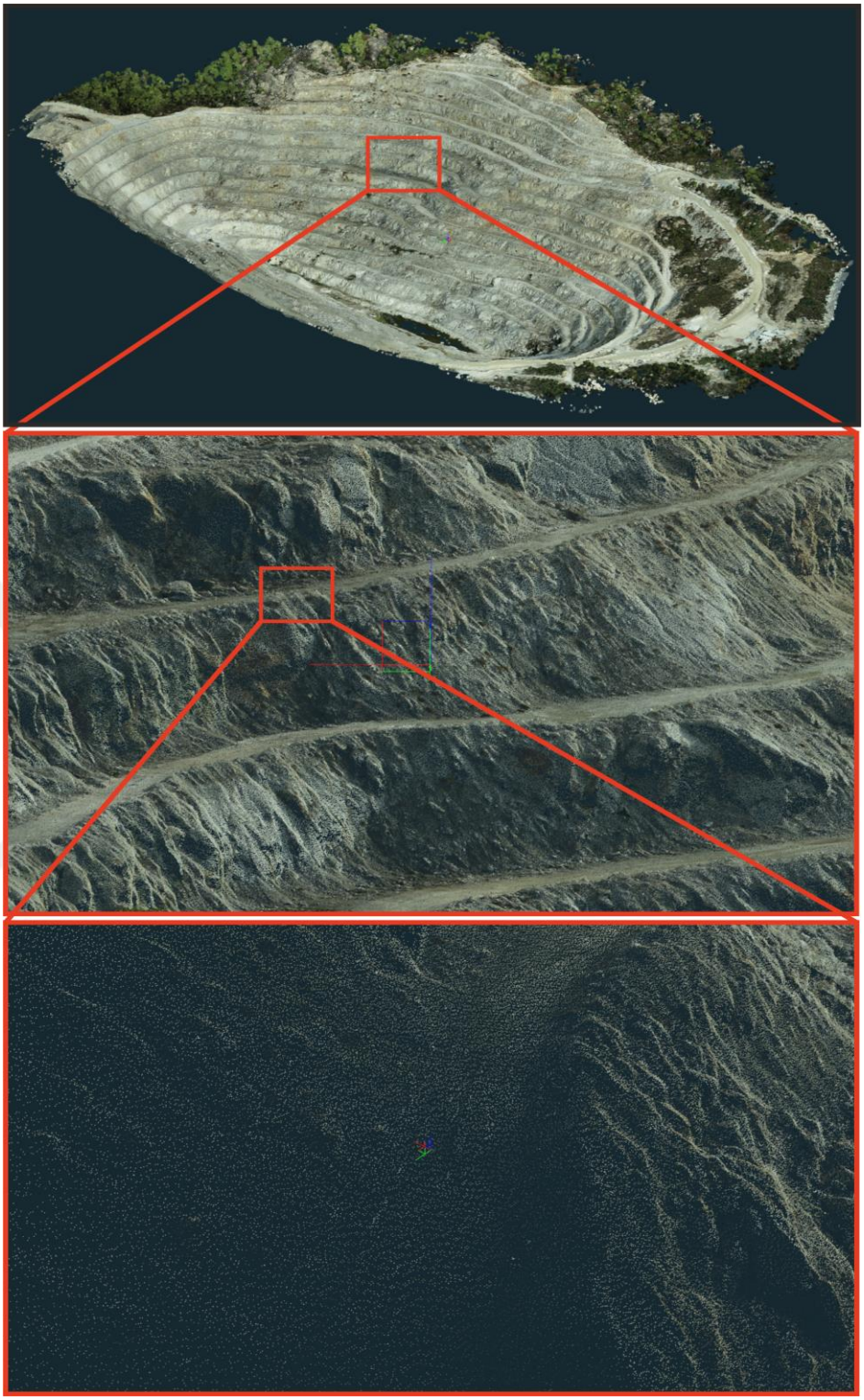

Figure 5.2 The "dense point cloud" data model with 144,786,888 points and its detailing

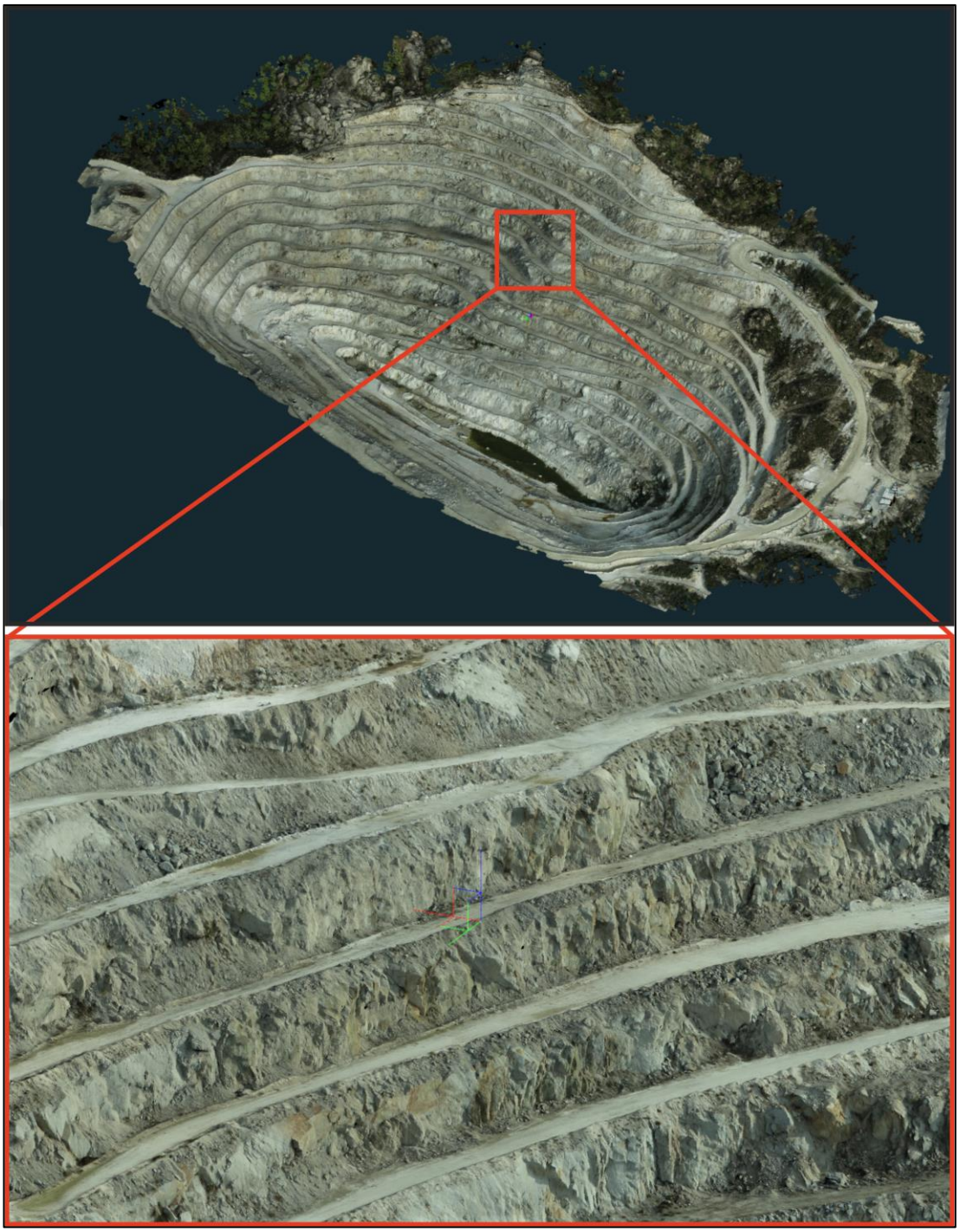

Figure 5.3 Textured mesh model created with 7.000.000 triangles and details from close-up view

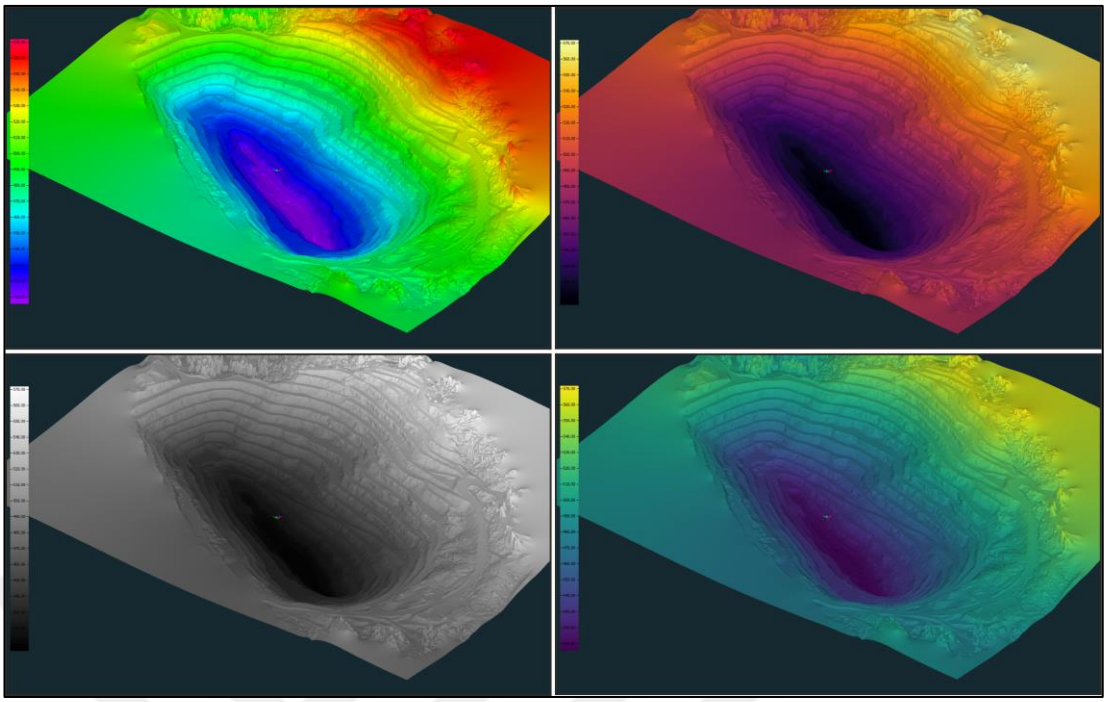

Figure 5.4 Digital elevation models (DEM) presented with different color palettes

After all these stages using 3D Survey photogrammetry software, the true orthophoto created by calculating from the 3D textured grid (mesh) model was transferred to the QGIS program. True orthophoto; It can be defined as the correct orthophoto created by using DSM (Digital Surface Model) by removing the irregularities and irregularities caused by the camera angles in the aerial photographs taken while the UAV is flying in the air. It is seen that this true orthophoto which is mentioned with the Google Sattaliete Hybrid image opened as a base in the QGIS program, overlaps exactly. These models and data types, whose location accuracy is proven with YKNs, are also shown as evidence of this overlap, which is described in the map shown in figure 43. It should be kept in mind that the image may appear as if it is not fully seated on the substrate due to the scarcity of overlaying aerial photographs at the boundaries of the formed orthophoton. However, the high overlapping rates, the correct reading of GCP's and their participation in the process, and the continuous "FIXED" verification of the UAV during flight also support position accuracy. In figure 43, the edges of the orthophoton are zoomed in and this accuracy is seen in the close view.

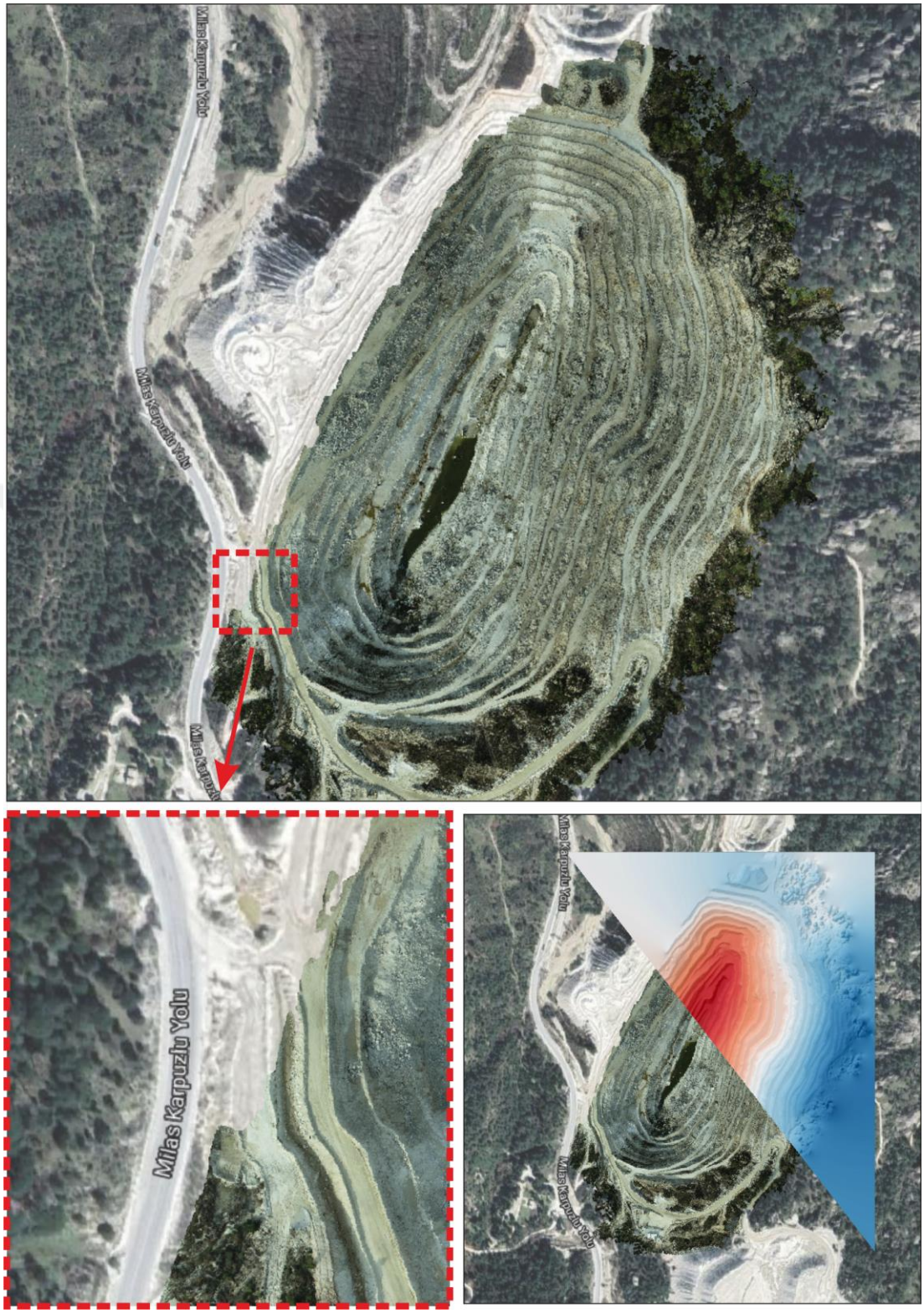

Figure 5.5 Proof of true orthophoto and digital elevation model fit on Google Satellite Hybrid image and positional accuracy

5.1.2.2 Monitoring With UAV

Within the scope of this study, flights were made considering the details and details given above. All of these flights were made on only 7 different days in June and December. According to the data received from the flights, the results of the flights on day 1 and day 7 are presented in the sections in the figure 5.6.

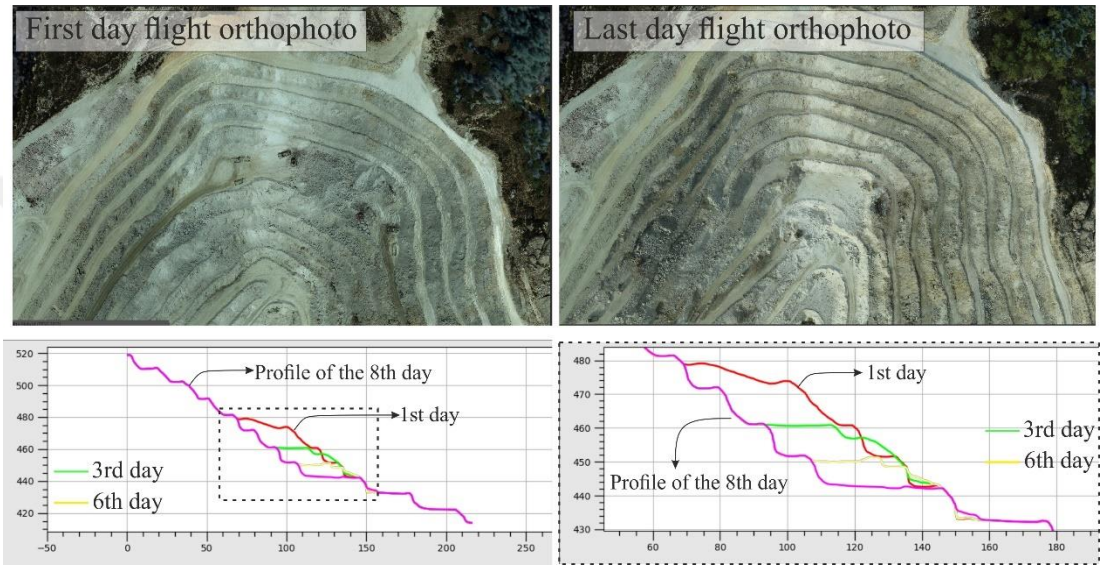

Figure 5.6 Difference analysis from the first and last day flights in the production region

As seen in the figure, according to the images taken from the drone, it can successfully analyze the difference in the region where the production is made. The difference analysis image of the northern region where the production is made is also presented in figure 5.7. It indicates that there is a volumetric difference in the region marked with red by the software and there is a change in this region. This difference has occurred in this region as albite production continues in the approximately north of the study area.

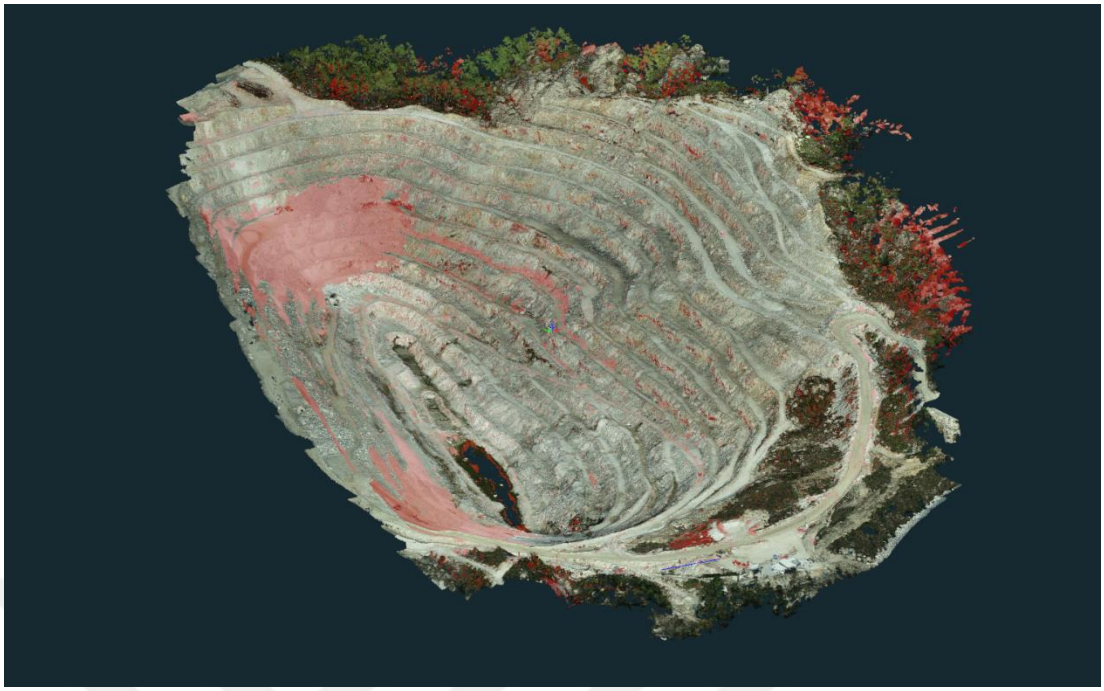

Figure 5.7 Analysis image showing the volume change in the production area

However, it also clearly shows the volume differences in the region at the time of the flight (Figure 5.8). The construction site vehicle in the figure is parked in the region during the flights on the 1st day. However, due to the fact that the same vehicle was not in that region on the 7th day flights, the event was viewed imaginatively in the difference analysis. This difference, which was made at different times, is seen as a result of the analyzes that can clearly reveal the displacement of a volume with the drone and the volume change that will occur as a result of this displacement.

The situation is not the same on the eastern side of the quarry, which is considered as the aim of the study and whose production has been stopped before. Figure 5.8 shows that there was no movement detection as a result of flights made during the summer periods. Certain changes were observed in the surface volume in the eastern region. The reason for this was seen as the displacement of the weathered gneiss unit along the slope surfaces due to the wind and rains that developed in certain periods (Figure 5.9).

Figure 5.8 The difference of the construction site vehicle in the field

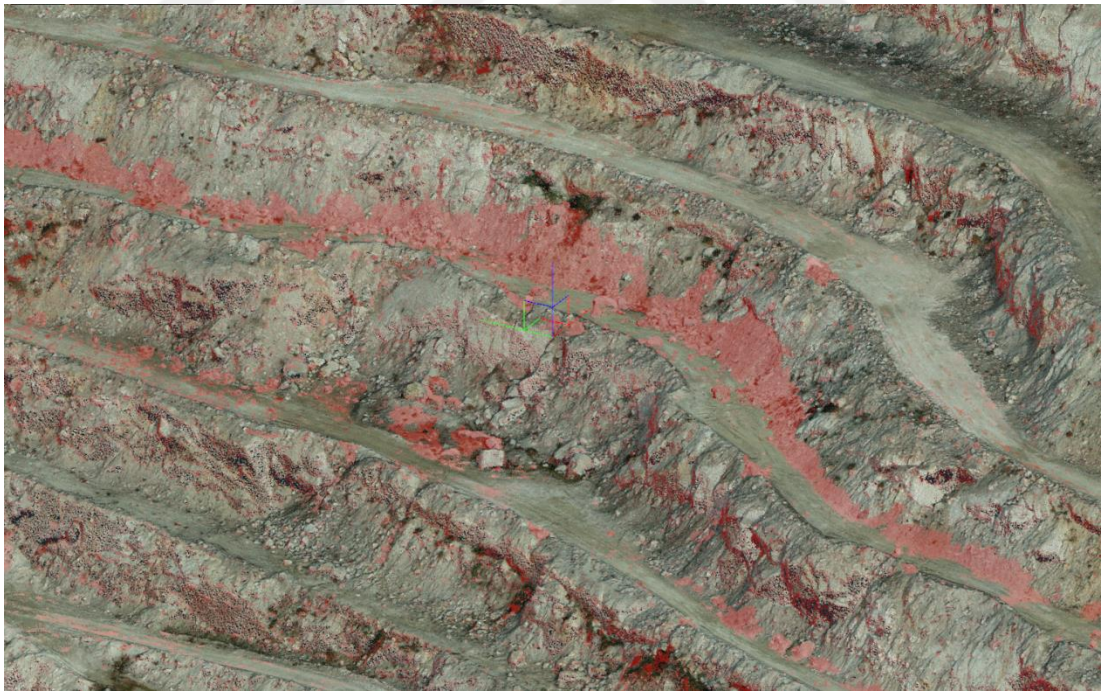

Figure 5.9 Material movement on the surface due to environmental factors

The reason why no surface movement was observed in the eastern region of the mining operation was determined as the fact that the production activities in this region were stopped and there was no force developing due to external factors during the measurement period. In other words, the absence of heavy rainfall during the flight period, the absence of freezing-thawing effects, and most importantly, the absence of a large-scale earthquake caused the surface movements in this region to cease to a certain extent. The section taken from the northern region where the production is located is shown in figure 5.10 and the section taken from the eastern region where the production stopped is shown in figure 5.11.

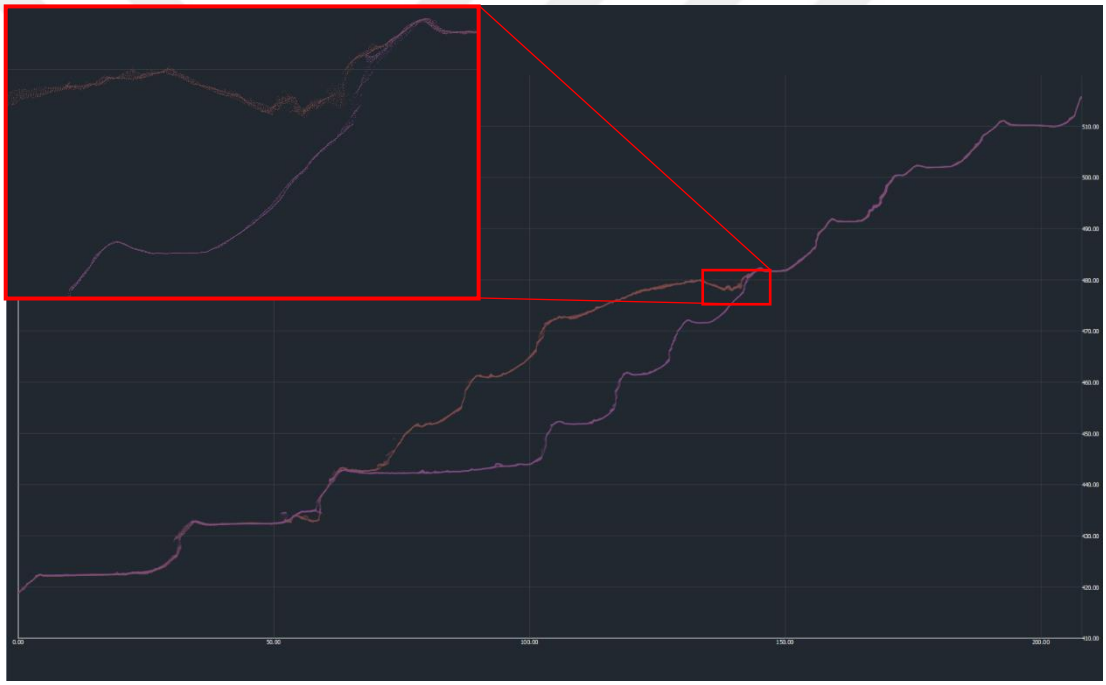

Figure 5.10 Difference analysis in the region of production

Figure 5.11 Eastern slopes where production is stopped (Only surface movement is observed)

5.2 Data Received From Total Station

In addition, motion tracking stations have been placed in some regions by the enterprise within the quarry. Thanks to these stations, slope movements in the region can be followed instantly. Thanks to this system, the movement of the slopes, which can be monitored electronically, due to exposure to any external force, helps the mine operator to follow the warning by sending a message. The locations of the motion tracking stations in this enterprise are presented in Figure 5.12.

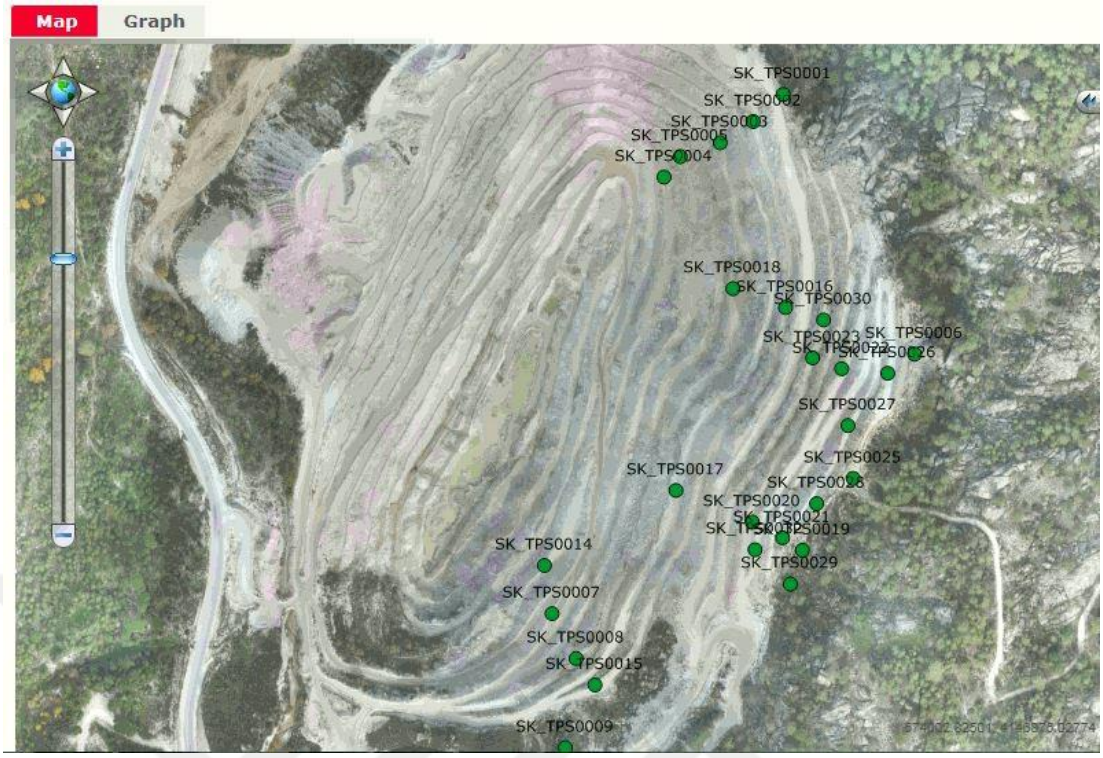

Figure 5.12 Locations of total stations in the mining area

According to the total station data obtained from the operation area, the data obtained in the last year in the eastern region are as in figure 5.13.

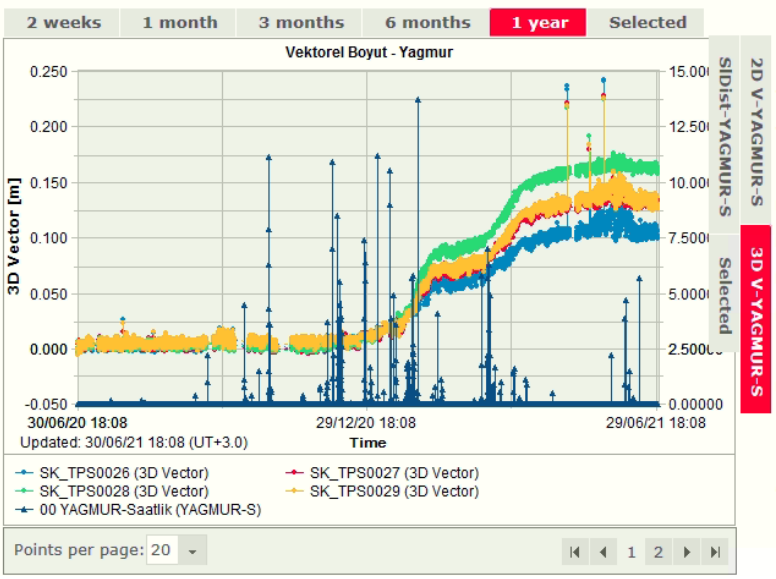

Figure 5.13 Data from total stations

According to these data, movement is observed after the months of January, February, March, when the rain is observed intensely. This may be due to the fact that the slopes become saturated with water after rainy periods. According to these data, no visible movement could be detected between the months of June 2020 and December 2020, when the study was conducted. The reason for this is that the region is both in the dry period during this time period and there is no production activity. At the same time, the absence of external factors (earthquake, production explosion, etc.) in the region during this time period and the complete cessation of production activities allowed the slopes to remain immobile. However, mm movements could be detected according to the data received from the station. The reason for this is that only the loose material on the slope surfaces has moved along the surface with the effect of periodic rain and wind.

CHAPTER SIX
NUMERICAL ANALYSES

In addition to scanline measurements kinematic analyzes and slope mass classification systems in the open pit mine the study was further detailed by numerical analysis Phase2 V 7.013. (2010) and Swedge V 5.013. (2010) software was used in this study. The analyzes made in the Phase2 V 7.013. (2010) program is performed by the finite element formulation method. This software is a 2-dimensional stress analysis program for engineering projects under different conditions and formations (RocScience 2010). Swedge V 5.013. (2010) is a software that performs two-dimensional limit-balance analysis and calculates the safety coefficient of simplified slope geometry according to the criterion suggested by Barton & Choubey (1977) (RocScience. 2010). Both SMR and Qslope classification systems were used to determine the area to be numerically analyzed. In the classification systems the slopes were tried to be classified as "low rock class" and an "unstable" region. In order to determine these regions. SMR and Qslope maps. which were depict before were used (Figure 6.1).

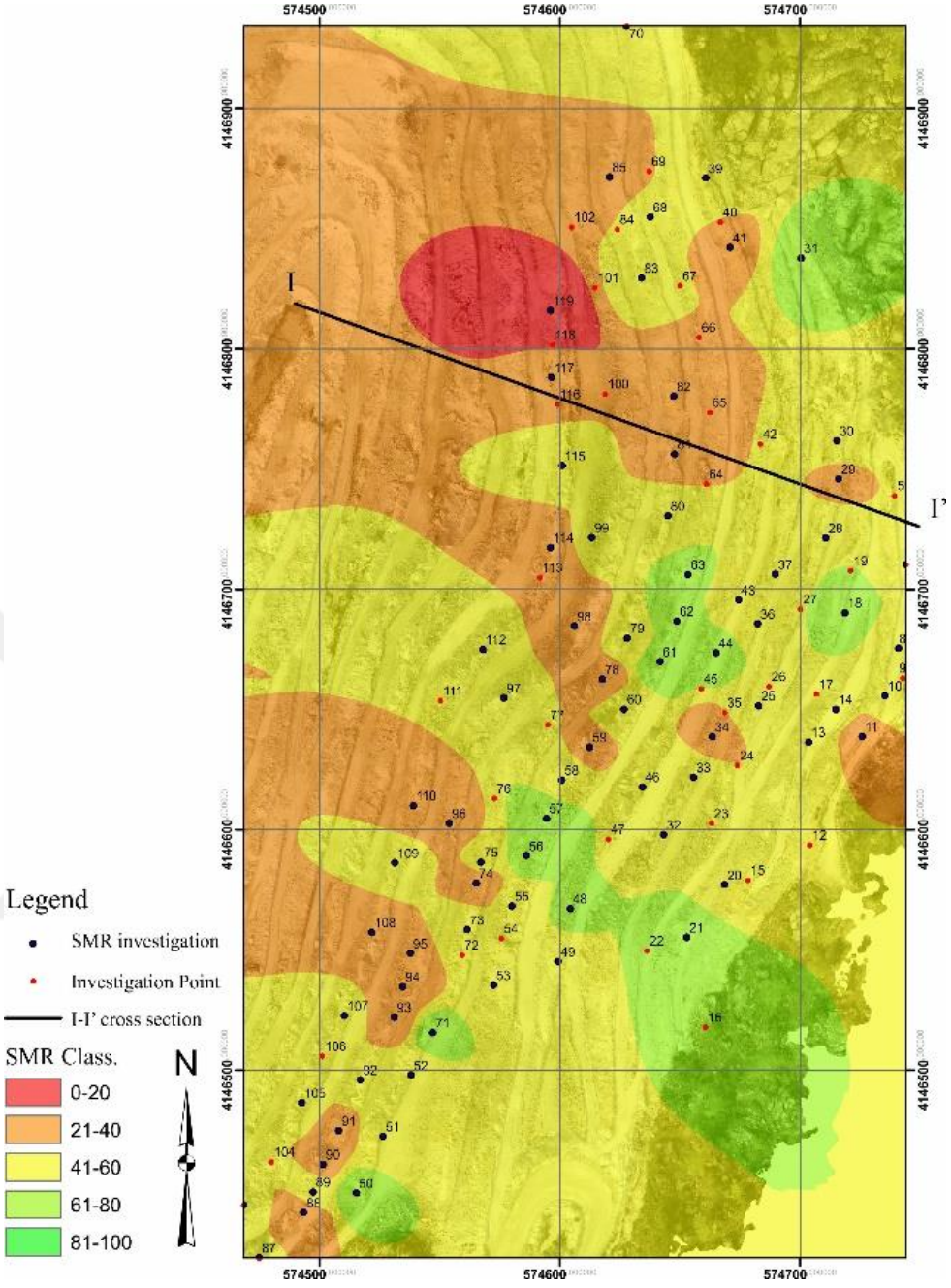

Figure 6.1 Interpolated state and cross section of the SMR system

As can be seen in the figure. the location where the I-I 'section is taken is the region where rock slopes of class III and IV in the SMR system are concentrated. In addition. many HW-EW regions were identified as a result of the field investigations in this region. Rocks in this region have lost their rock properties due to excessive weathering. The aforementioned observation points are marked with red point and are 6 in total north and south of the cross-section. In this cross-section. measurements could only be

made at the observation points 29, 81 and 117. These slopes can be examined from the tables given in the previous sections. Many slopes that cover an area of 20-30 meters of this cross-section line are in the unstable class. However, within the scope of this study. the slope points on the section line were used in numerical analysis.

After determining the location of the I-I 'section, the slope geometry was drawn in Phase2 V 7.013. (2010) software. These slope geometries and rock units seen along the cross-section were obtained from the business manager. EW-Gneiss. Gneiss and Albite units are observed from east to west along this section. For the evaluation of these geological units in numerical analysis the GSI table proposed by Hoek (2006) and Marinos & Hoek (2001) was used, which is a value used to classify a rock mass by visual inspection. The Generalized Hoek-Brown Criteria was proposed by Hoek et al. (2002) to more accurately estimate the rock mass strength based on rock material. Hoek-Brown constants in this criterion were determined by the program and used in numerical analysis. Mass properties according to the Generalized Hoek-Brown Criteria used in numerical analysis are given in the table 6.1. In addition the fault that cuts the open pit mine approximately north to south is shown in the software. The geomechanically properties of this fault are presented in table 6.2.

Table 6.1 Generalized Hoek-Brown Criterion constants used in numerical analysis

Rock Mass Type	Rock Mass and material properties										
	GSI	s	a	m_b	E_{rm} (MPa)	Poisson ratio (μ):	m_i	σ_{ci} (MPa)	Unit Volume Weight (MN/m^3)	Dilation Parameter	D
Gneiss	52	0.0003355	0.5050	0.746	1499.8	0.25	23	33	0.026		
EW-Gneiss	30	0.0000086	0.5223	0.155	564.5	0.3	23	1.5	0.018	0	1
Albite	60	0.0007	0.506	1.923	5364.09	0.25	-	72	0.026		

Table 6.2 Properties of the fault used in numerical analysis

Properties	c (MPa)	Φ (°)	kn (GPa/m)	ks (GPa/m)
Joints	0.03	21	100000	10000

Numerical analysis was performed in Phase2 V 7.013. (2010) software according to these values given in the table and slope geometries. In this numerical analysis the software has several input parameters requested from the user. These are parameters such as groundwater seismic coefficient. field stress. In addition to these parameters. support systems. if any can be entered into the program. Within the scope of this study. the groundwater level was determined beforehand from the boreholes drilled by the enterprise and entered into the program in this way. As a result of these operations. the SRF value was calculated after the slope geometry and input parameters were entered into the software (Figure 6.2).

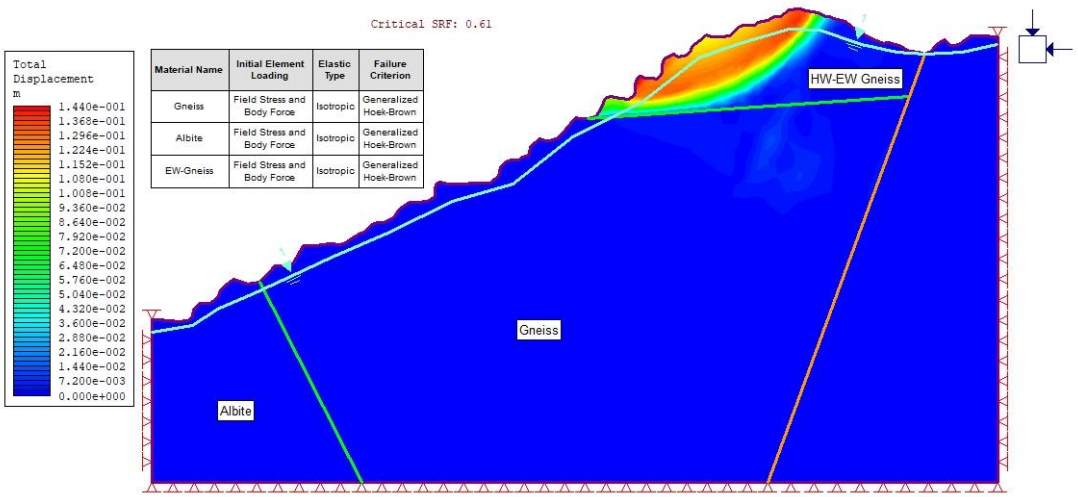

Figure 6.2 As a result of the data entered into the system. the SRF score in the I-I section (light blue line is GWT)

As a result of numerical analysis. the SRF score was found to be 0.61. According to Hoek and Bray this number should be between 1.2 and 1.4 on slopes in open pit mines. In slopes that are generally between these values. some movement can be observed during the life of the mine (Hoek & Bray, 2004). However, in the measurements made from this cross-section line a low safety coefficient was found throughout the whole slope. It is seen that this result is similar to the results in both Qslope and SMR systems, that is slopes classified as unstable are present in these regions in both systems. It is also possible to calculate the FOS simply on the step scale of the slopes on this section line. Improvements suggested by the Qslope and SMR system can be performed on the slopes on this cross-section line. To give an example, slope number 29 can be considered. Slope number 29 is in the unstable class in both systems. Since the failure mechanism in this slope is kinematically wedge type failure, the slope geometry can be simplified and FOS can be calculated using Swedge V 5.013. (2010) software. In the program, firstly parameters such as discontinuity causing wedge type failure, slope height slope direction and angle are entered. After entering these data external force parameters such as water condition on the slope seismic acceleration can also be entered. The maximum slope angle suggested in the Qslope system on this aforementioned slope is 48 degrees. However, the angle of this slope was determined as 53 degrees in the field. This caused the slope to be classified as Unstable in the Q slope system. The FOS coefficient was calculated by simplifying the current slope geometry and the slope geometries suggested by the system with the Swedge V 5.013. (2010) software (Figure 6.3). As seen in Figures A and B the safety factor for the current slope angle has been calculated as approximately 1.03. However, in the Qslope system. according to the formula developed by Barton & Bar (2015) at the steepest angle of the slope. which is 48 degrees for this slope the safety coefficient was found to be 1.35. This shows that if this slope is brought to the steepest angle suggested by Qslope it will fall into the stable class. But the one point to keep in mind is that this is a simplified slope geometry and does not include all parameters such as other sets of joints and discontinuities.

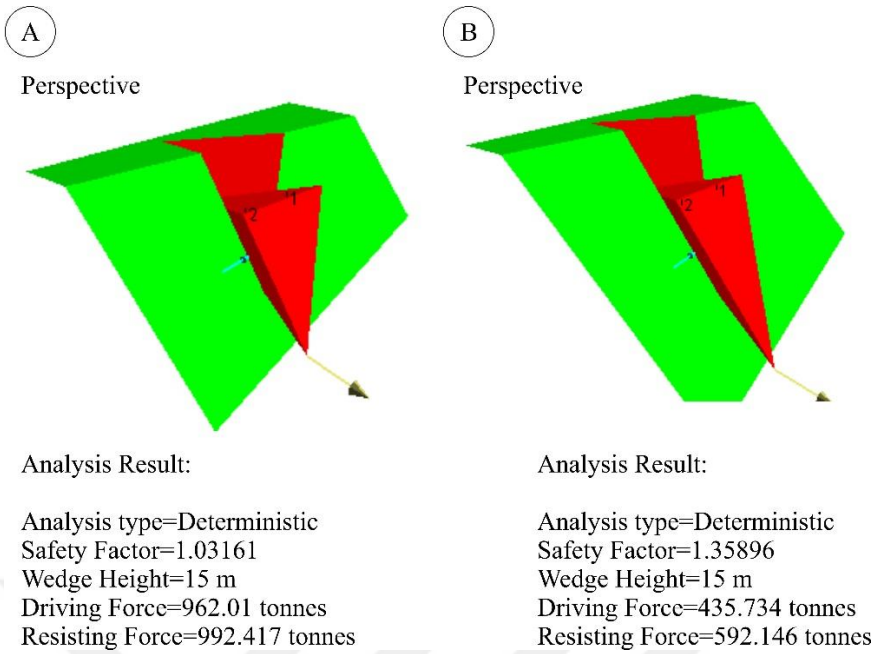

Figure 6.3 a) Simplified version of current slope geometry (slope =53º). b) Safety factor at steepest slope angle according to Qslope system (slope = 48º)

Improvement work provided by the SMR system can be carried out on the same slope. According to the improvement table developed by Romana (2003) for the slope number 29 “water drainage” was suggested in the rock slope. Again, Swedge V 5.013. (2010) software can be used for this process 2 cases have been considered for this process. The first case is when 90% of the slope is saturated with water and the second case is when the slope is saturated with 50% water. So, in the second case the slope is drained. When the analysis was made for both cases the results were as in the figure 6.4.

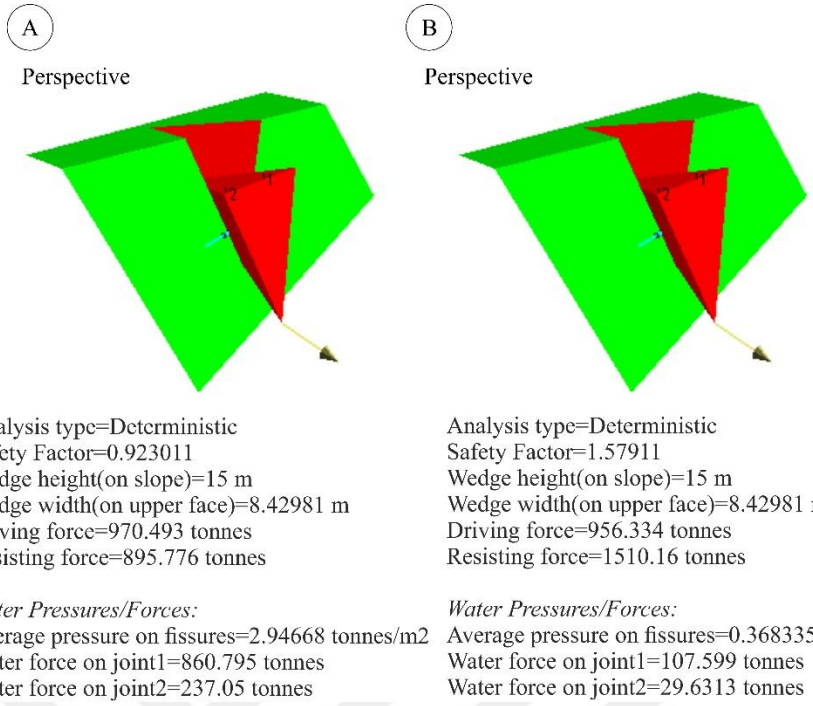

Figure 6.4 Safety coefficients of simplified geometries of slope; a) Slope is 90% saturated with water. b) Slope is 50% saturated with water (Both slopes are 53º).

In these analyzes it is seen that if the "water drainage" suggested in the SMR system is applied successfully, the safety coefficient of the slope increases from 1.03 to 1.5. In this last case, the safety factor is higher than the known range in the literature. In other words, if the slope is drained, its stability will increase. It has been shown in detail by numerical analysis that the classification systems made specifically for this mining operation have been successfully performed. In both SMR and Qslope systems, the values are almost completely in harmony with each other. Even if only one bench scale sample was made in this study, there is no doubt that similar results will be obtained in different analyzes to be made on different slopes. In the evaluations made according to the proposed improvement results of different classification systems, it is seen that the main factors affecting the durability of the slope steps or the overall slope in a mining operation can be the slope angle and water condition. It is seen both in different numerical analyzes and classification systems that the region where the I-I 'cross section is taken is a problematic region in terms of durability. If the improvement works proposed by different systems can be successfully implemented in this area, it is possible for the slope or the overall slope to become stable. In other words, it is seen

how important rock mass classification systems and numerical analysis are in the preliminary preparation stage of a mine planning. It is clear that these methods should be included in the planning stage of an enterprise.

CHAPTER SEVEN
CONCLUSIONS AND DISCUSSIONS

Production stopped completely after the movement in the eastern part of the open pit albite mine was detected. In order to restart the production in the most efficient way and to continue safely in this region, stability evaluations were made with different methods. First of all, a total of 1613 discontinuity measurements were taken to make kinematic analysis at 119 different points from the eastern part of the quarry. By means of these discontinuity measurements, the probable slip type of each slope was determined and the dominant joint sets throughout the quarry were determined. A total of 76 failures were observed in the eastern part of the quarry, including 44 wedges, 22 overturns and 10 planar failures. According to these numerical data, the dominant failure mechanism of the quarry was determined as wedge type failure with 58 percent. At the same time, 1613 discontinuities taken from the eastern part of the quarry were transferred to the DIPS software and 5 different joint sets were detected in the quarry by means of the program. During these studies, scanline measurements were made from 119 observation points and the engineering properties of the joint sets that caused the slips were determined. The uniaxial compressive strength of the discontinuities was determined by means of the Schmidt hammer test, thanks to previous laboratory studies in the neighboring quarry of the same enterprise. According to these data, the wall strength definition of the region was determined as “Medium strong rock” according to ISRM (2007) standards. It was desired to determine the better evaluation of the rock slopes and the improvement (reinforcement) processes that can be made accordingly at the beginning of the project. For this purpose, two different rock slope mass classification systems were used for stability evaluations. These are SMR (Slope mass rating) developed by Romana (1985) and Q-Slope systems developed by Barton & Bar (2015). The RMR system is also required to calculate the SMR score for rock slopes. For this purpose, RMR scoring was performed on 76 rock slopes. In addition, the kinematic analysis and the geometries of the slopes were determined and the SMR score of each slope was calculated as a result of the field studies. According to the SMR system of these slopes, 4 different classifications were made. These classes are; 1 bad. 22 bad. 41 is normal and 12 is good. Among these SMR classes, the most

dominant class is class III with 54 percent. This class can be eaten as "planar or big wedge" according to the definitions developed by Romana (1985). Kinematically, the dominant failure mechanism in this region is kinematic failure with 58 percent. In other words, in this study, it is seen that there is a harmony between the SMR system and the kinematic analysis. Again, the RMR system and SMR systems made within the framework of this study were also compared. The mentioned slopes are defined in only 2 classes according to the RMR score. According to the RMR system, no slope is “very bad rock. While they are not classified as “bad rock”, the rate of slopes that fall into these classes in the SMR system is determined as 30 percent. Although there are similar differences in other classes. The most obvious difference belongs to the “good rock” class. While this rate is 16 percent in SMR. It is set at 36 percent in the RMR class and is about 2 times higher than the SMR rate. In order to better observe these differences, thematic maps of SMR and RMR scores were prepared and an evaluation was made on the slope scale. However, there are exceptional cases. The reason for this is determined as slope geometries within the framework of this article. According to the SMR system, the instability of which is determined and the improvement works that can be done are determined separately for each slope. Most of these slopes III. “such as shotcrete. It has been revealed that one of the improvement operations such as “bolt anchors and toe ditch” can be done.

Another classification system, Qslope, is also used in this article in order to better evaluate slopes. Each parameter in the Qslope system was carefully defined from the field and appropriate scores were made in the suggested tables. According to these scores, the slope angles at 76 observation points were placed in the semi-logarithmic diagram developed by Barton & Bar (2015). At the same time, the slope angles for these slopes that can be stabilized without any strengthening were determined. According to the system, 41% of slopes are stable at current slope angles. It is calculated as 35% unstable and 24% uncertain. The same process was also done with the formula suggested by Barton & Bar (2015).

Kinematic analysis SMR. In addition to many different evaluation criteria such as RMR and Qlope, the safety factor was calculated with two different software for both

the accuracy of the scoring systems and the better evaluation of the unstable region by taking sections from a certain region of the slopes. First of all, the section line was determined and the slope geometries on this section line were drawn by an unmanned aerial vehicle. In order to be evaluated in Phase2 software, the geological structures in the section line were determined and the GSI values of the rocks in this region were determined by field observations. Accordingly, GSI value of Gneiss was determined as 52, EW-Gneiss as 30 and Albit as 60 and Generalized Hoek-Brown Criterion constants to be used in numerical analysis were determined.

SRF value was determined as 0.61 in the cross-section line determined as a result of the input parameters and slope geometries used. This rate is considerably less than the safety factor determined for an open business. Therefore, it is observed that the numerical analysis is in harmony with the information given by both qslope and smr systems. Another consideration is to perform a numerical analysis on simplified slope geometries. These analyzes were carried out to see how the safety factor changed when the improvement studies suggested by the Qslope and SMR system were applied in this particular quarry. The slope chosen for this is the slope number 29 passing through the section line. Since the kinematic failure mechanism of this slope is wedge failure, the Swedge program was used. According to both systems, this slope is classified as unstable. According to the Qslope system, this slope should be at most 48 degrees, but according to field studies, this slope was determined as 53 degrees.

Therefore, the slope falls into the unstable class according to the Qslope system. The factor of safety for the current slope angle was calculated as 1.03 according to the software. This value is not safe for a rock slope. However, when the slope angle suggested by the Qslope system was entered into the program, the safety factor was determined as 1.35. This value is in the range that can be considered safe for a slope. It is seen here that the slope can become stable if brought to the steepest slope angle suggested by Qslope. For the SMR system, the evaluation was made on the same slope and with the same software. According to the SMR system, “water drainage” should be made for this slope. Accordingly, in the software, the safety coefficient was calculated for the slope in the first case with 90% water saturated and the FOS was

determined as 1.03. In the second case, the slope was drained and made 50% irrigated. In this case, the safety factor increased to 1.5.

It is clearly seen here that unstable slopes in both systems and as a result of kinematic analysis can be stabilized by taking the improvement or strengthening measurements developed by the systems that can be made. In order for the quarry to become active again, these classification systems should be applied as a guide for the beginning of the project and production should be continued by making the necessary actions according to these evaluations.

As a result of the monitoring performed within the framework of the study, no movement was observed in the region. However, when the drone data from the region and total station data are compared, a few small-scale movements were observed in the superficial and only weathered gneiss unit due to environmental factors such as wind and/or rain. These are also not determined as movements that may affect production or cause production to stop. However, it can be said that the difference analyzes taken from the drone are very successful and in harmony with the total station data. Volumetric changes due to production activity or moving objects give very realistic results in difference analysis. It should be noted that this study was carried out during the summer periods and it should be known that there is no movement tracking within the scope of this study. In other words, in order to compare drone and total station data, it is necessary to fly with the drone as often as possible with certain periods. There is no doubt that it can give more accurate and precise results in winter periods when slopes are affected by external forces and when there is seismic activity.

REFERENCES

Anbalagan, R., Sharma, S., & Raghuvanshi, T. K. (1992). Rock mass stability evaluation using modified SMR approach. In *proceedings of the 6th National Symposium on Rock Mechanics,* 258-68.

Anon (1977). The description of rock masses for engineering purposes. *Quarterly Journal of Engineering Geology*, *10*, 355-388.

Bar, N., & Barton, N., (2017). The Q-slope method for rock slope engineering. *Rock Mech Rock Engineering*, *50*, 3307–3322.

Barton, N., & Bar, N., (2015). Introducing the Q-slope method and its intended use within civil and mining engineering projects. In *Schubert, Kluckner (eds) Future development of rock mechanics, proceedings of the ISRM regional symposium EUROCK 2015 and 64th Geomechanics Colloquium*, Salzburg, 7–10 Oct 2015, 157–162.

Barton, N., Lien, R., & Lunde, J., (1974). Engineering classification of rock masses for the design of tunnel support. *Rock Mechanics*, *6*(4), 189–236.

Barton, N., & Choubey, V., (1977). The shear strength of rock joints in theory and practice. *Rock Mechanisc*, *10*, 1-54.

Bell, F. G. (1992). *Engineering in rock masses*. Oxford: Butterworth-Heinemann.

Bieniawski, Z. T., (1973). Engineering classification of jointed rock masses. *Civil Engineer in South Africa*, *15*(12), 335-43.

Bieniawski, Z. T., (1989). Engineering rock mass classifications: a complete manual for engineers and geologists in mining, civil, and petroleum engineering. New York: Wiley.

Candan, O., Çetinkaplan, M., Oberhansli, R., Rimmele, G., & Akal, C., (2005). Alpinehigh-pressure. Low temperature metamorphism of Afyon Zone and implication for metamorphice evolution of western Anatolia. *Lithos, 84*, 24-102–.

Cernica, J. N., (1995). *Geotechnical Engineering: Soil Mechanics,* Kanada: John Wiley and Sons Inc.

Coduto, Donald P., (1999). *Geotechnical engineering: principies and practices.* New Jersey*:* Prentice-Hall Inc., 518.

Çelik, M., Yakar, İ., Hamal, S., Oğuz, G., & Kanun, E., (2020). Sfm Tekniği ile Oluşturulan 3B Modellerin Kültürel Mirasın Belgelenmesi Çalışmalarında Kullanılması: Gözne Kalesi Örneği. *Türkiye İnsansız Hava Araçları Dergisi, 2*(1), 22-27.

Das, B. M., (1994). *Principles of Geotechnical Engineering,* USA: PWS Publishing Company.

Deere, D. U., & Miller, R. P. (1966). *Engineering classification and index properties for intact rock.* Technical Report No: AFWL-TR-65-116, University of Illinois, Illionis.

Deere, D. U., (1963). Technical description of rock cores for engineering purposes. *Rock Mechanics and Engineering Geology*, Vienna. Springer. *1*(1), 16-22.

Erdoğan, B., & Yavuz, A. B., (2004). Kayaçların yapı taşı olarak kullanılabilirliğini belirlemede fiziko mekanik özelliklerin önemi, *Natural Stone Dergisi*, *6*, 22- 229.

Graciansky, P., (1965). Précisions sur le métamorphisme du massif de Menderes le long de sa bordure meridionale. *Bulletin of the Mineral Research and Exploration Institute of Turkey*, *64*, 9-23.

Goodman, R. E., & Bray, J., (1976). Toppling of rock slopes. *ASCE, Proc. Specialty Conf. on Rock Eng. for Foundations and Slopes,* Boulder, *2*, 201-34.

Hoek, E., (2006). Rock Mass Properties. *In practical rock engineering* (1-47). Canada: The University of Toronto Press.

Hoek, E., & Bray, J. W., (2004). *Rock Slope Engineering* (4rd Edition). London: Institution of Mining and Metallurgy.

Hoek, E., Carranza-Torres, C., & Corkum, B., (2002). Hoek-Brown criterion-2002 edition. *In Proceedings of North American Rock Mechanics Symposium*, Toronto, Canada, *1*, 267-273.

International Society for Rock Mechanics (ISRM) (2007). R. Ulusay, & J. A. Hudson, (Eds.). *The complete ISRM suggested methods for rock characterization, testing and monitoring: 1974-2006*. Suggested methods prepared by the Commission on Testing Methods, ISRM. Compilation arranged by the ISRM Turkish National Group, Ankara: Kozan Ofset.

Jorda´-Bordehore. L., (2017). Application of Qslope to assess the stability of rock slopes in Madrid province, Spain. *Rock Mechanics and Rock Engineering*, *50*(4), 1947-1957.

Kadakçı, K. T., & Koca, M. Y., (2014). Açık ocak albit işletmesindeki kaya şevlerinin sonlu elemanlar yöntemi kullanılarak duraylılık değerlendirmesi. *Jeoloji Mühendisliği Dergisi*, *38*(1), 1-19.

Kılıç, R., (2005). *Kaya Mekaniği Ders Notları* (61), Ankara: A.Ü.F.F Döner Sermaye İşletme Yayınları.

Kıncal, C., (2014). Application of two new stereographic projection techniques to slope stability problems. *International Journal of Rock Mechanics and Mining Sciences*, *66*, 136-150.

Laubscher, D. H., (1990). A geomechanics classification system for the rating of rock mass in mine design. *J S Afr Inst Min Metal*. *90*(10), 257–273.

Marinos, P., & Hoek, E., (2001). Estimating the geotechnical properties of heterogeneous rock masses such as flysch. *Bulletin of the Engineering Geology and the Environment*, *60*, 85-92.

Meteoroloji Genel Müdürlüğü Resmi İstatistikler (2019). Retreived December 12, 2019 from https://www.mgm.gov.tr/veridegerlendirme/il/ve/ilceler/istatistik.

Morales, M., (2017). Slope stability assessment of an open pit mine using three-dimensional rock mass modeling. *Bulletin of Engineering Geology and the Environment*, *78*(1), 1249-1264.

Norrich, N., & Wyllie, D., (1996). Rock slope stability analysis. In *Landslides: investigation and mitigation.* Transportation Research Board Special Report, National Research Council, 391–425.

Priest, S. D., & Hudson J., (1976). Discontinuity spacing in rock. *International Journal of Rock Mechanics and Mining Sciences & Geomechanics Abstracts*. *13*(5), 135-148.

Read, J., & Stacey, P., (2010). *Guidelines For Open Pit Slope Design Series*. Canada: CSIRO Publishing.

Robertson, A. M., (1988). Estimating weak rock strength. In *Sastry KVS (1th ed.) Proceedings of the SME annual meeting Society of Mining Engineering*, Phoenix, 1–5.

Rocscience (2007). *RocLab- Rock Mass Strength Analysis using the Generalized Hoek-Brown Failure Criterion* (Version 0.1) [Computer software].

Rocscience (2015). *Dips- graphical and statistical analysis of orientation data* (Version 6.017) [Computer software].

Rocscience (2019). *RS2- Two-dimensional finite element analysis program* (Version 10.012) [Computer software].

Romana, M., (1993). A geomechanical classification for slopes: Slope Mass Rating, in: Hudson, J.A. (Ed.), *Comprehensive Rock Engineering, Pergamon Press, Oxford*, pp. 575–599.

Romana, M., (1985). New adjustment ratings for application of bieniawski classification to slopes. *Proceedings of International Symposium on the Role of Rock Mechanics, ISRM,* Salzburg, 49–53.

Romana, M., Serón, J. B., & Montalar, E., (2003). "SMR geomechanics classification: application, experience and validation", *Proceedings of the 10th Congress of the International Society for Rock Mechanics*, South Africa, Sandton, South Africa.

Romana, M., Tomás, R., & Serón, J.B., (2015). Slope Mass Rating (SMR) geomechanics classification: thirty years review, *13th ISRM Congress,* 10.

Singh, Bhawani., & Goel, R. K., (2011). *Engineering rock mass classification, tunneling, foundations, and landslides*. London: Elsevier Inc.

Ulusay, R., & Sönmez, H., (2002). *Kaya kütlelerinin mühendislik özellikleri (Turkish),* Ankara: TMMOB Jeoloji Mühendisleri Odası Yayınları, *60*, 243.

APPENDICES

APPENDIX-1: Measured Discontinuities Of Joint Sets

Tablo A1.1 Discontinuity orientations

Location	J1	J2	J3	J4	J5	J6	J7
1	81/096	84/025	-	-	-	-	-
2	72/274	74/300	84/350	-	-	-	-
3	70/115	50/230	72/50	-	-	-	-
4	76/066	52/157	-	-	-	-	-
5	88/085	84/163	88/340	82/195	-	-	-
6	46/030	31/210	86/093	60/061	-	-	-
7	52/325	70/158	-	-	-	-	-
8	52/115	76/217	44/250	-	-	-	-
9	88/265	80/332	22/317	-	-	-	-
10	70/110	30/135	79/350	-	-	-	-
11	40/310	-	-	-	-	-	-
12	42/090	68/250	78/227	-	-	-	-
13	80/100	58/210	18/122	68/310	-	-	-
14	46/266	86/303	-	-	-	-	-
15	-	-	-	-	-	-	-
16	-	-	-	-	-	-	-
17	-	-	-	-	-	-	-
18	72/140	80/045	60/245	80/045	-	-	-
19	50/293	12/005	-	-	-	-	-
20	40/240	50/336	6/255	44/124	-	-	-
21	22/212	50/270	76/064	84/183	-	-	-
22	80/345	60/261	10/003	-	-	-	-
23	80/166	78/228	71/290	40/170	56/176		-
24	17/217	64/070	80/310	-	-	-	-
25	70/074	67/325	40/310	40/310	-	-	-
26	68/005	20/150	78/300	12/208	54/025	-	-
27	-	-	-	-	-	-	-
28	86/186	40/235	80/095	-	86/186	80/095	-
29	87/288	40/308	84/020	40/308	-	-	-
30	88/174	62/190	65/090	60/340	88/174	65/090	60/164
31	80/154	36/118	32/317	42/228	38/078	74/087	42/228
32	40/169	30/130	60/255	56/323	88/348	-	-
33	20/163	58/070	86/072	40/294	62/079	40/294	-
34	80/080	52/267	20/168	-	-	52/267	80/337
35	20/165	82/308	68/168	28/019	70/210	-	-

Tablo A1.1 continuies

36	55/273	20/113	52/012	-	55/273	52/012	
37	40/225	88/309	86/023	16/148	70/270	86/006	26/023
38	70/323	72/204	32/285	-	-	-	-
39	62/016	70/007	64/259	-	70/045	64/259	70/007
40	68/258	30/313	42/310	-	-	-	-
41	68/151	84/277	84/286	54/287	58/248	76/056	73/147
42	-	-	-	-	-	-	-
43	70/128	40/003	72/144	58/257	62/008	72/144	70/128
44	87/253	72/324	31/171	72/291	72/291	-	-
45	06/206	76/076	84/330	82/245	-	-	-
46	32/250	80/139	74/332	58/123	80/139	87/074	32/250
47	-	-	-	-	-	-	-
48	75/338	84/185	48/267	60/188	50/100	58/190	-
49	38/248	-	38/248	80/345	48/076	-	-
50	38/197	70/074	30/190	-	-	-	-
51	52/160	66/273	30/249	34/208	80/274	30/249	
52	40/242	77/337	64/156	-	-	-	-
53	82/97	80/323	40/222	57/337	-	-	-
54	-	-	-	-	-	-	-
55	72/101	80/110	28/287	80/046	28/287	63/080	62/139
56	72/135	75/147	56/326	34/207	60/180	70/088	
57	72/152	32/223	38/321	38/321	72/152	78/082	
58	80/161	88/064	80/161	88/253	34/258	32/086	20/184
59	42/261	44/327	62/154	82/65	-	-	-
60	82/011	40/267	80/121	63/147	82/011	74/262	88/311
61	46/143	64/320	86/251	65/321	84/157	47/141	17/203
62	88/076	76/301	87/256	68/283	44/214	40/130	64/293
63	47/190	70/321	87/119	87/089	83/076	62/094	82/154
64	-	-	-	-	-	-	-
65	-	-	-	-	-	-	-
66	-	-	-	-	-	-	-
67	-	-	-	-	-	-	-
68	47/284	70/180	73/285	80/190	73/259	70/025	-
69	-	-	-	-	-	-	-
70	70/185	82/348	80/013	82/348	78/176	18/205	56/178
71	80/297	68/196	12/097	-	-	-	-
72	-	-	-	-	-	-	-
73	66/265	72/063	80/082	63/120	63/120	72/63	52/126
74	36/310	50/280	82/210	57/341	10/190	22/124	18/105
75	40/284	68/253	62/327	78/086	40/214	70/194	84/310

Tablo A1.1 continuies

76	83/087	88/341	45/292	82/163	-	-	-
77	-	-	-	-	-	-	-
78	45/287	51/324	60/248	50/323	74/112	80/089	81/160
79	28/285	48/257	60/331	75/108	74/113	60/131	88/097
80	76/109	14/040	-	-	-	-	-
81	54/210	50/310	74/113	85/115	50/248	60/035	77/310
82	84/341	60/195	82/101	69/081	84/030	70/081	79/284
83	57/224	40/336	84/084	88/348	86/160	59/153	87/253
84	-	-	-	-	-	-	-
85	63/205	86/003	87/099	74/130	88/340	78/341	71/325
86	33/283	67/045	70/136	-	-	-	-
87	86/141	60/206	-	-	-	-	-
88	50/288	45/309	86/194	46/309	60/092	60/092	80/184
89	41/067	71/284	70/148	47/182	60/196	23/123	61/266
90	38/351	69/251	58/357	67/155	72/197	61/065	30/169
91	42/290	39/283	45/271	42/290	40/283	78/288	48/143
92	37/308	58/358	60/212	83/080	81/109	88/175	70/105
93	40/319	50/039	74/267	70/325	89/280	53/185	20/090
94	50/277	64/200	47/336	77/092	67/101	55/110	80/183
95	40/259	60/190	50/327	80/088	87/094	85/358	77/007
96	30/292	35/241	73/011	78/090	80/095	73/011	87/171
97	68/344	89/007	79/284	10/131	70/071	30/139	-
98	70/227	70/005	74/146	74/146	74/159	84/275	65/075
99	80/247	50/355	80/080	82/105	80/075	81/107	27/131
100	-	-	-	-	-	-	-
101	-	-	-	-	-	-	-
102	46/262	58/356	46/262	79/090	79/175	82/033	62/019
103	45/256	70/008	83/356	83/337	-	-	-
104	-	-	-	-	-	-	-
105	30/282	36/267	54/255	61/335	80/091	63/055	80/181
106	-	-	-	-	-	-	-
107	39/204	62/333	79/088	68/094	68/094	60/154	74/004
108	45/260	45/260	57/339	71/088	70/097	68/128	70/097
109	45/312	47/314	70/353	81/095	72/090	81/060	72/090
110	56/290	54/308	69/191	86/090	70/066	75/159	67/337
111	-	-	-	-	-	-	-
112	55/302	44/013	30/280	85/116	61/102	61/102	60/184
113	82/157	80/095	-	-	-	-	-
114	-	-	-	-	-	-	-
115	60/284	79/161	60/284	67/008	78/161	58/159	-

Tablo A1.1 continuies

116	-	-	-	-	-	-	-
117	70/330	67/192	85/270	70/206	30/093	-	-
118	-	-	-	-	-	-	-
119	50/270	50/270	78/180	83/184	78/180	-	-

APPENDIX-2: Discontinuity Spacing

Table A2.1 Discontinuity spacing measurements taken from the field

Location	DS(m)=		Frequency (m-1)	
6	DS(m)=	0,25	λ=	4.00
8	DS(m)=	0,15	λ=	6.67
10	DS(m)=	0,1	λ=	10.00
11	DS(m)=	0,2	λ=	5.00
13	DS(m)=	0,19	λ=	5.26
14	DS(m)=	0,2	λ=	5.00
18	DS(m)=	0,08	λ=	12.50
20	DS(m)=	0,15	λ=	6.67
21	DS(m)=	0,25	λ=	4.00
25	DS(m)=	0,15	λ=	6.67
28	DS(m)=	0,15	λ=	6.67
29	DS(m)=	0,14	λ=	7.14
30	DS(m)=	0,09	λ=	11.11
31	DS(m)=	0,11	λ=	9.09
32	DS(m)=	0,12	λ=	8.33
33	DS(m)=	0,13	λ=	7.69
34	DS(m)=	0,08	λ=	12.50
36	DS(m)=	0,09	λ=	11.11
37	DS(m)=	0,12	λ=	8.33
39	DS(m)=	0,08	λ=	12.50
41	DS(m)=	0,05	λ=	20.00
43	DS(m)=	0,11	λ=	9.09
44	DS(m)=	0,15	λ=	6.67
46	DS(m)=	0,13	λ=	7.69
48	DS(m)=	0,1	λ=	10.00
49	DS(m)=	0,08	λ=	12.50
50	DS(m)=	0,12	λ=	8.33
51	DS(m)=	0,06	λ=	16.67
52	DS(m)=	0,09	λ=	11.11
53	DS(m)=	0,15	λ=	6.67
55	DS(m)=	0,1	λ=	10.00
56	DS(m)=	0,22	λ=	4.55
57	DS(m)=	0,17	λ=	5.88
58	DS(m)=	0,12	λ=	8.33
59	DS(m)=	0,15	λ=	6.67

Table A2.1 continuies

60	DS(m)=	0,19	λ=	5.26
61	DS(m)=	0,2	λ=	5.00
62	DS(m)=	0,23	λ=	4.35
63	DS(m)=	0,15	λ=	6.67
68	DS(m)=	0,14	λ=	7.14
70	DS(m)=	0,1	λ=	10.00
73	DS(m)=	0,11	λ=	9.09
74	DS(m)=	0,15	λ=	6.67
75	DS(m)=	0,06	λ=	16.67
78	DS(m)=	0,12	λ=	8.33
79	DS(m)=	0,13	λ=	7.69
80	DS(m)=	0,07	λ=	14.29
81	DS(m)=	0,1	λ=	10.00
82	DS(m)=	0,11	λ=	9.09
83	DS(m)=	0,1	λ=	10,00
85	DS(m)=	0,09	λ=	11,11
87	DS(m)=	0,104	λ=	9,62
88	DS(m)=	0,216	λ=	4,63
89	DS(m)=	0,08	λ=	12,50
90	DS(m)=	0,1	λ=	10,00
91	DS(m)=	0,11	λ=	9,09
92	DS(m)=	0,15	λ=	6,67
93	DS(m)=	0,109	λ=	9,17
94	DS(m)=	0,062	λ=	16.13
95	DS(m)=	0,17	λ=	5.88
96	DS(m)=	0,05	λ=	20.00
97	DS(m)=	0,09	λ=	11.11
98	DS(m)=	0,21	λ=	4.76
99	DS(m)=	0,19	λ=	5.26
103	DS(m)=	0,08	λ=	12.50
105	DS(m)=	0,05	λ=	20.00
107	DS(m)=	0,06	λ=	16.67
108	DS(m)=	0,112	λ=	8.93
109	DS(m)=	0,13	λ=	7.69
110	DS(m)=	0,12	λ=	8.33
112	DS(m)=	0,15	λ=	6.67
114	DS(m)=	0,05	λ=	20.00
115	DS(m)=	0,091	λ=	10.99
117	DS(m)=	0,056	λ=	17.86
119	DS(m)=	0,05	λ=	20.00

APPENDIX-3: Schmidt Re-Bounce Counts

Table 3A.1 Values from discontinuity surfaces

Location	Rebound Value										Total	Average
1	24	25	28	27	24	33	28	28	29	18	264	26.4
2	23	40	34	32	34	39	38	34	45	44	363	36.3
3	48	56	30	32	25	51	48	34	28	52	404	40.4
4	25	20	12	16	18	19	20	14	12	15	171	17.1
5	19	15	11	12	14	12	12	18	10	14	137	13.7
6	40	34	41	26	28	32	24	35	16	22	298	29.8
7	18	19	14	22	32	19	24	19	21	11	199	19.9
8	12	10	14	34	16	28	11	13	10	23	171	17.1
9	38	35	28	37	27	32	25	28	30	23	303	30.3
10	27	28	24	24	28	18	18	11	32	34	244	24.4
11	11	21	15	25	23	26	14	18	15	10	178	17.8
12	22	17	24	10	22	15	14	30	40	15	209	20.9
13	19	10	15	20	16	11	22	18	11	15	157	15.7
14	15	31	22	21	28	26	15	44	30	34	266	26.6
15	20	21	23	21	30	12	20	18	21	13	199	19.9
16	17	11	13	19	25	18	14	21	17	25	180	18
17	15	28	35	28	25	36	18	26	46	40	297	29.7
18	30	22	34	24	21	18	40	32	34	28	283	28.3
19	19	28	22	20	15	24	18	30	34	15	225	22.5
20	15	26	29	48	40	40	19	38	30	15	300	30
21	23	28	24	20	22	15	30	28	15	18	223	22.3
22	18	21	12	11	24	13	20	18	13	11	161	16.1
23	29	31	38	28	40	29	25	30	30	33	313	31.3
24	22	28	31	20	24	22	25	28	28	20	248	24.8
25	30	27	24	33	25	21	31	30	27	26	274	27.4
26	28	25	30	31	38	31	34	28	22	33	300	30
27	24	22	32	27	23	24	30	27	24	25	258	25.8
28	34	30	31	33	40	37	31	27	28	32	323	32.3
29	38	40	34	39	36	28	27	42	37	39	360	36
30	13	19	20	27	24	11	21	27	19	21	202	20.2
31	12	16	21	24	16	19	22	21	18	23	192	19.2
32	28	22	24	21	26	20	23	25	28	31	248	24.8
33	24	28	23	22	44	32	29	32	22	30	286	28.6
34	39	32	25	23	30	24	26	27	34	28	288	28.8
35	28	42	27	42	41	27	28	44	44	38	361	36.1
36	22	20	33	26	42	29	23	48	39	36	318	31.8

Table 3A.1 continues

37	25	39	30	26	38	44	29	41	32	29	333	33.3
39	31	42	26	30	28	36	25	38	25	43	324	32.4
40	29	31	44	48	39	34	34	45	39	27	370	37
41	33	32	30	33	32	31	28	34	29	31	313	31.3
42	32	33	28	37	31	28	27	41	33	27	317	31.7
43	34	20	25	16	18	24	22	20	29	26	234	23.4
44	28	37	31	31	24	38	34	38	28	33	322	32.2
45	40	46	32	30	35	35	34	31	36	39	358	35.8
46	23	26	29	31	35	25	24	28	36	34	291	29.1
48	28	34	24	40	31	27	25	40	28	33	310	31
49	20	22	19	21	18	19	21	24	20	25	209	20.9
50	34	35	31	39	28	30	38	33	36	29	333	33.3
51	25	27	24	27	22	18	14	25	26	23	231	23.1
52	24	18	19	17	19	21	16	19	20	21	194	19.4
53	12	11	14	11	14	13	12	14	14	16	131	13.1
54	12	20	16	15	24	20	23	19	25	17	191	19.1
55	14	11	10	10	12	10	12	12	13	10	114	11.4
56	10	13	10	18	14	13	12	20	11	12	133	13.3
57	24	28	26	18	20	24	18	20	24	20	222	22.2
58	18	14	16	18	14	16	14	17	18	25	170	17
59	16	26	18	44	22	18	20	16	36	28	244	24.4
60	39	41	46	26	32	39	43	24	28	35	353	35.3
61	30	31	36	33	22	23	26	30	32	21	284	28.4
62	41	28	31	27	28	34	50	24	40	41	344	34.4
63	37	38	42	42	38	37	45	38	41	38	396	39.6
64	17	16	14	20	11	17	16	11	16	13	151	15.1
65	20	25	18	15	18	27	29	25	33	21	231	23.1
66	14	18	12	12	20	21	21	13	14	14	159	15.9
67	30	40	24	33	27	40	18	21	16	24	273	27.3
68	50	47	41	40	38	36	44	41	42	40	419	41.9
69	12	21	18	16	25	19	12	22	17	15	177	17.7
70	20	19	12	17	12	14	21	18	16	18	167	16.7
71	37	33	30	48	35	30	43	37	41	47	381	38.1
72	36	24	30	26	24	24	26	21	20	20	251	25.1
73	17	19	21	22	12	24	16	25	17	20	193	19.3
74	30	37	29	27	30	37	35	27	38	33	323	32.3
75	19	27	25	22	19	20	28	27	22	18	227	22.7
78	28	35	33	35	36	22	30	35	33	29	316	31.6
79	29	31	27	36	41	44	27	30	33	41	339	33.9
80	33	29	28	31	27	34	22	25	34	32	295	29.5
81	26	19	18	12	17	20	16	16	14	21	179	17.9
82	24	26	30	26	31	28	27	25	21	27	265	26.5

Table 3A.1 continues

83	39	33	29	45	37	40	42	37	40	29	371	37.1
84	18	17	22	12	20	17	19	18	13	16	172	17.2
85	22	24	31	24	30	20	33	28	30	33	275	27.5
86	12	20	28	17	23	21	20	22	15	17	195	19.5
87	12	24	20	18	24	21	13	17	15	15	179	17.9
88	20	19	14	20	16	14	12	11	20	17	163	16.3
89	14	11	12	14	13	11	16	15	14	11	131	13.1
90	28	25	20	18	16	14	23	27	20	25	216	21.6
91	27	25	17	32	17	26	20	19	20	23	226	22.6
92	21	27	25	30	31	20	20	29	30	32	265	26.5
93	22	19	26	28	20	24	24	19	21	20	223	22.3
94	40	37	41	35	31	45	40	40	47	37	393	39.3
95	35	30	40	44	45	25	27	35	30	32	343	34.3
96	28	34	26	20	29	27	31	30	32	31	288	28.8
97	32	40	41	40	39	44	47	35	41	42	401	40.1
98	27	30	25	32	34	41	40	37	38	28	332	33.2
99	40	39	38	35	28	27	30	27	33	25	322	32.2
100	30	25	24	22	27	23	29	31	32	25	268	26.8
101	20	22	19	10	14	11	12	17	18	13	156	15.6
102	15	20	17	19	18	15	19	17	14	16	170	17
103	22	30	25	28	32	31	22	26	28	26	270	27
104	26	24	30	27	24	20	27	26	30	27	261	26.1
105	23	31	21	25	28	29	33	29	35	25	279	27.9
106	20	22	25	27	26	22	29	22	24	27	244	24.4
107	29	25	38	26	21	35	28	37	27	29	295	29.5
108	32	28	29	30	27	35	33	28	29	22	293	29.3
109	34	35	34	35	22	24	20	19	21	26	270	27
110	24	28	30	22	23	25	24	37	27	29	269	26.9
111	40	39	44	46	36	40	34	35	45	40	399	39.9
112	34	40	38	29	31	27	25	36	30	37	327	32.7
113	37	30	40	35	36	42	28	32	36	35	351	35.1
114	35	41	40	39	35	39	38	22	34	44	367	36.7
115	30	30	38	30	31	40	31	28	25	25	308	30.8
116	24	26	28	27	22	28	30	25	22	24	256	25.6
117	34	30	32	27	23	35	40	43	27	25	316	31.6
118	30	27	29	20	35	23	32	34	27	35	292	29.2
119	28	23	30	20	20	35	20	32	33	21	262	26.2

APPENDIX-4: SMR classification in study area

Table 4A.1 SMR classification of location point

		SMR Classifications				
Location	Failure Type	V (0-20)	IV (21-40)	III (41-60)	II (61-80)	I (81-100)
1						
2						
3						
4						
5						
6	T			X		
7						
8	W			X		
9						
10	T			X		
11	P		X			
12						
13	T			X		
14	P			X		
15						
16						
17						
18	W				X	
19						
20	W			X		
21	T				X	
22						
23						
24						
25	P			X		
26						
27						
28	W			X		
29	W		X			
30	W			X		
31	W				X	
32	W			X		
33	W			x		
34	P		X			
35						
36	W			X		

Table 4A.1 continues

37	W			X		
38						
39	T			X		
40						
41	T		X			
42						
43	T			X		
44	W				X	
45						
46	T			X		
47						
48	W				X	
49	P			x		
50	T				X	
51	W			X		
52	W			X		
53	W			X		
54						
55	T			X		
56	W				X	
57	W				X	
58	T			X		
59	W		X			
60	T			X		
61	W				X	
62	T				X	
63	W				X	
64						
65						
66						
67						
68	W			X		
69						
70	W			X		
71	T				X	
72						
73	W			X		
74	W		X			
75	W			X		
76						
77						
78	W		X			

Table 4A.1 continues

79	W			X		
80	T			X		
81	W		X			
82	W		X			
83	T			X		
84						
85	W		X			
86						
87	T			X		
88	P		X			
89	T			X		
90	W		X			
91	P		X			
92	W			X		
93	P		X			
94	W		X			
95	W		X			
96	T		X			
97	W			X		
98	W		X			
99	T			X		
100						
101						
102						
103	W			X		
104						
105	W			X		
106						
107	T			X		
108	P		X			
109	T			X		
110	W		x			
111						
112	W			X		
113						
114	P		X			
115	W			X		
116						
117	W		X			
118						
119	W	X				

APPENDIX-5: Qslope classsification in study area

Table 5A.1 QSLOPE classification of location point

	QSLOPE Classifications				
Location	UNSTABLE	SEMİ-STAB	STABLE	Current Slope Angles	Stable Slope Angles
1					
2					
3					
4					
5					
6			X	41	71.41
7					
8			X	58	67.22
9					
10			X	56	69.31
11			X	48	76.13
12					
13			X	50	53.63
14			X	48	73.63
15					
16					
17					
18			X	48	60.21
19					
20			X	45	62.67
21			X	47	50.39
22					
23					
24					
25			X	59	65.17
26					
27					
28		X		50	48.69
29	X			53	48.49
30			X	56	58.92
31			X	44	60.23
32		X		55	52.60
33		X		50	48.28
34		X		57	46.58
35					
36		X		57	50.77

Table 5A.1 continues

37	X			58	50.00
38					
39	X			74	48.73
40					
41		X		54	44.65
42					
43			X	54	54.10
44	X			73	67.22
45					
46			X	47	52.71
47					
48			X	40	49.31
49			x	44	49.08
50			X	47	57.95
51			X	51	50.57
52			X	53	58.36
53			X	43	50.63
54					
55			X	45	45.79
56			X	41	61.42
57			X	39	67.52
58			X	35	60.45
59			X	39	55.18
60			X	46	59.65
61			X	73	77.82
62	X			76	63.36
63			X	45	77.32
64					
65					
66					
67					
68			X	44	47.93
69					
70			X	39	40.33
71	X			79	50.04
72					
73			X	51	52.27
74	X			55	41.20
75	X			63	48.63
76					
77					
78	X			57	52.60

Table 5A.1 continues

79		X		60	58.84
80		X		50	49.81
81	X			48	35.33
82	X			50	40.33
83			X	45	51.88
84					
85	X			42	31.84
86					
87			X	43	47.00
88	X			57	51.68
89		X		58	54.25
90			X	54	47.44
91		X		47	42.72
92			X	54	65.34
93		X		60	55.48
94		X		50	46.38
95			X	45	42.99
96		X		56	46.71
97			X	55	53.43
98	X			55	49.29
99			X	60	59.65
100					
101					
102					
103			X	45	44.65
104					
105			X	54	54.19
106					
107	X			63	50.11
108	X			60	52.27
109	X			60	52.71
110	X			56	48.06
111					
112		X		58	48.69
113					
114	X			62	54.54
115	X			68	47.00
116					
117	X			44	31.45
118					
119	X			60	42.15